

Solitons and matter waves

Jean Dalibard
Collège de France, chair *Atoms and radiation*

Lecture series 2024-25



COLLÈGE
DE FRANCE
— 1530 —

Contents

Introduction	7	4-1	The speed of sound in a uniform condensate	26	
I Bright solitons	11	4-2	Modulational instability	27	
1	A bright soliton at rest	11	4-3	Observation of a soliton train	27
1-1	The Gross–Pitaevskii energy functional	12	4-4	A soliton gas	28
1-2	Some general properties	13	II Bright soliton dynamics and the IST method	31	
1-3	Stationary solution: the fundamental soliton	14	1	Temporal evolution of a soliton	31
1-4	The quantum version of the problem	15	1-1	Eigenmodes of a soliton?	31
2	The bright soliton in motion	16	1-2	Damped oscillations	33
2-1	Soliton in uniform motion	16	1-3	Experimental study	34
2-2	Action of a force on a soliton	17	1-4	Case of a (relatively) large initial deviation	34
2-3	Observation of a single soliton	17	2	The IST method	35
2-4	The validity of the one-dimensional approach	19	2-1	A reminder: Eigenstates decomposition	35
3	Beyond the stationary soliton	20	2-2	The Lax pair of operators	36
3-1	Soliton collisions	21	2-3	Scattering data associated with \hat{L}	38
3-2	Kuznetsov-Ma structure	22	2-4	The evolution of scattering data	39
3-3	The Peregrine breather	24	2-5	Inversion of scattering data	40
4	Dynamic instability and soliton train	25	3	The fundamental soliton	41

3-1	The fundamental soliton at rest	41	3-5	Does a quantum soliton stay dark?	68
3-2	Variants around the soliton at rest	42	4	Transitions to other states	69
3-3	The fundamental soliton in motion	43	4-1	The instability of the nodal plane	69
4	Higher-order solitons	44	4-2	The different possible stationary states	70
4-1	N solitons of different velocities	45	4-3	Observations on a superfluid Fermi gas	71
4-2	Multi-solitons (or composite solitons)	45			
4-3	Experimental observations	47	IV Magnetic solitons and Bloch oscillations		73
4-4	Can a multi-soliton be decomposed?	48	1	The ferromagnetic chain	73
			1-1	The relevant energy scales	73
III Gray solitons		51	1-2	Dynamics of a magnetic moment	74
1	The wave function of a grey soliton	51	1-3	Switching to a continuous description	75
1-1	The speed of sound in a uniform condensate	51	1-4	Lagrangian approach	76
1-2	The healing length	52	1-5	Link with the nonlinear Schrödinger equation	77
1-3	Dark soliton (at rest)	53	2	A binary mixture of condensates	78
1-4	The grey soliton (in motion)	53	2-1	Coupled Gross-Pitaevskii equations	78
2	Energy and momentum of a grey soliton	56	2-2	Manakov regime	79
2-1	Using the Gross-Pitaevskii functional	56	2-3	Bath at rest: the magnetic chain regained	80
2-2	Local momentum vs. total momentum	57	2-4	Unconstrained bath	81
2-3	Why two momenta? The case of a straight line	59	3	The magnetic soliton	83
2-4	Why two momenta? The case of a ring	60	3-1	General structure of the solution	84
2-5	Effective soliton mass	61	3-2	The magnetic soliton at rest	84
3	Gray soliton dynamics	62	3-3	Experimental realization of a soliton at rest	86
3-1	The soliton seen as a quasi-particle	62	3-4	The magnetic soliton in motion	88
3-2	Oscillation in a harmonic trap	64	4	Bloch oscillations of a magnetic soliton	89
3-3	Experimental observations	65	4-1	"Usual" Bloch oscillations	89
3-4	Collision between two grey solitons	67	4-2	Force on a magnetic soliton	90

4-3	Observation of Bloch oscillations	91
4-4	The origin of the periodicity of $E(P)$	92

Références

Introduction

Solitons are fascinating objects that appear in many fields of science, from hydrodynamics to biology, mathematics, theoretical physics and chemistry. Their existence is based on a nonlinear process, making them intrinsically difficult to describe. It is hardly surprising, then, that the concept has taken a long time to establish itself in all its generality: it is only since the 1960s that the universal nature of solitonic structures has been understood, beyond the various contexts in which they appear.

In this course, we will discuss a relatively recent field of research, based on the use of coherent matter waves to generate and characterize solitons. This field emerged around 25 years ago, with the possibility of manipulating and shaping Bose-Einstein condensates formed from laser-cooled and trapped atoms. It has developed considerably since then, and we will be presenting several remarkable achievements.

The date of birth of the scientific study of solitons is known¹: in August 1834, the Scottish engineer John Scott Russell (1808-1882), inspecting the canal linking Edinburgh and Glasgow, observed the birth of a wave generated by the sudden stop of a boat. He described the phenomenon as follows:

I was observing the motion of a boat which was rapidly drawn along a narrow channel by a pair of horses, when the boat suddenly stopped – not so the mass of water in the channel which it had put in motion; it accumulated round the prow of the vessel in a state of violent agitation, then suddenly leaving it behind, rolled forward with great velocity, assuming the form of a large solitary elevation, a rounded, smooth and well-defined heap of water, which continued its course along the channel apparently without change of form or diminution of speed. I followed

¹The historical aspects described here are mainly taken from Ablowitz & Segur (1981), Drazin & Johnson (1989), Dauxois & Peyrard (2006) and Marin (2012). One can also consult the comprehensive article by Darrigol (2003).

it on horseback, and overtook it still rolling on at a rate of some eight or nine miles an hour, preserving its original figure some thirty feet long and a foot to a foot and a half in height. Its height gradually diminished, and after a chase of one or two miles I lost it in the windings of the channel. Such, in the month of August 1834, was my first chance interview with that singular and beautiful phenomenon which I have called the Wave of Translation

The main characteristics of a soliton are identified: "large solitary elevation", "without diminution of speed", "preserving its original figure". Over the next ten years, Russell devoted a great deal of time, both theoretically and experimentally, to characterizing this "translation wave" (which he also called the "large solitary wave"). He even went so far as to build a 10-meter-long pond in his garden for measurements. Russell published all his results in Russell (1844), but his work was met with skepticism from his contemporaries, especially Airy and Stokes. The latter's arguments were in fact irrelevant, as they were based on a linear approach – the only one known at the time – to wave propagation; yet the solitons observed by Russell are intrinsically nonlinear. Unfortunately, Russell did not have the right wave equation to answer these objections, so he abandoned his research.

Towards the end of the 19th century, the Frenchman Boussinesq (1871), the Englishman Rayleigh (1876), then the Dutchmen Korteweg and de Vries (1895), understood the wave structure observed by Russell and established its equation of motion². For a relatively narrow channel of axis x and for shallow water, this equation can be written (in reduced units and

²The genesis of the ideas around the KdV equation is described by Darrigol (2003) and by De Jager (2006). See also R.K. Bullough's contribution in Lakshmanan (1988).

in an appropriate reference frame):

$$u_t = -u_{xxx} - 6uu_x \quad (1)$$

where $u(x, t)$ represents the height of the water above its reference level³. The solitonic solution of this equation is

$$u(x, t) = -\frac{v/2}{\cosh^2[\sqrt{v}/2(x - vt)]} \quad v > 0, \quad (3)$$

i.e. a structure that propagates without deformation at speed v .

Once this solution was known, interest in this type of problem waned. It was not until the early 1950s, with the work of Fermi, Pasta, Ulam and Tsingou⁴ (Fermi, Pasta, et al. 1955) to see solitonic behavior emerge again. This article actually describes the first digital experiment, as Fermi sought to use the brand-new computer at his disposal, the MANIAC, to explore physical phenomena. The initial idea was to solve the equations of motion of 64 nonlinearly coupled oscillators, in order to demonstrate a thermalization phenomenon. The conclusion of this work was non ambiguous⁵: *The results show very little, if any, tendency toward equipartition of energy among the degrees of freedom.*

What was going on? One had to wait another ten years for the work of Zabusky & Kruskal (1965) to elucidate the paradox. These authors first showed that the problem studied by Fermi and his collaborators boiled down to solving the Korteweg – de Vries equation. They also understood that the initial condition chosen by Fermi fragments into several solitons, which collide with each other without deforming, before reproducing the initial state almost identically. Zabusky & Kruskal (1965) introduced the word "soliton"⁶ and wrote:

³In this course, we will use the notations :

$$u_t \equiv \partial_t u \equiv \frac{\partial u}{\partial t} \quad u_x \equiv \partial_x u \equiv \frac{\partial u}{\partial x} \quad u_{xxx} \equiv \partial_x^3 u \equiv \frac{\partial^3 u}{\partial x^3}. \quad (2)$$

⁴The article (actually a classified report from Los Alamos) is signed by the first three authors only, but it explicitly mentions that the work was done by the three signatories and Mary Tsingou [see, for example, Dauxois (2008)].

⁵In fact, we now know that if Fermi and his collaborators had used a significantly stronger nonlinearity, they would have reached a threshold where the dynamics of their system would have become chaotic, leading to equipartition of energy.

⁶They first tried "solitron", but this word had already been pre-empted by a company.

In other words, solitons "pass through" one another without losing their identity. Here we have a nonlinear physical process in which interacting localized pulses do not scatter irreversibly.

Since then, solitons have remained at the forefront of the scientific scene, with considerable impact in a wide variety of fields. They can appear in any system governed by a nonlinear equation, and they result from a competition between two terms, one tending to spread the solitonic object in question, the other tending on the contrary to compress it. The nonlinear nature of the problem links the size of the object to its amplitude, as seen on the solution (3) of amplitude v and width $\sim 1/\sqrt{v}$. These solitons are found in particular in optics and hydrodynamics, with fruitful parallels between the two fields.

As mentioned above, this series of lectures will focus on the physics of solitons generated from matter waves in ultra-cold atomic gases. The necessary nonlinearity will come from the interaction between atoms, which we will describe using a mean-field approach, limiting ourselves to one-dimensional systems for simplicity. The outline of this lecture series will be as follows:

- The first two chapters will be devoted to the case of an attractive interaction, for which the soliton consists of an aggregate of atoms, generally propagating on a dark background. In Chapter 1, we will establish the evolution laws of a soliton based on the nonlinear Schrödinger equation. We will then generalize these laws to the case of several solitons, and demonstrate the possibility of generating large-amplitude "rogue waves" from an almost uniform wave (figure 1). Then, in chapter 2, we will introduce an extremely powerful theoretical approach to studying these solitons, called *inversion scattering transform* (IST), and discuss the possibility of generating and analyzing "multi-solitons".
- Chapter 3 will be devoted to the case of repulsive interaction, which allows the realization of dark solitons, i.e. density holes with the right phase profile to obtain stable structures propagating at constant velocity. We will also tackle the tricky problem of defining the momentum of a soliton, which we will link to the counterflow existing in the bath on either side of the density hole.
- In Chapter 4, we turn to a broader class of solitons, called *magnetic*



Figure 1. The Great Wave of Kanagawa, print by Katsushika Hokusai, 1831. The connection with a rogue wave is explained by Cartwright & Nakamura (2009) and Dudley, Sarano, et al. (2013).

solitons. We will see how these can be realized in a mixture of condensates, and we will study a remarkable property of these magnetic solitons: when subjected to a constant force, they do not undergo a uniformly accelerated motion as one would intuitively expect, but take on an oscillatory motion, reminiscent of the Bloch oscillations of a quantum particle in a spatially periodic lattice. We will analyze this phenomenon and describe its very recent experimental demonstration.

On a subject as vast as solitons, this series of lectures can by no means claim to be exhaustive. Our aim is to illustrate some salient properties of these objects, linked to their robustness and the consequences of the integrability of the underlying evolution equations. We refer readers wishing to delve deeper into the subject to recent articles or books, such as Malomed (2022), Dudley, Finot, et al. (2023), Suret, Randoux, et al. (2024) and Malomed (2024) for multi-dimensional aspects.

Acknowledgements I am very grateful to Jérôme Beugnon, Guillaume Brochier, Raphael Lopes, Sylvain Nascimbene and Franco Rabec for multiple discussions on the subject and for proofreading a preliminary version (in French) of these lecture notes.

Chapter I

Bright solitons

The first chapter of this course is devoted to the simplest configuration for the emergence of a solitonic structure for matter waves: a set of interacting atoms forced to move along a straight line. The soliton then appears as the ground state of the system, with the N atoms forming a bound state. The spatial extension of this state results from a balance between attractive interactions, which tend to reduce the size of the soliton as much as possible, and the kinetic energy linked to particle confinement, which tends on the contrary to extend the atomic wave packet.

This structure is called a "bright soliton" because the atoms form a density peak located at an arbitrary position on the straight line along which they can move. Outside this density peak, the probability of finding a particle is negligible. We will see that the wave function describing this state is the solution of lowest energy for the nonlinear Schrödinger equation (also known as the Gross–Pitaevskii equation) in the one-dimensional geometry.

Once we have understood this solitonic structure, we will turn our attention to more complex structures than this simple bright soliton. In particular, we will show that solitons behave like particles when they interact with each other, i.e. they emerge "unchanged" from a binary soliton-soliton collision. We will also present structures that are non-stationary, but can recur periodically over time (*breathers*).

The chapter ends with a model to explain the formation of soliton trains in gases whose interactions are suddenly changed from repulsive to attractive. We will say a few words about the dynamics of an assembly of atoms



Figure I.1. A gas of particles forced to move along a straight line. Particles interact with each other through a contact potential.

with energies well above the ground state, giving rise to a gas of solitons. This dynamic provides a model to explain the existence of "rogue waves" in hydrodynamics, i.e. waves with a very large amplitude that may emerge in an otherwise nearly flat sea.

Many of the results shown in this chapter are related to the integrability of the 1D nonlinear Schrödinger equation. Here, we will restrict ourselves to pointing out these integrability signatures. We will return to this notion in greater detail in Chapter II.

1 A bright soliton at rest

Most of this course will be devoted to effectively one-dimensional situations for quantum fluids. These are obtained by strongly confining the fluid along two directions in space (noted here as y and z), so that the two corresponding degrees of freedom can be considered frozen. On the other hand, motion along the x direction is free, and this is what we will be fo-

cusing on (figure I.1). We will come back in §2-4 to the validity conditions for this one-dimensional approach.

For the electromagnetic field, this one-dimensional situation is obtained by sending light through a single-mode optical fiber. For atoms or molecules, confinement in the y, z directions can be achieved with a strong magnetic field gradient or by using light beams to create an optical lattice, for example. In what follows, we will start from the case of a gas of atoms to construct solitons, but the results obtained will also apply to the case of light pulses propagating in a fiber.

1-1 The Gross–Pitaevskii energy functional

Throughout this course, we will assume that interactions between atoms are binary, short-range and describable by a contact potential. For two atoms located at x_1 and x_2 , we will assume

$$V(x_1, x_2) = g \delta(x_1 - x_2) \quad (\text{I.1})$$

where the real coefficient g characterizes the strength of the interactions. The cases $g < 0$ and $g > 0$ correspond to attractive and repulsive interactions, respectively. The 1D situation considered here is much simpler than the three-dimensional case, where the contact interaction must be regularized to avoid uncontrolled divergences (see courses 2020-21 and 2021-22). Here, the Dirac distribution simply corresponds to the limit of a potential well ($g < 0$) or a potential bump ($g > 0$), with a width small compared to all the physical quantities of the problem (in particular the distance between particles).

We assume in this paragraph that the quantum fluid is well described by a classical field approach. The state of the fluid at an instant t is therefore characterized at a point x by a complex wave function $\psi(x, t)$, normalized by the total number of particles along the length accessible to the gas, which we will assume here to be infinite:

$$\int_{-\infty}^{+\infty} |\psi(x, t)|^2 dx = N \quad (\text{I.2})$$

and corresponding to the spatial density at point x :

$$\rho(x, t) = |\psi(x, t)|^2. \quad (\text{I.3})$$

The total energy of the gas is given by the Gross–Pitaevskii functional

$$E^{(1D)}[\psi] = \frac{\hbar^2}{2m} \int \left| \frac{\partial \psi}{\partial x} \right|^2 dx + \frac{1}{2} \iint \rho(x) V(x, x') \rho(x') dx dx' \quad (\text{I.4})$$

where the first term corresponds to kinetic energy and the second to interaction energy. This expression is simplified for contact interaction (I.1) to

$$E^{(1D)}[\psi] = \frac{\hbar^2}{2m} \int \left| \frac{\partial \psi}{\partial x} \right|^2 dx + \frac{g}{2} \int |\psi(x)|^4 dx \quad (\text{I.5})$$

This energy functional corresponds to a mean-field description of the fluid, where each particle evolves in a potential proportional to the local fluid density $\rho(x)$.

The equation of motion deduced from the energy functional (I.5) is the nonlinear Schrödinger equation (or Gross–Pitaevskii equation):

$$i\hbar \frac{\partial \psi}{\partial t} = -\frac{\hbar^2}{2m} \frac{\partial^2 \psi}{\partial x^2} + g|\psi|^2 \psi \quad (\text{I.6})$$

We will often use a dimensionless version of this equation. For this, let us introduce a unit of length x_0 and a unit of time t_0 (which are arbitrary at this stage)

$$\tilde{x} = \frac{x}{x_0} \quad \tilde{t} = \frac{t}{t_0}. \quad (\text{I.7})$$

We link these units of length and time by

$$t_0 = \frac{2mx_0^2}{\hbar} \quad (\text{I.8})$$

and we simultaneously make the function change

$$u(\tilde{x}, \tilde{t}) = \sqrt{\frac{x_0}{N}} \psi(x, t) \quad (\text{I.9})$$

so that the norm of u is related to that of ψ by:

$$\int |u(\tilde{x}, \tilde{t})|^2 d\tilde{x} = \frac{1}{N} \int |\psi(x, t)|^2 dx. \quad (\text{I.10})$$

The nonlinear Schrödinger equation is then written as

$$i \frac{\partial u}{\partial \tilde{t}} = -\frac{\partial^2 u}{\partial \tilde{x}^2} + 2G|u|^2 u \quad \text{with} \quad G = \frac{Nm x_0}{\hbar^2} g. \quad (\text{I.11})$$

At this stage, the length scale x_0 is still arbitrary. In what follows, we will choose it so that $G = +1$ for repulsive interactions ($g > 0$) and -1 for attractive interactions ($g < 0$):

$$x_0 = \frac{\hbar^2}{Nm|g|} \quad (\text{I.12})$$

with the associated time scale given the link (I.8) between t_0 and x_0 :

$$t_0 = \frac{2\hbar^3}{N^2 m g^2}. \quad (\text{I.13})$$

We will therefore write the equation for the evolution of the function u in the form :

$$\boxed{i u_t + u_{xx} \pm 2|u|^2 u = 0} \quad (\text{I.14})$$

where we have omitted the $\tilde{\cdot}$ above the variables x and t to simplify the writing and where we have adopted here the usual notation

$$u_t = \frac{\partial u}{\partial t} \quad u_{xx} = \frac{\partial^2 u}{\partial x^2}. \quad (\text{I.15})$$

The $+$ sign in (I.14) corresponds to the attractive case $g < 0$ (called the focusing case in nonlinear optics), on which we will concentrate in this chapter. The $-$ sign corresponds to the repulsive (defocusing) case, which we will describe in chapter III, and gives rise to dark solitons.

This equation appears in many other physics problems, such as the propagation of the envelope of a light pulse in an optical fiber, or deep-water wave dynamics [see, for example, Dudley, Genty, et al. (2019) and refs. in]. Note that in the case of a light pulse propagating in an optical fiber, the roles of space and time variables are reversed: the variable \tilde{t} in the above equation represents the position along the fiber and the variable \tilde{x} is related to time (Dauxois & Peyrard 2006).

1-2 Some general properties

The nonlinear Schrödinger equation has a number of general properties, independent of the chosen initial condition, which will play a crucial role in what follows. These properties are well known for the usual (i.e. linear) Schrödinger equation as a consequence of the Hermitian character of the Hamiltonian, and they remain valid in the presence of the nonlinearity of (I.6).

Conservation of the number of particles. The number of particles is given by the squared norm of the function $\psi(x, t)$, as indicated in (I.2). We simply check that

$$\frac{dN}{dt} = \int (\partial_t \psi^*) \psi + \int \psi^* (\partial_t \psi) \quad (\text{I.16})$$

vanishes. To do this, simply use the evolution equation (I.6) and its complex conjugate, then perform integration by parts for the kinetic energy term:

$$\int (\partial_x^2 \psi^*) \psi = - \int (\partial_x \psi^*) (\partial_x \psi) = \int \psi^* (\partial_x^2 \psi). \quad (\text{I.17})$$

We have assumed here that ψ is sufficiently regular and tends to 0 fast enough at infinity for these manipulations to be legitimate.

Momentum conservation. The momentum associated with the wave function ψ is obtained by taking the average of the momentum operator $\hat{p} = -i\hbar \partial_x$:

$$p = -i\hbar \int \psi^* (\partial_x \psi) \quad (\text{I.18})$$

and we can check that

$$\frac{dp}{dt} = 0. \quad (\text{I.19})$$

The cancellation of the kinetic energy term is ensured as above (as for the linear Schrödinger equation), and the contribution of the interaction terms is proportional to $\int \partial_x |\psi|^4$, which cancels out assuming that ψ decreases fast enough at infinity.

Energy conservation. This conservation is in fact assured insofar as the evolution equation (I.6) is obtained from the energy functional (I.5). It can also be checked directly by taking the derivative with respect to time of the functional (I.5) and ensuring that all terms cancel out after the appropriate integrations by parts.

Homothety. We can check that if $\psi(x, t)$ is a solution to (I.6), then

$$\psi_\kappa(x, t) \equiv \kappa \psi(\kappa x, \kappa^2 t) \quad (\text{I.20})$$

is also a solution of this equation for the same mass m and the same interaction parameter g , with each term of the nonlinear Schrödinger equation multiplied by κ^3 . Note that ψ and ψ_κ correspond to different numbers of particles:

$$\int |\psi(x, t)|^2 dx = N \quad \Rightarrow \quad \int |\psi_\kappa(x, t)|^2 dx = \kappa N. \quad (\text{I.21})$$

1-3 Stationary solution: the fundamental soliton

For the moment, we will not attempt to give families of time-dependent solutions to the equation (I.6) and we will restrict ourselves to stationary solutions:

$$\psi(x, t) = \psi(x) e^{-i\mu t/\hbar} \quad (\text{I.22})$$

satisfying the equation

$$-\frac{\hbar^2}{2m} \frac{d^2\psi}{dx^2} + g|\psi(x)|^2\psi(x) = \mu\psi(x). \quad (\text{I.23})$$

For a gas of atoms, the quantity μ corresponds to the chemical potential, i.e. the energy required to add a particle to the system. We will check this property a little further on.

In a box of size $L \rightarrow +\infty$ and for a finite number of particles N , the equation (I.6) always has as its solution the constant function corresponding to a density $\rho = N/L \rightarrow 0$, i.e. zero chemical potential. The energy (I.5) associated with this uniform solution is also zero.

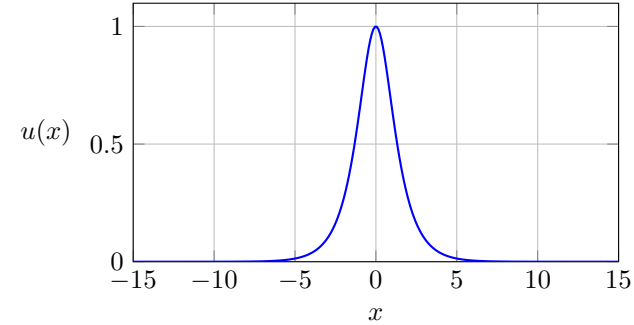


Figure I.2. Profile of the bright soliton given by equation (I.24).

In the attractive case we are interested in here, it is possible to find stationary solutions of (I.6) or (I.14) corresponding to negative μ and E . In the dimensionless version (I.14), a possible solution is:

$$u(x, t) = \frac{e^{it}}{\cosh x} \quad \int |u|^2 dx = 2 \quad (\text{I.24})$$

with the chemical potential equal to -1 . This function is plotted for $t = 0$ in figure I.2. More generally, given the homothety property mentioned above, we find the family of solutions

$$u(x, t) = \frac{\kappa}{\cosh(\kappa x)} e^{i\kappa^2 t} \quad \int |u|^2 dx = 2\kappa. \quad (\text{I.25})$$

Let us express the solution (I.25) with dimensioned variables, choosing $\kappa = 1/2$ so that the link (I.10) between the norms of u and ψ results in

$$\kappa = 1/2 : \quad \int |u|^2 dx = 1 \quad \Rightarrow \quad \int |\psi|^2 dx = N. \quad (\text{I.26})$$

We then find

$$\psi(x, t) = \frac{\psi_0}{\cosh(x/2x_0)} e^{-i\mu t/\hbar} \quad \text{with} \quad x_0 = \frac{\hbar^2}{Nm|g|} \quad \psi_0 = \sqrt{\frac{N}{4x_0}} \quad (\text{I.27})$$

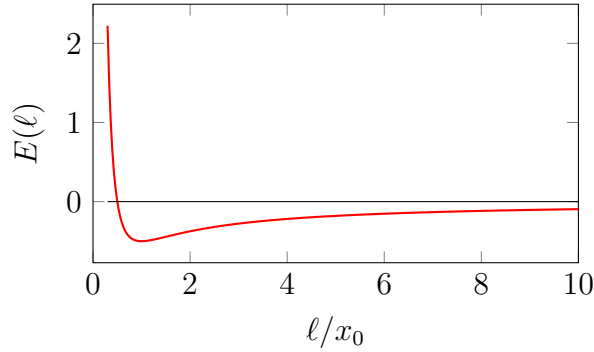


Figure I.3. Variation of total energy with wave packet size.

with the chemical potential :

$$\mu = -3\alpha N^2 \quad \text{with} \quad \alpha = \frac{1}{24} \frac{mg^2}{\hbar^2} \quad (\text{I.28})$$

The energy of the Gross–Pitaevskii functional associated with this wave function is $E = E_{\text{kin}} + E_{\text{int}}$ with

$$E_{\text{kin}} = \alpha N^3 \quad E_{\text{int}} = -2\alpha N^3 \quad (\text{I.29})$$

so that

$$E = -\alpha N^3 \quad (\text{I.30})$$

We then recover the relationship between the chemical potential and the energy:

$$\mu = \frac{\partial E}{\partial N}. \quad (\text{I.31})$$

The fact that the energy is negative indicates that we are dealing with a bound state: the (negative) interaction energy is greater in absolute value than the kinetic energy, and the N -particle system minimizes its energy by forming a wave packet of size x_0 , inversely proportional to the number of particles N . More precisely, for a wave packet of size ℓ , these two energies vary as follows

$$E_{\text{kin}} = N \frac{\hbar^2}{2m\ell^2} \quad E_{\text{int}} = -N^2 \frac{|g|}{\ell} \quad (\text{I.32})$$

so that the total energy $E_{\text{kin}} + E_{\text{int}}$ has the shape shown in figure I.3, with a minimum for $\ell \sim x_0$.

We have considered here the solution centered at $x = 0$, but as the problem is invariant by translation, the function $\psi(x - a)$, where a is any distance, is also a solution for the same energy.

Note: norm of a soliton. For the wave function (I.27), we find as indicated that $\int |\psi(x)|^2 dx = N$. In the literature, this situation is frequently referred to as the " N -norm soliton". In the usual sense of the norm of wave functions, it is the square of the norm of ψ that is N and the wave function is of norm \sqrt{N} . One must therefore be careful to re-establish the true normalization of the wave function in question, depending on the context.

1-4 The quantum version of the problem

Remarkably, certain physical quantities of a 1D assembly of quantum particles obeying Bose statistics and in contact interaction can be calculated exactly, both in the repulsive and in the attractive case.

The system's Hamiltonian can be written as

$$\hat{H} = \sum_i \frac{\hat{p}_i^2}{2m} + g \sum_{i < j} \delta(\hat{x}_i - \hat{x}_j). \quad (\text{I.33})$$

In the repulsive case ($g > 0$), Lieb & Liniger (1963) determined the spectrum of the Hamiltonian and the corresponding eigenstates using Bethe's ansatz. In the attractive case of interest here, McGuire (1964) calculated exactly the energy of the ground state:

$$E = -\frac{mg^2}{24\hbar^2} N(N^2 - 1). \quad (\text{I.34})$$

The associated wave function is written, to within a normalization coefficient [Castin & Herzog (2001) and refs. in]:

$$\Psi(x_1, \dots, x_N) = \exp \left[-\frac{m|g|}{2\hbar^2} \sum_{i < j} |x_i - x_j| \right] \quad (\text{I.35})$$

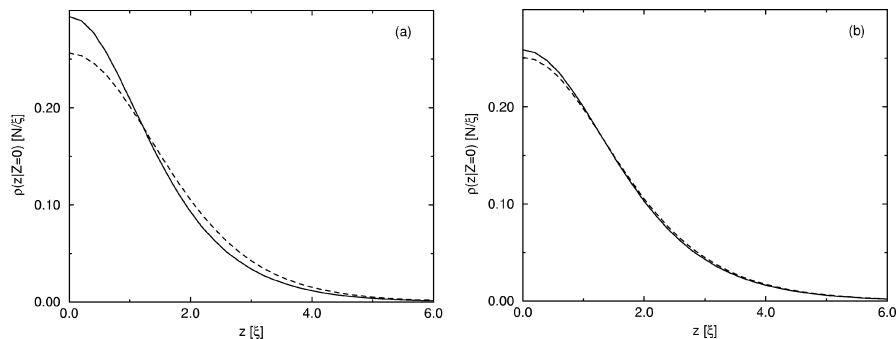


Figure I.4. Function $\rho(z|Z_{\text{cm}} = 0)$ giving the probability of finding a particle at point z , knowing that the center-of-mass of the N particles is located at $Z = 0$. Solid line: result obtained for the N -body wave function (I.35) of the ground state. Dashed line: result obtained for the wave function $\psi(x)$ of a soliton in the classical field approach, breaking the translational invariance of the quantum problem. Left (resp. right) panel: $N = 10$ (resp. $N = 45$).

In the limit of a number of atoms much larger than 1, the energy is very close to that found using the functional (I.30), the relative difference being of order $1/N^2$.

As far as the states are concerned, we immediately note a major difference between the soliton wave function, $\psi(x) \propto 1/\cosh(x/2x_0)$ and the N -body wave function (I.35): the former is localized in the vicinity of $x = 0$, whereas the latter is completely delocalized, a natural consequence of the translational invariance of the quantum many-body problem. To explore this point further, Castin & Herzog (2001) have calculated, from the N -body wave function, the probability of finding a particle at z , knowing the position Z_{cm} of the center-of-mass of the ensemble. This quantity is plotted in figure I.4 for $N = 10$ and $N = 45$ particles. We can see that it is very close to the classical field result obtained from $\psi(x)$, the agreement being all the better as N is larger.

The situation encountered here is an example of a very general problem, where a broken-symmetry description of a system (here, the wavefunction $\psi(x)$ solution of the nonlinear Schrödinger equation) is compared with the exact many-body wavefunction of the system (here, the state (I.35)), which

itself respects this symmetry. Another example of this issue is the determination of the relative phase of two condensates (Javanainen & Yoo 1996; Castin & Dalibard 1997).

2 The bright soliton in motion

2-1 Soliton in uniform motion

The Schrödinger equation has a Galilean invariance that is not modified by the addition of the nonlinear term in (I.6). Starting from a stationary solution (I.22), we can generate a family of solutions corresponding to the transition to a frame of reference in uniform translation with respect to the initial frame of reference:

$$\psi(x, t) \longrightarrow \psi(x - vt, t) e^{im(vx - v^2t/2)/\hbar}. \quad (\text{I.36})$$

Each solution here corresponds to a soliton whose envelope (i.e. the modulus of ψ) is moving at speed v , its total energy being the sum of its internal energy (I.30) and the kinetic energy of the center of mass $Nmv^2/2$. The corresponding momentum is $P = Nmv$ and the wave function is:

$$\psi(x, t) = \frac{\psi_0 e^{imvx/\hbar}}{\cosh[(x - vt)/2x_0]} e^{-it(\mu + mv^2/2)/\hbar}. \quad (\text{I.37})$$

As shown by Dauxois & Peyrard (2006), this family of solitons corresponds to the set of possible solutions of the nonlinear Schrödinger equation when we impose the form

$$\psi(x, t) = \mathcal{A}(x - v_a t) e^{i\theta(x - v_p t)} \quad (\text{I.38})$$

where v_a and v_p correspond to the propagation velocities for the amplitude and the phase. Note that it is not possible to have a solution with a constant profile, i.e. $v_a = v_p$, unlike in the case of the Korteweg–de Vries and sine-Gordon equations.

2-2 Action of a force on a soliton

Galilean invariance is just a special case of a more general invariance of the Schrödinger equation (linear or nonlinear). We can check that if the function $\psi(x, t)$ is a solution of

$$i\hbar \frac{\partial \psi}{\partial t} = -\frac{\hbar^2}{2m} \frac{\partial^2 \psi}{\partial x^2} + g|\psi|^2\psi, \quad (\text{I.39})$$

then the function $\phi(x, t)$ defined by

$$\phi(x, t) = \psi\left[x - \xi(t)\right] \exp\left[\frac{im}{\hbar} \left(\xi x - \frac{1}{2} \int_0^t \dot{\xi}^2 dt\right)\right] \quad (\text{I.40})$$

is solution of

$$i\hbar \frac{\partial \phi}{\partial t} = -\frac{\hbar^2}{2m} \frac{\partial^2 \phi}{\partial x^2} + g|\phi|^2\phi - m\ddot{\xi}x\phi. \quad (\text{I.41})$$

Galilean invariance (I.36) corresponds to the case $\xi(t) = vt$ with a velocity v independent of time, but the result (I.41), sometimes called *extended Galilean invariance* (Greenberger 1979), can be used to deal with the transition to non-inertial reference frames, or to solve problems where particles are subjected to a uniform force F , hence a potential $V(x) = -Fx$, knowing the solution for $F = 0$.

Consider a soliton initially at rest with wave function $\psi_0/\cosh(x/2x_0)$ [cf. (I.27)]. From this result, we deduce that if we apply a force $F = ma$ that is uniform in space and constant in time, this soliton will undergo a uniformly accelerated motion without any deformation of its envelope, whatever the value of the force. Its wave function at time t is written:

$$\phi(x, t) = \frac{\psi_0}{\cosh[(x - at^2/2)/2x_0]} e^{-it(\mu - Fx + F^2t^2/6m)/\hbar}. \quad (\text{I.42})$$

This result is no longer valid if the force is not uniform. For example, the application of an inverted harmonic potential $V(x) = -m\omega^2x^2/2$, corresponding to the force $F = m\omega^2x$, can destabilize the soliton if the number of atoms N does not reach a critical value (Carr & Castin 2002).

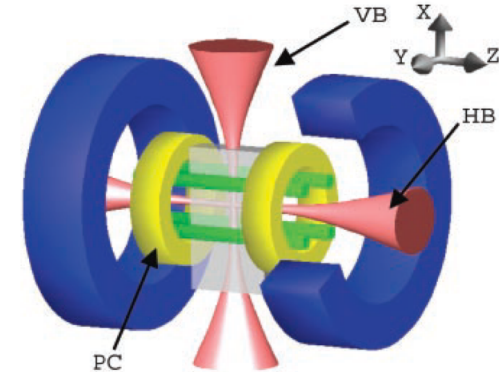


Figure I.5. Schematic diagram of the Khaykovich, Schreck, et al. (2002) experiment that revealed a bright matter-wave soliton. Atoms are initially confined to the intersection of two light beams, one horizontal (HB), the other vertical (VB). The scattering length is controlled by a Fano–Feshbach resonance by adjusting the magnetic field.

2-3 Observation of a single soliton

The prediction of the existence of solitons for the nonlinear Schrödinger equation dates back to a paper by Hasegawa & Tappert (1973) on the propagation of light in an optical fiber. This type of soliton was then demonstrated experimentally by Mollenauer, Stolen, et al. (1980). See Dudley, Finot, et al. (2023) for a recent review of the study of solitons in this nonlinear optics context.

The first observation of a bright soliton for matter waves was made by Khaykovich, Schreck, et al. (2002). These authors started with a spherical condensate containing $\sim 20\,000$ atoms of lithium (isotope 7, i.e. a boson). These atoms were trapped at the intersection of two focused laser beams, and the scattering length a was positive, of the order of 2 nanometers (figure I.5).

One of the two light beams is then slowly extinguished (200 ms), preparing the atoms in a quasi-1D geometry, and the scattering length a is changed by a Fano-Feshbach resonance (see lecture series 2020-21) to a final value that is zero or negative. The cloud of atoms is then allowed to

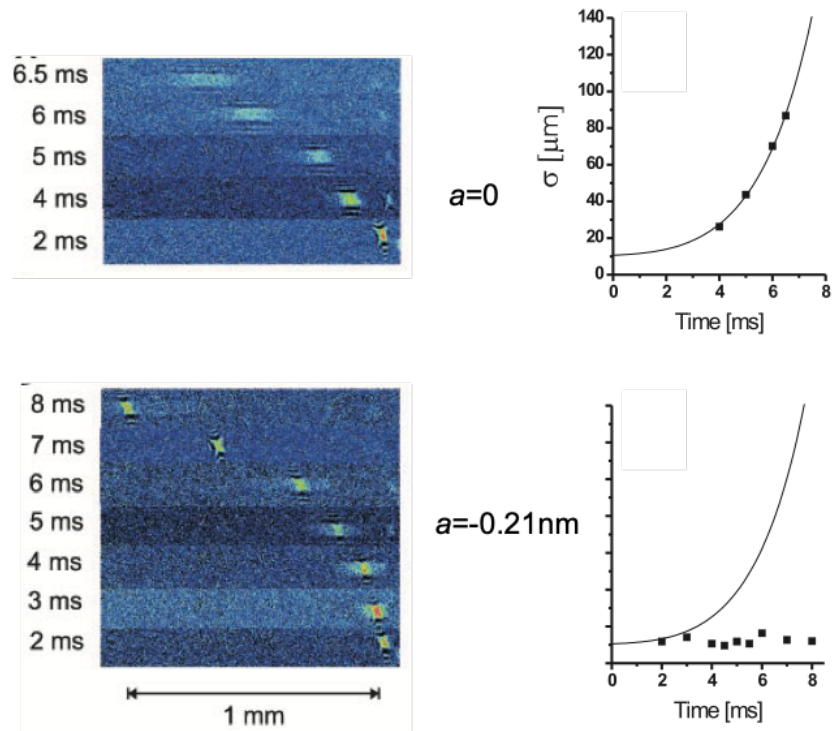


Figure I.6. Evolution of a cloud of atoms in the horizontal laser beam of figure I.5, with the vertical beam switched off. The top line is obtained with a zero scattering length (perfect gas), and the atom cloud is seen to spread out (σ represents the width of the cloud). The bottom line is obtained with a negative scattering length and corresponds to a soliton of around 6000 atoms. There is no detectable spreading. The acceleration observed in both cases is due to an expelling force exerted by a residual magnetic field gradient. Figure taken from Khaykovich, Schreck, et al. (2002).

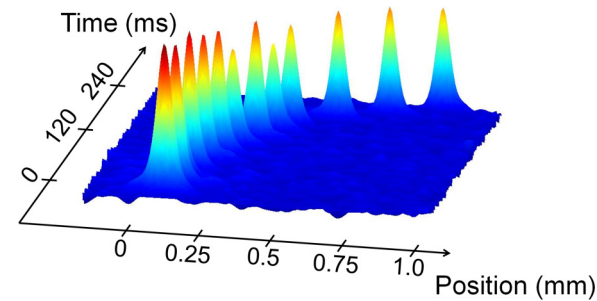


Figure I.7. Evolution of a soliton from $N = 4500$ to 6000 atoms of ^{39}K with $a = -1.5 a_0$ where a_0 is the Bohr radius. The soliton is stable as long as $a > -2.15 a_0$, above which the one-dimensional approach ceases to be valid (see §2-4). Figure taken from Lepoutre, Fouché, et al. (2016).

evolve in this configuration for an adjustable time, before its size is measured.

If the final scattering length is zero, the atom cloud behaves like a perfect gas, and we therefore expect it to spread out because of its initial kinetic energy. This is indeed what is observed in figure I.6, top. On the other hand, for a negative scattering length, we observe a cloud that remains constant in size: this is the soliton we are looking for. The number of atoms in the soliton is $N \approx 6000$.

In the Khaykovich, Schreck, et al. (2002) experiment, the atoms making up the soliton are subjected to a force from a magnetic field gradient, which accelerates the soliton. The authors checked that the soliton trajectory was identical to that of a material point of the same mass and subjected to the same force. A similar experiment was carried out by Lepoutre, Fouché, et al. (2016), from which we have extracted figure I.7. It shows a soliton formed by 6000 ^{39}K atoms evolving in a light trap providing strong radial confinement, with longitudinal acceleration.

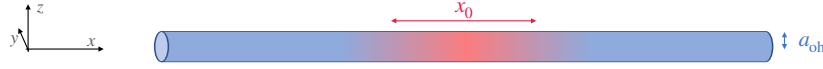


Figure I.8. Quasi-1D gas of x axis obtained by strong confinement in the y and z directions.

2-4 The validity of the one-dimensional approach

The solitons we have just described are actually formed in our usual three-dimensional space. In this section, we will briefly revisit the 3D description of a Bose gas and explain under which conditions the 1D approach developed above is valid.

For a stationary Bose–Einstein condensate confined in a potential $V(\mathbf{r})$ and described by the mean-field approach, the Gross–Pitaevskii energy functional is written:

$$E^{(3D)}[\Psi] = \int \left[\frac{\hbar^2}{2m} |\nabla \Psi|^2 + V(\mathbf{r}) |\Psi(\mathbf{r})|^2 + \frac{1}{2} g^{(3D)} |\Psi(\mathbf{r})|^4 \right] d^3r \quad (\text{I.43})$$

where the interaction constant $g^{(3D)}$ is related to the scattering length a characterizing low-energy collisions between two atoms:

$$g^{(3D)} = \frac{4\pi\hbar^2 a}{m}. \quad (\text{I.44})$$

The wave function $\Psi(\mathbf{r})$ is assumed to be normalized by:

$$\int |\Psi(\mathbf{r})|^2 d^3r = N. \quad (\text{I.45})$$

To obtain an effectively one-dimensional system along the x axis, we apply a strongly confining potential in the two orthogonal directions y and z (figure I.8). As an example, let us take a harmonic potential:

$$V(\mathbf{r}) = \frac{1}{2} m\omega^2 (y^2 + z^2) \quad (\text{I.46})$$

whose energy levels are $E_n = (n + 1)\hbar\omega$, $n \in \mathbb{N}$. We assume that the interaction energy between atoms is low enough for the gas wave function

to be written to a good approximation

$$\Psi(\mathbf{r}) = \chi_0(y, z) \psi(x) \quad (\text{I.47})$$

where χ_0 is the single-particle ground state of motion in the xy plane normalized to 1, i.e. the Gaussian

$$\chi_0(y, z) = \frac{e^{-(y^2+z^2)/2a_{\text{oh}}^2}}{a_{\text{oh}}\sqrt{\pi}} \quad \text{with} \quad a_{\text{oh}} = \sqrt{\frac{\hbar}{m\omega}}. \quad (\text{I.48})$$

We can then simply transfer the ansatz (I.47) into the 3D energy functional written in (I.43) to arrive at

$$E^{(3D)}[\Psi] = \hbar\omega + E^{(1D)}[\psi] \quad (\text{I.49})$$

with the link between the 1D and 3D coupling constants given by

$$g = g^{(3D)} \int |\chi_0(y, z)|^4 dy dz = 2\hbar\omega a. \quad (\text{I.50})$$

This result calls for several comments:

- The use of the relation (I.44) linking $g^{(3D)}$ to the scattering length a assumes that collisions retain their three-dimensional nature despite confinement along the y and z directions. This assumption is only correct if the extension a_{oh} of the ground state along these directions is much greater than the scattering length itself (or its absolute value), which imposes:

$$|a| \ll a_{\text{oh}}. \quad (\text{I.51})$$

When this condition is not satisfied, the collision process must be described by explicitly taking into account the transverse confinement potential $V(\mathbf{r})$ (Olshanii 1998).

- For the frozen transverse motion approximation to be correct, the energies involved in forming the soliton must be small compared with the quantum $\hbar\omega$. Otherwise, it is likely that a correct description of the atomic motion will have to take into account the excited levels in the potential $V(y, z)$. A necessary condition is therefore

$$|\mu| \ll \hbar\omega \quad \Rightarrow \quad N \ll \frac{a_{\text{oh}}}{|a|} \quad (\text{I.52})$$

which limits the number of atoms in the soliton.

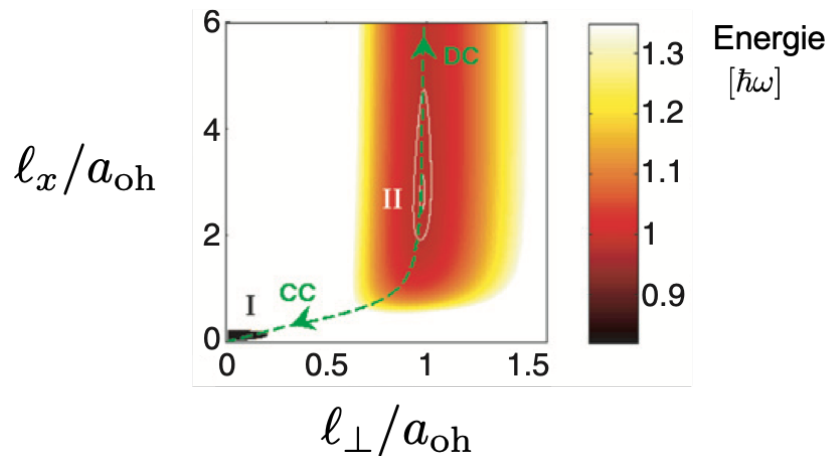


Figure I.9. Energy landscape of a soliton in a transverse harmonic trap as a function of longitudinal ℓ_x and transverse ℓ_\perp sizes, obtained by a variational ansatz for the 3D energy functional of equation (I.43). The soliton represents a metastable state, with the minimum energy state ($E \rightarrow -\infty$) corresponding to $\ell_x, \ell_\perp \rightarrow 0$. The abbreviations "cc" and "dc" stand for "collapse channel" and "dispersive channel". Figure adapted from Parker, Cornish, et al. (2007).

- The soliton we have constructed is an essentially one-dimensional object, with extension x_0 along the x axis. For this construction to be valid, its transverse size in the y and z directions must be very small compared with x_0 , which imposes:

$$a_{\text{oh}} \ll x_0 \quad \Rightarrow \quad N \ll \frac{a_{\text{oh}}}{|a|}. \quad (\text{I.53})$$

We recover the validity condition (I.52).

- Finally, it is important to note that we are interested here in the attractive case $g < 0$, i.e. a negative scattering length a according to (I.50), which poses a problem of principle: A 3D gas of bosons with a negative scattering length tends to implode on itself. This result is easy to understand: if we assume that the N particles occupy a ball of radius

R , the (negative) interaction energy varies as follows

$$E_{\text{int}} \propto -|a| \frac{N^2}{R^3} \quad (\text{I.54})$$

which tends to minimize R . The kinetic energy cost resulting from this confinement varies as follows

$$E_{\text{kin}} \propto \frac{N}{R^2} \quad (\text{I.55})$$

and it is not enough to compensate for this tendency to collapse when $R \rightarrow 0$. It follows that an attractive 1D gas is not actually a stable system, but only metastable, i.e. a local minimum for the 3D energy functional.

Carr & Castin (2002) studied this problem using a variational approach and showed that this local minimum is indeed present when the validity condition (I.52) is satisfied. The result of a similar analysis by Parker, Cornish, et al. (2007) is shown in figure I.9. A numerical study of the energy landscape carried out by these authors shows that the local minimum corresponding to the soliton exists only if

$$\frac{N|a|}{a_{\text{oh}}} < 0.675 (\pm 0.005). \quad (\text{I.56})$$

See also the articles by Perez-Garcia, Michinel, et al. (1998) and Gammal, Frederico, et al. (2001) on the analysis of this problem.

In conclusion, solitons obtained in a quasi-one-dimensional gas with a negative scattering length are metastable objects. They are all the more robust as the above inequalities are well verified, but it will still be possible to lower the gas energy (towards $-\infty$ in the mean-field approximation) by making a cloud of size $\ll a_{\text{oh}}$ in all three directions of space.

3 Beyond the stationary soliton

The stationary soliton found in the first part of this chapter represents the lowest-energy state of the system, at least when limited to strictly 1D motion. We now turn our attention to states of higher energy than this ground

state, in which several solitons may co-exist, or other states, corresponding to oscillating structures in time or space. In the next chapter, we will look at other complex structures (high-order solitons), resulting from the integrability of the problem considered here.

3-1 Soliton collisions

A remarkable property of bright solitons is that they emerge intact from a collision between them. This property was discovered for the Korteweg–de Vries equation by Zabusky & Kruskal (1965). We will see in the next chapter that it can be explained by the integrable nature of the nonlinear Schrödinger equation, and is a direct consequence of the IST approach (*Inverse Scattering Transform*). This property is illustrated in figures I.10 and I.11. The former shows a collision between solitons of the same mass, and the latter a collision between solitons of different masses.

This fundamental characteristic of a system described by an integrable nonlinear equation has been observed experimentally in many systems, notably in hydrodynamics and optics [see, for example, Mitschke & Mollenauer (1987) for the first demonstration in an optical fiber]. It can also be shown that, although the solitons emerge from the collision unchanged, there is an effective interaction between them, resulting from the interference between the two wave packets, the attractive or repulsive nature of which depends on their relative phase (Gordon 1983): two solitons of the same phase attract each other, while two solitons whose phases differ by π repel each other (see figure I.10). Figure I.12, taken from Copie, Suret, et al. (2023), illustrates this phase sensitivity for the collision of two solitons propagating in an optical fiber.

For matter waves, Nguyen, Dyke, et al. (2014) have provided an elegant illustration of this collisional property using ^7Li atoms. The principle of the experiment is described on the left of figure I.13:

- A stable condensate is formed in an elongated harmonic trap by choosing a positive scattering length ($a = +140 a_0$).
- A potential barrier formed by a focused laser beam is switched on around the center of the trap, cutting the cloud in two parts.

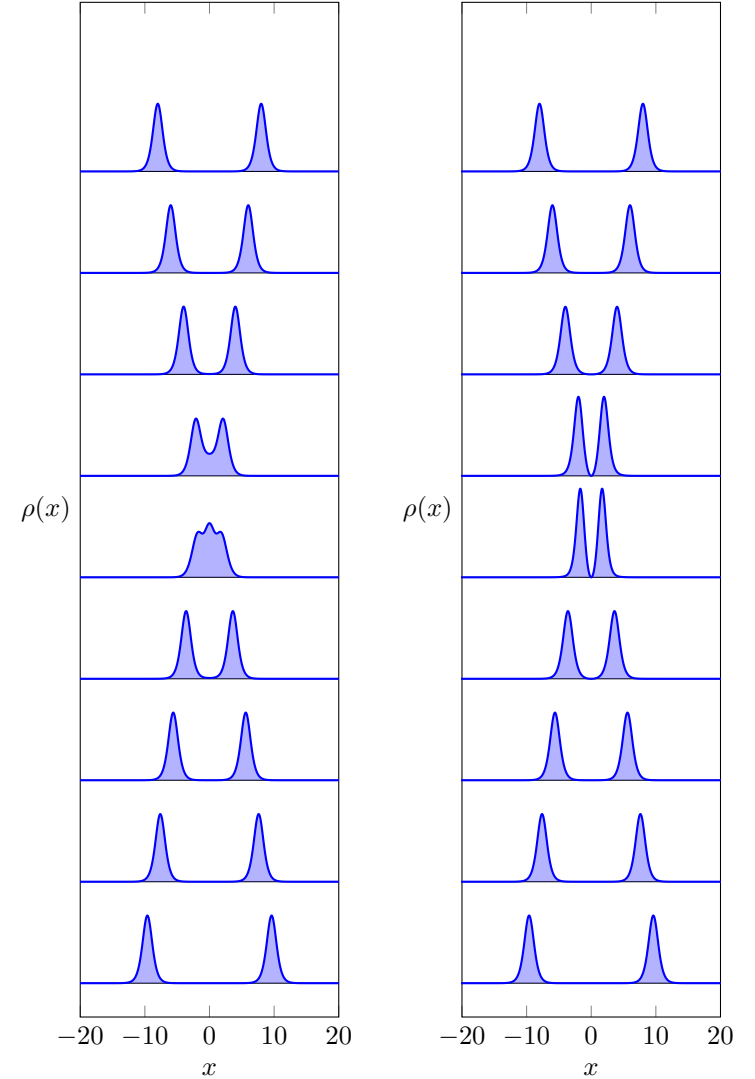


Figure I.10. Numerical solution of the nonlinear Schrödinger equation (I.14) for an initial condition involving two solitons of opposite velocities, same mass ($\kappa = 1$ in (I.25)), and equal phases (left) or phases differing by π (right).

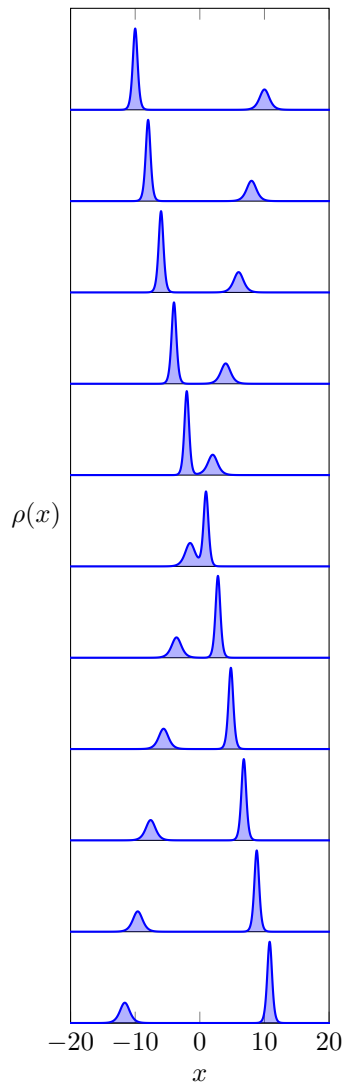


Figure I.11. Numerical solution of the nonlinear Schrödinger equation (I.14) for an initial condition with two solitons of opposite velocities and different masses, corresponding to $\kappa = 1$ and $\kappa = 4$ in (I.25).

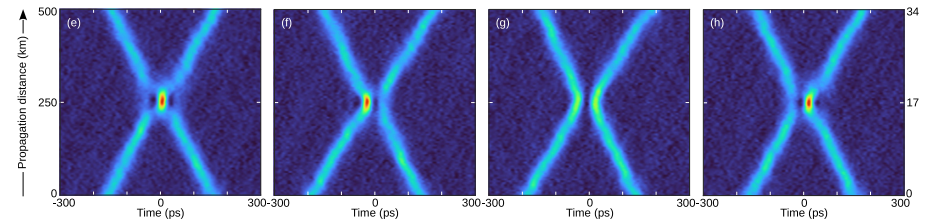


Figure I.12. Collision of two solitons propagating in an optical fiber. Tracking the collision is made possible by a recirculation loop that provides a "stroboscopic" view of the solitons' propagation. The relative velocity of the solitons is adjusted using electro-optical amplitude and phase modulators to control the group velocity of each soliton. Each sub-figure corresponds to a given value of relative phase. For these fiber-optic experiments, time and space play opposite roles to the case of quantum gases. Figure taken from Copie, Suret, et al. (2023).

- The scattering length is brought to a negative value $a = -0.57 a_0$ to transform these two clouds of atoms into bright solitons.
- The barrier is released and the solitons move towards the center of the trap, where they collide.

Nguyen, Dyke, et al. (2014) use an imaging system based on phase contrast, enabling them to take several images of the same cloud. This is important because the relative phase of the solitons fluctuates from one realization to the next, so not all images of the collision are identical. The two sequences shown in figure I.13 correspond to a phase close to 0 for one and close to π for the other.

3-2 Kuznetsov-Ma structure

The bright soliton we studied in § 1 is a stationary solution of the nonlinear Schrödinger equation. Non-stationary solutions are of course possible, but it is generally difficult to provide analytical forms for them.

There are, however, relatively simple expressions corresponding to localized structures in time and/or space (*breathers*). We will not go into de-

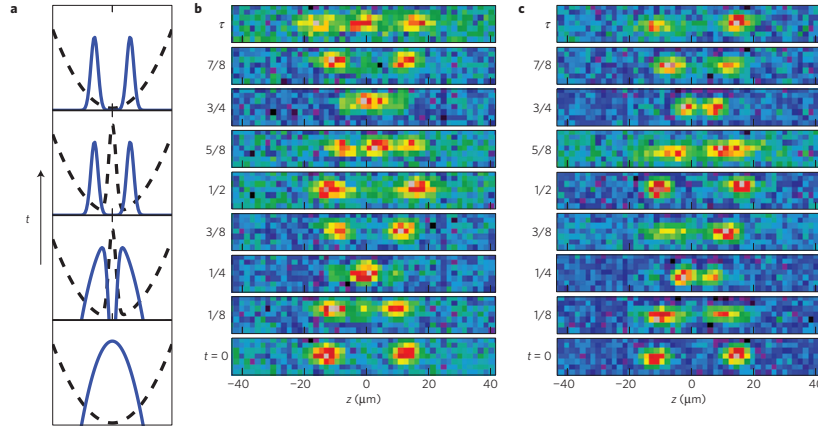


Figure I.13. Left: preparation sequence for a pair of solitons (read from bottom to top). Middle and right: two different realizations of a collision between solitons oscillating in a harmonic trap, obtained using phase-contrast imaging. They correspond to a relative phase of 0 (middle) and π (right). Figure taken from Nguyen, Dyke, et al. (2014).

tail on all of them here, but we will focus on the Kuznetsov-Ma "breathing structure" (Kuznetsov 1977; Ma 1979). We refer readers interested in a general discussion of these structures to the recent articles by Dudley, Genty, et al. (2019), Akhmediev (2021) and Karjanto (2021).

The Kuznetsov-Ma solution centered at $x = 0$ is written for the dimensionless version of the nonlinear Schrödinger equation¹ :

$$\psi_\nu(x, t) = \left[\frac{\nu^2 \cos(\rho t) + i\rho \sin(\rho t)}{2 \cos(\rho t) - \frac{\rho}{\nu} \cosh(\nu x)} + 1 \right] e^{2it} \quad (\text{I.57})$$

with $\rho = \nu\sqrt{4 + \nu^2}$ and with a possible offset in time ($t \rightarrow t - t_0$) and space ($x \rightarrow x - x_0$). The result, plotted in figure I.14 for $\nu = 0.3$, is spectacular: for $\nu \ll 1$, the spatial density is almost uniform and very close to 1 most of the time, but it periodically takes on a value close to 9 in $x = 0$.

¹In practice, the study of this type of solution can be made difficult by the modulational instability studied in §4-2, which develops from noise on the preparation of the initial state.

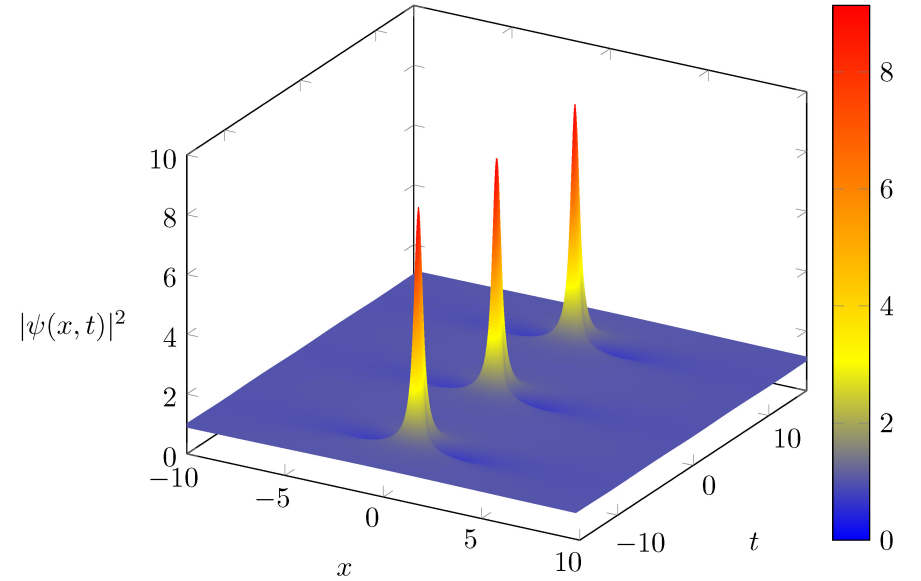


Figure I.14. "Breathing structure" of Kuznetsov-Ma, whose analytical formula is given in (I.57), plotted here for $\nu = 0.3$.

This possibility of seeing successive appearances of density peaks much larger than the mean value of this density constitutes a prototype of a *rogue wave*, i.e. an event *a priori* very unlikely within the framework of a linear analysis, but made more frequent by the nonlinearity of the problem (Shrira & Geogjaev 2010). We will come back to these rogue waves in section §4-4.

Akhmediev structure. There is also an analytical expression for a structure that is only significant around a given time (here $t = 0$) and spatially periodic:

$$\psi_\nu(x, t) = \left[\frac{\nu^2 \cosh(\sigma t) + i\sigma \sinh(\sigma t)}{2 \cosh(\sigma t) - \frac{\sigma}{\nu} \cos(\nu x)} - 1 \right] e^{2it} \quad (\text{I.58})$$

with $\sigma = \nu\sqrt{4 - \nu^2}$. The Kuznetsov-Ma and Akhmediev structures were experimentally realized on light pulses propagating in an optical fiber by

Kibler, Fatome, et al. (2012).

3-3 The Peregrine breather

It is interesting to consider the limiting case of the Kuznetsov-Ma structure when $\nu \rightarrow 0$ [see Karjanto (2021) for a precise definition of this limit]. We then find the structure proposed by Peregrine (1983):

$$\psi(x, t) = \left[1 - \frac{4(1 + 4it)}{1 + 4x^2 + 16t^2} \right] e^{2it} \quad (I.59)$$

The $\mu \rightarrow 0$ limit has the effect of making the period of the recurrence of the central peak tend towards infinity, so that all that remains is the emergence of a single peak at $t = 0$. When $t \rightarrow \pm\infty$, the wave function $\psi(x, t)$ is virtually flat and equal to 1 at every point in space, apart from one global phase. However, in the vicinity of time $t = 0$, it is strongly peaked in $x = 0$, with the value $\psi(0, 0) = -3$. The density at $x = 0$ and $t = 0$ is therefore 9 times greater than the quasi-uniform density at long times.

Observation of the Peregrine structure. The Peregrine structure was observed in an optical fiber by Kibler, Fatome, et al. (2010). Here we describe a very recent achievement in a cold atomic gas by Romero-Ros, Katsimiga, et al. (2024). The experiment was carried out on a gas of $N \approx 130\,000$ ^{87}Rb atoms confined in a highly elongated trap (frequencies $2.5 \times 250 \times 250$ Hz), with an effective scattering length set to the negative value $a = -2.41 a_0$ at time $t = 0$ (we will come back to the method used to obtain a negative scattering length for rubidium atoms in a moment). To initiate the formation of the Peregrine structure, an auxiliary light beam is focused in the vicinity of $x = 0$, where it creates a Gaussian-shaped potential well. At time $t = 0$ (figure I.16 a), there is a slight density surplus around this point.

The presence of this slight initial density bump is sufficient to generate a much more significant local density maximum at a later instant, of the order of 65 ms in the experiment (figure I.16). After this instant, the density hump becomes much less significant. At long times, the profile measured or calculated from this initial condition differs markedly from that of the Peregrine structure, with three similar density maxima around $t \sim 90$ ms (figure I.17).

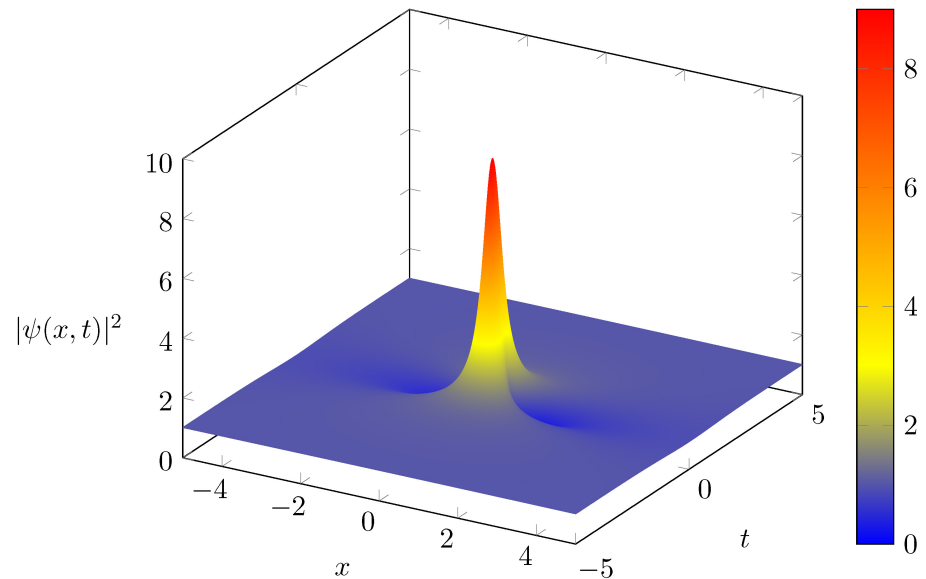


Figure I.15. Peregrine breather, whose analytical formula is given in (I.59).

How to get $a < 0$ with ^{87}Rb atoms? For a pair of rubidium atoms prepared in a given Zeeman sub-level j of the ground electronic level, the scattering length a_{jj} is always positive and of the order of $100 a_0$. However, if we start with a bath of atoms prepared in one sublevel j and transfer a small proportion of the atoms to another sublevel i , these atoms will evolve under the effect:

- $i - i$ interactions characterized by the scattering length a_{ii} ;
- interactions mediated by the much denser bath, which can under certain conditions be modeled by the scattering length $-a_{ij}^2/a_{jj}$.

Interactions between atoms in state i are then described by the effective scattering length

$$a_{ii}^{\text{eff}} = a_{ii} - \frac{a_{ij}^2}{a_{jj}} \quad (I.60)$$

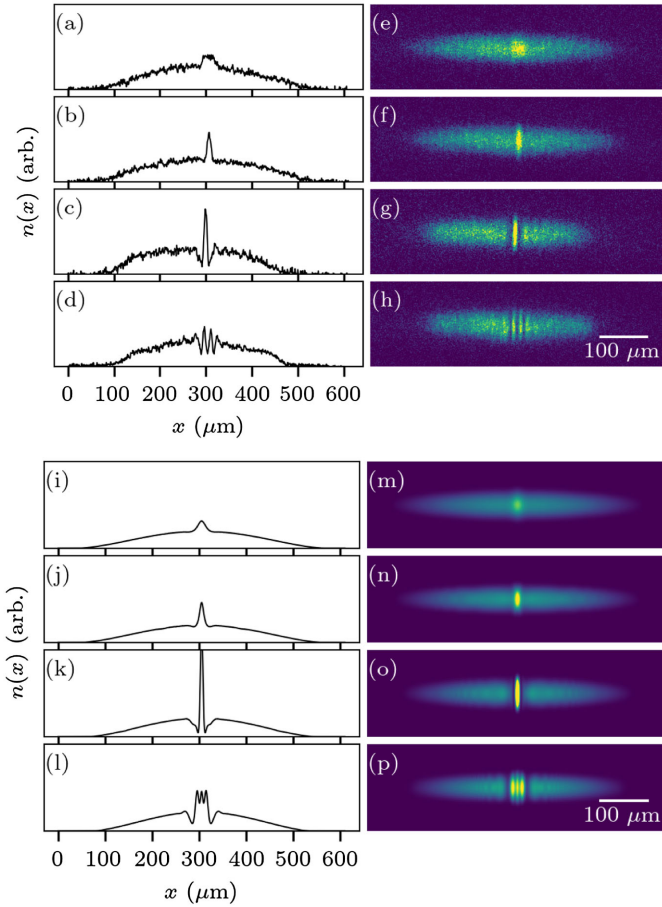


Figure I.16. Observation of a structure close to the Peregrine breather in a 1D condensate. The series of images correspond to times $t = 10, 30, 65, 85$ ms after the switch to a negative effective scattering length. Top series: experimental results, bottom series: 3D simulation of the experiment. Figure taken from Romero-Ros, Katsimiga, et al. (2024).

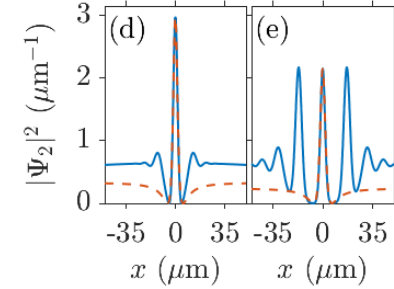


Figure I.17. Comparison between the Peregrine breather profile (red dotted line) and the density profile calculated under experimental conditions (blue solid line) for $t = 33.6$ ms (left) and $t = 94.9$ ms (right). Figure taken from Romero-Ros, Katsimiga, et al. (2024).

which is much smaller than each of the initial scattering lengths (since they are all neighbors) and can be negative for a suitable choice of the i and j sublevels (Bakkali-Hassani, Maury, et al. 2021; Bakkali-Hassani, Maury, et al. 2023). This approach was used in the experiment by Romero-Ros, Katsimiga, et al. (2024).

4 Dynamic instability and soliton train

In most experiments on bright solitons performed with atomic gases, the starting point is not a small spherical cloud, as in the experiment of Khaykovich, Schreck, et al. (2002) described above, but a very elongated cloud. This cloud is prepared in the positive scattering length regime, and the scattering length is suddenly brought to a negative value. One then observes the formation of a train of solitons, as a result of a modulational instability.

We will describe this observation of a soliton train in §4-3. Before that, we will look at the nature of this modulational instability, which was first described in a hydrodynamic context by Benjamin & Feir (1967). We will recover it from Bogoliubov dispersion relation, which characterizes the dynamics of a condensate subjected to small initial perturbations.

4-1 The speed of sound in a uniform condensate

Let us first consider a condensate of uniform density ρ_0 and determine the value of the speed of sound in this medium. As this problem has been dealt with in detail in previous lecture series (see, for example, the 2016 course, Chapter III, and the 2024 course, Chapter III), we will confine ourselves here to its simplest version; we will not therefore discuss the different regimes that may appear in addition to the phonons we are interested in here.

The dynamics of the condensate is described by the Gross–Pitaevskii equation

$$i\hbar\partial_t\psi = -\frac{\hbar^2}{2m}\partial_x^2\psi + g|\psi|^2\psi \quad (\text{I.61})$$

where $\psi(x, t)$ is a complex wave function. For $g > 0$, the minimum-energy state of the condensate corresponds to

$$\psi(x, t) = \sqrt{\rho_0} e^{-i\mu t/\hbar} \quad \text{with} \quad \mu = g\rho_0. \quad (\text{I.62})$$

The quantity μ represents the chemical potential, i.e. the energy required to add a particle to the system. We characterize the deviation from equilibrium by two complex numbers U and V , and the parameter ϵ assumed to be small in front of 1:

$$\psi(x, t) = \sqrt{\rho_0} \left\{ 1 + \epsilon \left[U e^{i(kx - \omega t)} + V^* e^{-i(kx - \omega^* t)} \right] \right\} e^{-i\mu t/\hbar}. \quad (\text{I.63})$$

It is necessary to introduce simultaneously these two numbers U and V , amplitudes of the two plane waves of wave number $\pm k$ and frequency $+\omega$ and $-\omega^*$, because of the simultaneous presence of ψ and ψ^* in the evolution equation (I.61).

Let us look for the dispersion relation between k and ω . When we transfer the form (I.63) into (I.61), we find at order zero in ϵ the relationship (I.62) between μ and ρ_0 . At order 1 in ϵ , we find the system

$$\begin{cases} (g\rho_0 + \epsilon_k - \hbar\omega)U + g\rho_0 V & = 0 \\ g\rho_0 U^* + (g\rho_0 + \epsilon_k + \hbar\omega^*)V^* & = 0 \end{cases} \quad (\text{I.64})$$

where we set $\epsilon_k \equiv \hbar^2 k^2 / 2m$ and we used $\mu = g\rho_0$. Let us take the complex conjugate of the second equation; we then obtain a linear system in

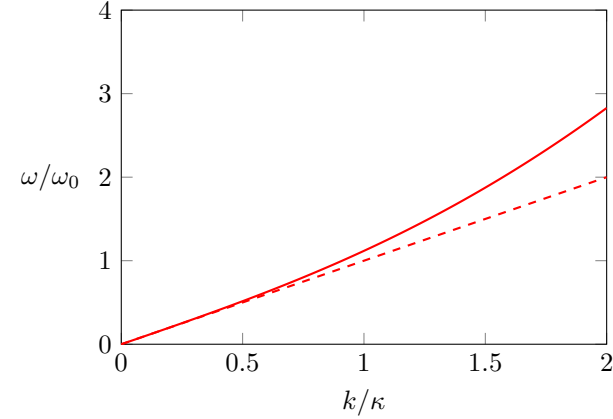


Figure I.18. Bogoliubov dispersion relation (I.66) for $g > 0$. The dotted line corresponds to the phonon limit, with the dispersion relation $\omega = ck$, the speed of sound c being given by $c = \sqrt{g\rho_0/m}$. We define $\hbar^2 \kappa^2 / m = \hbar\omega_0 = g\rho_0$.

(U, V) which admits a non-zero solution if and only if the determinant of the system cancels out:

$$\begin{vmatrix} g\rho_0 + \epsilon_k - \hbar\omega & g\rho_0 \\ g\rho_0 & g\rho_0 + \epsilon_k + \hbar\omega \end{vmatrix} = 0. \quad (\text{I.65})$$

This leads to the Bogoliubov dispersion relation

$$(\hbar\omega)^2 = \epsilon_k^2 + 2\epsilon_k g\rho_0, \quad (\text{I.66})$$

plotted in figure I.18 for $g > 0$ and in figure I.19 for $g < 0$.

For repulsive interactions ($g > 0$), the frequencies ω are all real: a small initial disturbance will propagate without attenuating or amplifying. On the other hand, for attractive interactions ($g < 0$), we find a range of k values for which ω^2 is negative, i.e. pure imaginary ω . This can lead to an exponential increase in the amplitude of the perturbation with time, stemming from the $e^{|\omega|t}$ term: this is the origin of the modulation instability.

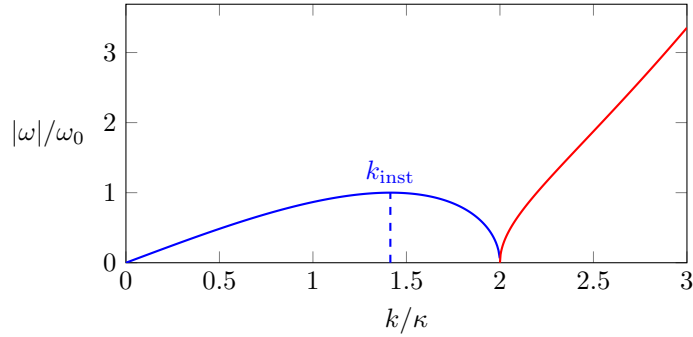


Figure I.19. Bogoliubov dispersion relation (I.66) for $g < 0$. The blue line corresponds to a pure imaginary ω frequency, the red line to real ω . The instability zone extends between $k = 0$ and $k = 2\kappa$, with $\hbar^2 \kappa^2 / m = \hbar \omega_0 = |g| \rho_0$. The point of maximum instability is obtained for $k_{\text{inst}} = \sqrt{2} \kappa$.

4-2 Modulational instability

As we saw in the previous paragraph, an attractive uniform gas ($g < 0$) is unstable with respect to perturbations whose wavenumber k is such that $\epsilon_k - 2|g|\rho < 0$. If noise is initially present at all wavenumbers, the wavenumber leading to the largest value of $|\omega|$ is expected to grow fastest and become dominant after a certain time. This wave number k_0 is such that (see figure I.19):

$$\frac{\hbar^2 k_{\text{inst}}^2}{2m} = |g| \rho_0 \quad k_{\text{inst}} = \frac{2\sqrt{|a|\rho_0}}{a_{\text{oh}}} \quad (\text{I.67})$$

where we used the relationship between g and the 3D scattering length given in (I.50).

The initially quasi-uniform gas will then break up into approximately evenly-spaced particle packets with spatial period $\ell_{\text{inst}} = 2\pi/k_{\text{inst}}$. The characteristic time for this instability to develop is $1/|\omega(k_{\text{inst}})| = \hbar/|g|\rho_0$. Each packet contains approximately $N_a = \rho_0 \ell_{\text{inst}}$ atoms, which gives using

(I.67):

$$N_a = \pi \sqrt{\frac{\rho_0 a_{\text{oh}}^2}{|a|}}. \quad (\text{I.68})$$

Each cluster of atoms will form a soliton, at least if the metastability condition with respect to 3D collapse (I.56) is met. The peak density ρ_{peak} of each soliton (once a stationary regime has been reached) can be deduced from the study carried out in §1-3 and we find $\rho_{\text{peak}} = \rho_0 \pi^2 / 2$. Given the result obtained above for N_a , the metastability condition is written:

$$\frac{N_a |a|}{a_{\text{oh}}} \lesssim 0.7 \quad \Rightarrow \quad \rho_0 |a| \lesssim 0.05. \quad (\text{I.69})$$

For a gas with a given initial density ρ_0 , prepared with a positive scattering length, this condition limits the exploitable range for the transition to negative scattering lengths. A more detailed theoretical study of modulational instability in quasi-1D atomic gases can be found in Salasnich, Parola, et al. (2003) and Carr & Brand (2004).

4-3 Observation of a soliton train

The splitting of a gas of 1D bosons with a negative scattering length was observed in the early 2000's in Hulet's group in Houston, then in Wieman's group in Boulder. This type of experiment has been taken up more recently by several teams, the Houston team first (Nguyen, Luo, et al. 2017), then by Everitt, Sooriyabandara, et al. (2017) and Mežnaršič, Arh, et al. (2019).

We show in figure I.20 the result obtained by Nguyen, Luo, et al. (2017) on a gas of ^7Li atoms prepared in an elongated trap ($7 \times 350 \times 350$ Hz). The gas is first prepared with a positive scattering length ($+3 a_0$) before being switched to the negative value $a = -0.18 a_0$ by a ramp lasting 1 ms. This group uses a phase-contrast optical detection method, which enables several successive images to be taken of a sample without destroying it (see also figure I.13). During the time explored in this figure (20 ms), the total number of atoms is virtually constant (8×10^5). The number of solitons formed, $N_s \sim 12$, is in excellent agreement with the estimate obtained from the total length of the condensate and the spatial period ℓ_0 expected for the modulational instability.

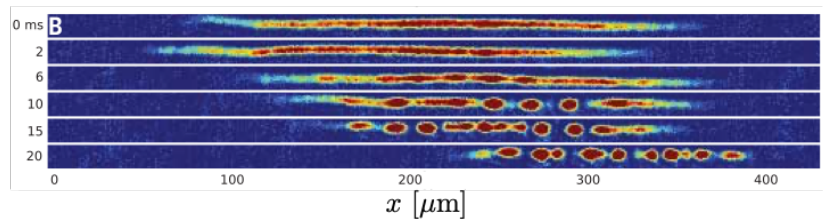


Figure I.20. Formation of a soliton train in a 1D condensate of ${}^7\text{Li}$ when the scattering length is brought to the negative value $a = -0.18 a_0$. Figure taken from Nguyen, Luo, et al. (2017).

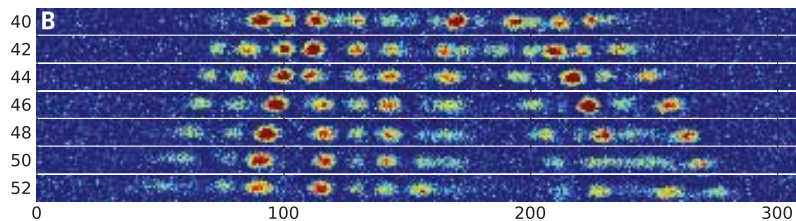


Figure I.21. Evolution of a train of solitons under the effect of the trap's axial confinement potential (breathing mode). The relative motion of the solitons indicates a repulsive interaction between them. Figure taken from Nguyen, Luo, et al. (2017).

Nguyen, Luo, et al. (2017) indicate that the onset of the instability is due to noise present in the initial cloud, which may be of thermal or quantum origin. This conclusion is based on the fact that the instability first starts in the center of the gas, where the density $\rho(x)$ and therefore the imaginary part of the frequency $|\omega|$ are greatest.

Phase contrast imaging enables one to follow a given soliton train over a wide time range. In this way, one can observe a breathing mode of the soliton train in the axial harmonic potential. The fact that the solitons remain relatively well separated from each other during this oscillation indicates that two neighboring solitons interact repulsively, i.e. they have a phase difference close to π . This phase distribution between adjacent solitons emerges spontaneously from the development of modulational instability,

as shown numerically by Salasnich, Parola, et al. (2003).

4-4 A soliton gas

The notion of soliton gas was introduced to describe the behavior of a dilute assembly of bright solitons propagating in both directions of an infinite line. A detailed review of the history of this concept and its connection with *integrable turbulence* is presented in the recent review article by Suret, Randoux, et al. (2024). Since this notion has not yet been implemented with matter waves², we will limit ourselves here to the description of numerical and observational work on light propagation in an optical fiber. This work in optics is particularly important because its results can be directly mapped onto observations of waves on the ocean surface, in particular of *rogue waves* (Dudley, Genty, et al. 2019).

We will be relying here on two papers by Soto-Crespo, Devine, et al. (2016) and Akhmediev, Soto-Crespo, et al. (2016). These authors have solved the dimensionless nonlinear Schrödinger equation (I.14) with an initial condition of the form

$$u(x, 0) = \frac{1}{\sqrt{Q}} [1 + \mu f(x)] \quad (\text{I.70})$$

where $f(x)$ is a complex function, whose real and imaginary parts are independent random functions of zero mean value and variance 1, generated from Gaussian distributions of equal correlation length L_c . The normalization factor Q is adapted so that the spatial mean value of $\rho(x, 0) = |u(x, 0)|^2$ remains equal to 1 for different choices of parameters μ and L_c . For each choice of parameters, we calculate the quantity $\sigma^2 = \langle \rho^2 \rangle - \langle \rho \rangle^2$ for the incident field.

The authors solve the nonlinear Schrödinger equation (I.14) to obtain $u(x, t)$ and study the probability distribution function (PDF) for the density $\rho(x, t)$. They give their results for three values of σ : 0.1, 0.5, 0.9, the calculations being made with $L_c = 0.76$. This distribution first evolves and then stabilizes after a time $t \gtrsim 20$. Figure I.22 shows the result obtained for $t = 100$. For the smallest value of σ , we find to a good approximation the

²see nevertheless the recent work of Sivovitz, Lannig, et al. (2023) and Mossman, Katsimiga, et al. (2024) on multicomponent condensates.

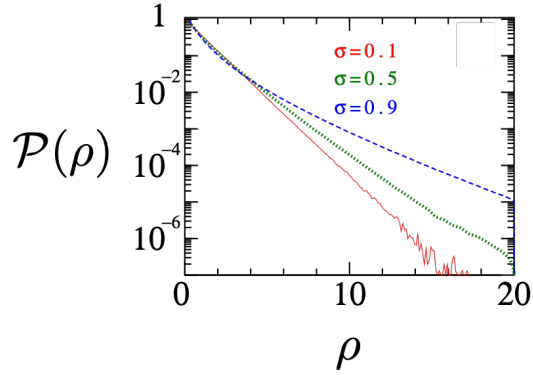


Figure I.22. Distribution law of the density $\rho(x)$ at a given instant ($t = 100$) for the three noises considered for the incident field. Figure taken from Soto-Crespo, Devine, et al. (2016).

exponential law for the density ρ [i.e. a Rayleigh statistic for the amplitude $|u|$] (Bromberg & Cao 2014):

$$P(\rho, 0) = e^{-\rho} \quad (\text{I.71})$$

characteristic of a Gaussian field, as is the case with speckle in optics, for example. On the other hand, as σ increases, large deviations become much more important. For example for $\sigma = 0.9$, the probability of finding $\rho = 16$ at a point is 500 times greater than the value given by the exponential law, while the mean $\langle \rho \rangle = 1$ remains unchanged by construction. This is a signature of the existence of rogue waves, which occur with a much greater probability than might be assumed from the simple exponential law (I.71).

In the regime of strong fluctuations, the plot of the density versus time reveals the predominant role of solitons with significant velocities, incessantly colliding with each other (figure I.23, right). On the other hand, for weak fluctuations (figure I.23, left), Soto-Crespo, Devine, et al. (2016) show that the dynamics is dominated by near-zero velocity solitons or quasi-immobile structures of the *breather* type (Peregrine or Akhmediev), generated from the modulational instability described above. See recent articles by Gelash, Agafontsev, et al. (2019) and Congy, El, et al. (2024) for a discussion of the link between these "integrable turbulence" dynamics and

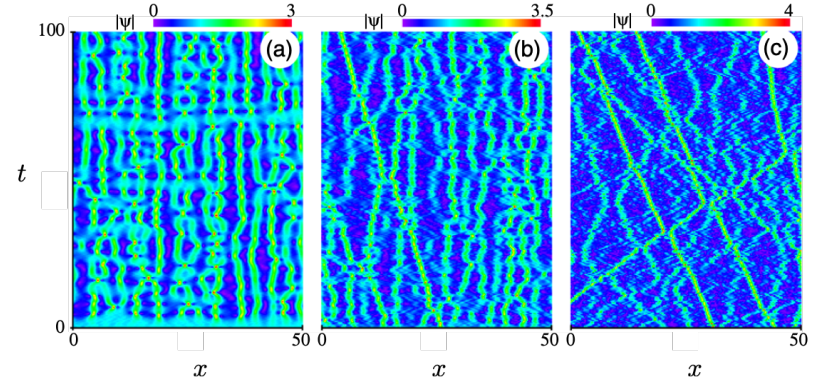


Figure I.23. Variations of $|u(x, t)|$ for the three values of σ considered in figure I.22. Figure taken from Soto-Crespo, Devine, et al. (2016).

the spectrum obtained from the IST method (*Inverse Scattering Transform*), which we will present in the next chapter.

The study of light propagation in an optical fiber has revealed a phenomenology very similar to that just described. Since Solli, Ropers, et al. (2007)'s initial observation, a great deal of work has been carried out on rogue waves in optics and hydrodynamics, and we refer interested readers to Dudley, Genty, et al. (2019)'s review article. In figure I.24 we show the comparison between the intensity distribution of a random light field before and after traversing a nonlinear optical fiber (Walczak, Randoux, et al. 2015). This clearly shows the emergence of a very wide distribution tail, with a considerably increased probability of extreme events. Shortly afterwards, Suret, Koussaifi, et al. (2016) developed a "time microscope", to analyze the structure of light pulses at the fiber output with 0.25 picosecond resolution, which enabled them to identify the respective roles of solitons and Peregrine-like structures in the emergence of a wide distribution tail [see also Kraych, Agafontsev, et al. (2019) for an experimental study in the regime dominated by modulational instability]. The essential role of non-linearity in the emergence of these rare events was highlighted in a 2D experiment by Safari, Fickler, et al. (2017).

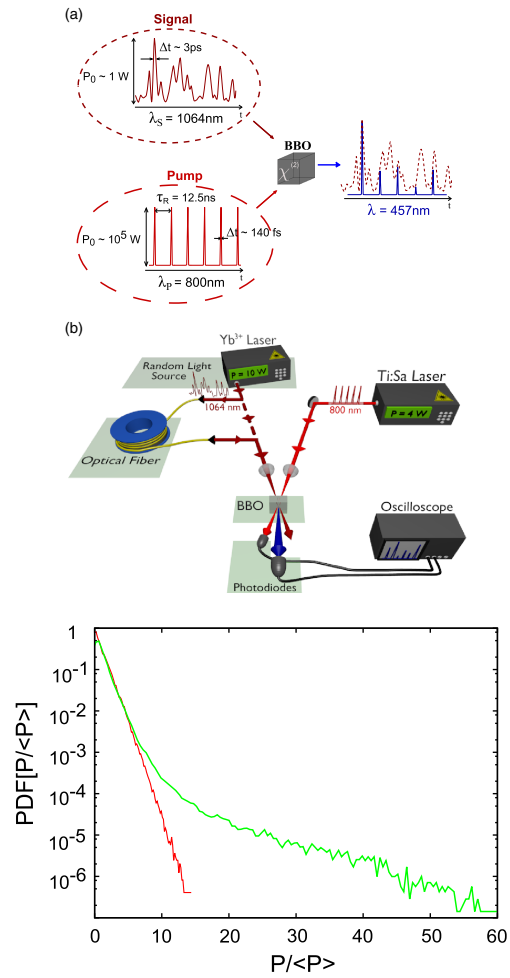


Figure I.24. Top: device for sampling the intensity of a random light field at regular intervals. Bottom: instantaneous power distribution at the input of the nonlinear medium (red) and at the output (green). Figure taken from Walczak, Randoux, et al. (2015).

Chapter II

Bright soliton dynamics and the IST method

In the previous chapter, we started from the nonlinear Schrödinger equation to obtain the shape of a bright soliton, an object that can be stationary or moving at constant speed. We put the soliton's wave function into the form $\psi(x) = \psi_0 / \cosh(x/2x_0)$, and established the link between the soliton's width x_0 and the number of particles it contains.

We have also shown that solitons are robust objects: two bright solitons emerge intact from a binary collision, whatever their masses and velocities. In this chapter, we continue to explore the robustness of bright solitons. In particular, we will consider imperfect preparation. This may result, for example, from a width ill-suited to its number of atoms, or from an envelope that does not have the canonical $1/\cosh x$ form. We will see that, in these cases, the wave packet evolves by oscillating and ejecting particles, eventually forming a stationary soliton, slightly smaller than the starting object, but which is an exact solution of the nonlinear Schrödinger equation.

This robustness was behind the suggestion to use optical solitons for fiber-optic telecommunications [see Haus & Wong (1996) for a review]. It should be noted, however, that the implementation of this technique eventually came up against practical problems and this route did not meet with the initially expected success (Hasegawa 2022; Dudley, Finot, et al. 2023).

In this chapter, we will first illustrate a few facets of this robustness, before placing it in the general context of integrable systems. To this end, we will introduce the inverse scattering transform (IST) method for the case of the nonlinear Schrödinger equation. We will see that solitons are

associated with very specific eigenvalues of a spectral problem, and that these eigenvalues remain constant over time: the robustness of solitons follows immediately from this.

We conclude this chapter with the study of "multi-solitons", composite solitons formed by the superposition of elementary solitons, which also form stable structures but are less robust than basic solitons, and which have recently been demonstrated with cold atomic gases.

1 Temporal evolution of a soliton

1-1 Eigenmodes of a soliton?

A bright soliton is a stationary wave packet that results from the balance between two opposing phenomena: kinetic energy is minimized by taking the largest possible wave packet; interaction energy, on the other hand, is minimized by taking the most concentrated possible wave packet. If we note ℓ the size of this wave packet, we have for these two contributions (to numerical factors unimportant here):

$$E_{\text{kin}} = N \frac{\hbar^2}{m\ell^2} \quad E_{\text{int}} = -N^2 \frac{|g|}{\ell} \quad (\text{II.1})$$

so that the total energy $E_{\text{kin}} + E_{\text{int}}$ has the shape shown in figure II.1, with a minimum for $\ell = x_0$ with $x_0 \equiv \hbar^2 / (Nm|g|)$, a result we had already found

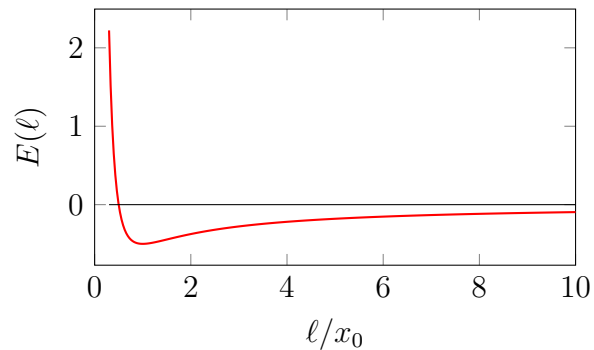


Figure II.1. Variation of total energy with wave packet size.

in the previous chapter.

This figure suggests that if we prepare the wave packet with a size close to x_0 , we will be able to observe small oscillations of the soliton size, which would correspond to a soliton eigenmode. This idea is *stricto sensu* incorrect, as we shall now explain.

To tackle the problem, we can use Bogoliubov's method, which we introduced in the previous chapter to study modulational instability. We are interested in the evolution of a small perturbation of the initial condition ψ_0 by posing

$$\psi(x, t) = \{ \psi_0(x) + \epsilon [U(x)e^{-i\omega t} + V(x)e^{i\omega t}] \} e^{-i\mu t/\hbar}, \quad (\text{II.2})$$

where $\psi_0(x)$ here represents the wave function of the unperturbed soliton, varying as $1/\cosh(x/2x_0)$, with chemical potential $\mu = -mg^2N^2/(8\hbar^2)$. The quantity $\hbar\omega$ represents the energy to be supplied to the soliton to excite the eigenmode in question, the functions $U(x)$ and $V(x)$ characterize the spatial structure of this mode and $\epsilon \ll 1$ is the perturbative development parameter. We inject this expression for $\psi(x, t)$ into the nonlinear Schrödinger equation

$$i\hbar \frac{\partial \psi}{\partial t} = -\frac{\hbar^2}{2m} \frac{\partial^2 \psi}{\partial x^2} + g|\psi|^2\psi \quad (\text{II.3})$$

and we obtain at order 1 in ϵ a linear differential system for the functions

$U(x)$ and $V(x)$:

$$\begin{aligned} (\mu + \hbar\omega) U &= \left[-\frac{\hbar^2}{2m} \partial_x^2 - 2|g|\psi_0^2 \right] U - |g|\psi_0^2 V \\ (\mu - \hbar\omega) V &= \left[-\frac{\hbar^2}{2m} \partial_x^2 - 2|g|\psi_0^2 \right] V - |g|\psi_0^2 U. \end{aligned} \quad (\text{II.4})$$

Solving this system (which we will not do here) shows that all these eigenmodes (except two, see remark below) vary as $e^{\pm ikx}$ for $|x| \rightarrow +\infty$ with $k \in \mathbb{R}$; they are therefore non-localized traveling waves (Kaup 1990; Castin & Herzog 2001). The energy spectrum of these delocalized modes is

$$\hbar\omega = \frac{\hbar^2 k^2}{2m} + |\mu|, \quad (\text{II.5})$$

which means that to excite them, we must first pay the energy $|\mu|$ to extract a particle from the soliton, then the kinetic energy $\hbar^2 k^2/2m$ to set this particle in motion with the momentum $\hbar k$. There is therefore no *discrete* eigenmode, localized in the vicinity of the soliton and with energy $\hbar\omega$ less than $|\mu|$, which would correspond, for example, to an undamped oscillation of the soliton size around its equilibrium value x_0 .

Note 1. There are in fact two localized modes, of frequency $\omega = 0$, which correspond to the fact that we can, without paying energy, change the position or the phase of the soliton. These are the two Goldstone modes that correspond to gauge invariance (for phase) and translational invariance (for position). Their existence in no way invalidates our conclusion on the absence of localized eigenmodes, which would correspond to undamped oscillation of the soliton's width.

Note 2. The absence of other localized modes, corresponding for example to an oscillation of the soliton width, is a consequence of the integrable nature of the nonlinear Schrödinger equation, as we will see in the following sections. If we modify this evolution equation by adding terms that break the integrability, then localized modes may appear, as discussed by Kivshar, Pelinovsky, et al. (1998) and Pelinovsky, Kivshar, et al. (1998).

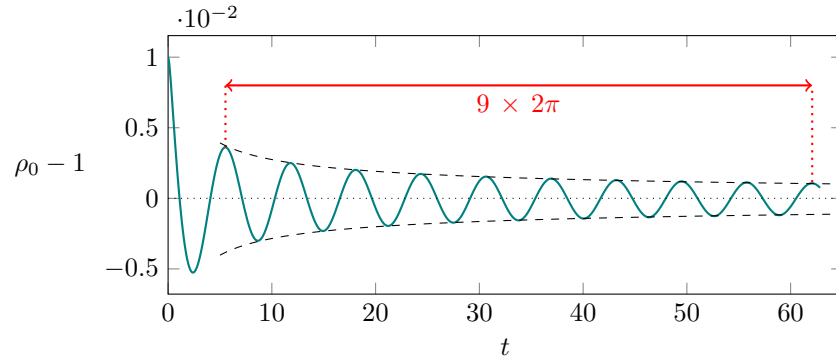


Figure II.2. Damped oscillations of the central density $\rho_0(t) = |u(0,t)|^2$ of a solitonic packet with the initial condition (II.10) for $\epsilon = 0.01$. The dashed black curves correspond to a decay of the oscillation envelope in $1/\sqrt{t}$. Calculated on a box of length 640 with discretization on 32768 points.

1-2 Damped oscillations

The absence of localized eigenmodes does not prevent oscillations of the soliton amplitude and width from being observed for an appreciable period of time. To convince ourselves of this, we can first turn to a numerical simulation. Consider the nonlinear Schrödinger equation in its dimensionless version¹

$$iu_t + u_{xx} + 2|u|^2u = 0 \quad (\text{II.7})$$

a particular soliton of which is given by

$$u(x) = \frac{1}{\cosh x}, \quad (\text{II.8})$$

of mass M and energy E given by

$$M = \int_{-\infty}^{+\infty} |u|^2 dx = 2 \quad E = \int_{-\infty}^{+\infty} (|\partial_x u|^2 - |u|^4) dx = -\frac{2}{3}. \quad (\text{II.9})$$

¹Recall the choice of length and time units that lead to this equation:

$$x_0 = \frac{\hbar^2}{Nm|g|} \quad t_0 = \frac{2mx_0^2}{\hbar}. \quad (\text{II.6})$$

Figure II.2 shows the evolution of the central density associated with the function $u(x,t)$, taking as initial condition

$$u(x,0) = \frac{\sqrt{1+\epsilon}}{\cosh[x(1+\epsilon)]} \quad \text{with } \epsilon \ll 1. \quad (\text{II.10})$$

So we still have a mass $\int |u(x,0)|^2 dx = 2$, but with a central density slightly too large and a width slightly too small (by a factor of $1+\epsilon$) to correspond to the stationary soliton (II.8).

The time evolution of the central density reveals a damped oscillation, with a decay in $1/\sqrt{t}$ and an asymptote very slightly below 1. The fact that the excitation decays irreversibly is characteristic of coupling to a continuum: if we had excited only one discrete mode, the oscillation would occur at the frequency ω of that mode without damping. At long times, we find a stationary soliton, with a mass slightly reduced compared with the initial mass.

The interpretation of the result shown in figure II.2 is straightforward within the framework of Bogoliubov's analysis: non-localized modes are excited by the choice $\epsilon \neq 0$ in (II.10) and the time evolution of these modes corresponds to particle or radiation emission (depending on the nature of the objects – matter or light – that are described). The period of oscillation is, to a good approximation, $2\pi\hbar/\mu$ (2π for these reduced units), which means that it is essentially modes at the bottom of the continuum (II.5) that are excited². On the other hand, we can understand the decay law in $1/\sqrt{t}$ as follows. Let us decompose the initial state $u(x,0)$ onto the final solitonic state, $u_s(x)$, to which is added the small wave packet $\delta u(x,0)$ formed by the Bogoliubov modes. Initially, this wave packet is localized at $u(x,0)$, but we know that it will spread, since the Bogoliubov modes are not bound. Its width will increase linearly with time and its central amplitude will therefore decrease as $1/\sqrt{t}$, since its norm must remain constant over time. The decreasing oscillation of $|u(0,t)|^2$ shown in figure II.2 demonstrates the interference between $u_s(x)$ and $\delta u(0,t)$.

The calculation of the evaporated mass in this particular case is presented by Carr & Castin (2002), who show that it is a term of order 2 in ϵ , so very small in relative value ($\sim 10^{-4}$) for the example in figure II.2. We

²More precisely, it is the final value of the chemical potential that determines the frequency of oscillation, as discussed by Sroyngoen & Anglin (2025).

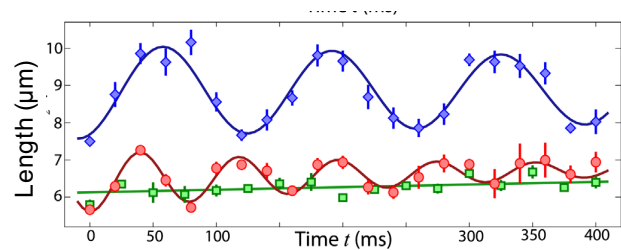


Figure II.3. Oscillations of the length of a cloud of cesium atoms confined in an elongated harmonic trap. Blue dots: standard Bose-Einstein condensate regime (repulsive interactions). The oscillation frequency is equal to $\sim \sqrt{3}$ times the axial confinement frequency. Red dots: solitonic regime (attractive interactions). The damped oscillation corresponds to an "eigenmode" of the soliton and is similar to that shown in figure II.2. The green dots also correspond to the solitonic regime, but the excitation of axial motion is negligible. Figure taken from Di Carli, Colquhoun, et al. (2019).

will see later how the IST method can be used to calculate the mass of the soliton reached at long times, by solving the eigenvalue problem of the Lax operator \hat{L} for the initial condition $u(x, 0)$.

1-3 Experimental study

Di Carli, Colquhoun, et al. (2019) have studied the variation over time of the width of a soliton prepared in a highly elongated harmonic trap (figure II.3). The transverse frequencies of this trap are of the order of 100 Hz, while the longitudinal frequency can be varied between 1 and 10 Hz. The authors used cesium atoms initially forming a "standard" Bose-Einstein condensate, with ~ 2000 atoms in repulsive interaction. For this condensate (blue dots in figure II.3), a "breathing" mode can be excited for which the condensate length oscillates with a frequency equal to $\sqrt{3}\omega_x$, as theoretically expected (Menotti & Stringari 2002).

The authors then placed their gas in the vicinity of a Fano-Feshbach resonance to switch the scattering length from a positive value ($\sim 7a_0$ where a_0 represents the Bohr radius) to $-5a_0$. They then form a bright soliton

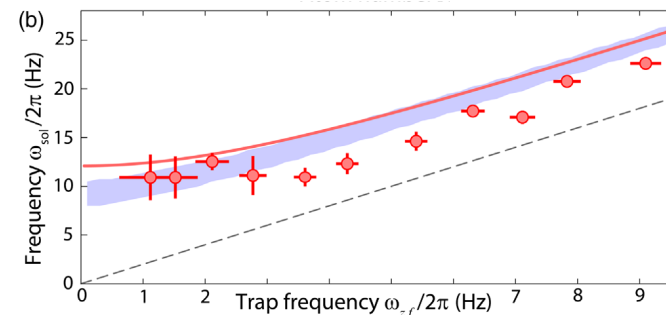


Figure II.4. Variation of the oscillation frequency of the soliton length with the axial frequency of the trap confining the atoms. The limit of zero confinement frequency corresponds to a free soliton. Colored area: result of a numerical solution of the 1D nonlinear Schrödinger equation for a number of atoms between 1300 and 1500. The dashed line gives the prediction for an ideal gas. Figure taken from Di Carli, Colquhoun, et al. (2019).

and observe a faster, damped oscillation of the cloud length (red dots in figure II.3). This "mode" corresponds to the oscillation described above (see figure II.2).

Di Carli, Colquhoun, et al. (2019) verified that the frequency associated with damped oscillations of the soliton length became quasi-independent of the trap's axial frequency when this frequency was strongly reduced (figure II.4). This limit therefore corresponds to an intrinsic characteristic of the soliton. The experimental results are in good agreement with theoretical predictions based on the numerical solution of the one-dimensional nonlinear Schrödinger equation (shaded area in figure II.4).

1-4 Case of a (relatively) large initial deviation

The emergence of a stationary soliton at long times is not restricted to the case where the initial condition is close to a solitonic wave function. We show in figures II.5 and II.6 the evolution of an initially triangular wave function under the effect of the dimensionless equation (II.7). We can see that, at the cost of losing around 1% of the particles, the wave function

evolves towards a solitonic solution $\kappa / \cosh(\kappa x)$. The missing particles are "radiated" and thus form a background of asymptotically zero density in the limit of a box of infinite length L . For these calculations, we have taken $L = 640$.

2 The IST method

The IST method, which stands for inverse scattering transform, was initiated by Gardner, Greene, et al. (1967) to solve the KdV equation. It was then generalized to other nonlinear equations by several authors, in particular by Zakharov & Shabat (1972) for the nonlinear Schrödinger equation of interest here. We will present it schematically in the version proposed by Lax (1968). We will restrict ourselves here to the case where the wave function $u(x, t)$ tends to 0 at infinity [see, for example, Shrira & Geogjaev (2010), Roberti, El, et al. (2021) and refs. in for nonzero boundary conditions, which correspond to the cases of the Kuznetsov–Ma, Akhmediev and Peregrine structures, for example].

The IST method is an extremely powerful technique for tackling many integrable nonlinear problems. It has been the subject of several reference books, such as Ablowitz & Segur (1981), Novikov, Manakov, et al. (1984), Drazin & Johnson (1989), Zakharov (1991), and Korepin, Korepin, et al. (1997). One can also consult Dauxois & Peyrard (2006) for a remarkably clear presentation in the case of the KdV equation.

2-1 A reminder: Eigenstates decomposition

In simplified terms, we can think of the IST method as a generalization of the eigenmode decomposition for solving the evolution of a linear system. Let us start by recalling the principle of this decomposition. We are given an evolution equation, for example the (linear) Schrödinger equation for a function $\psi(x, t)$ describing the evolution of a particle in a potential $V(x)$:

$$i\hbar \partial_t \psi = \hat{H} \psi \quad \text{with} \quad \hat{H} = \frac{\hat{p}^2}{2m} + V(x) \quad (\text{II.11})$$

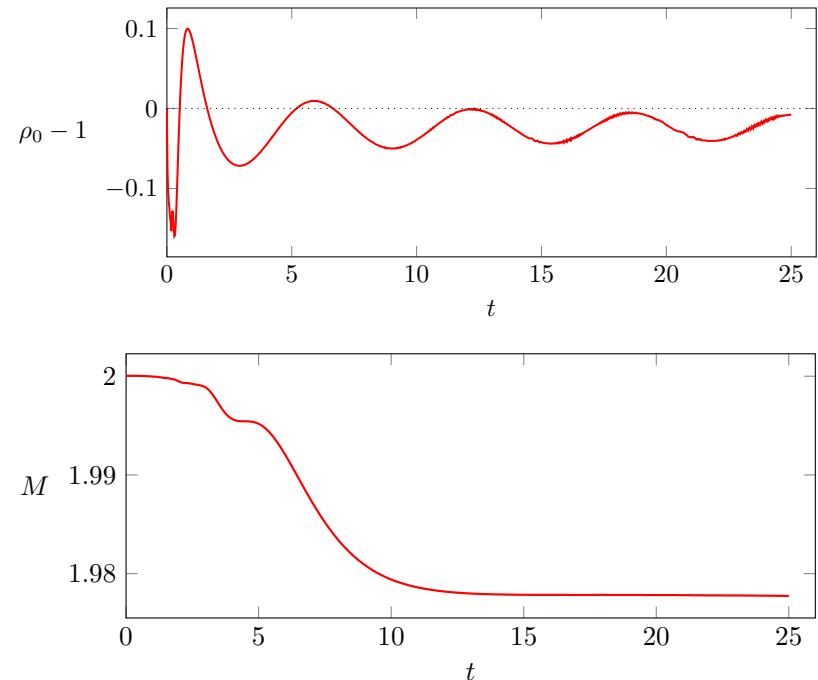


Figure II.5. Evolution of an initial triangular wave function. The number of atoms N_s is defined as $\int_{-a}^{+a} |u(x, t)|^2 dx$ with the (somewhat arbitrary) choice $a = 20$. The calculation is performed on a segment of length $L = 640$ with discretization on 32 768 points.

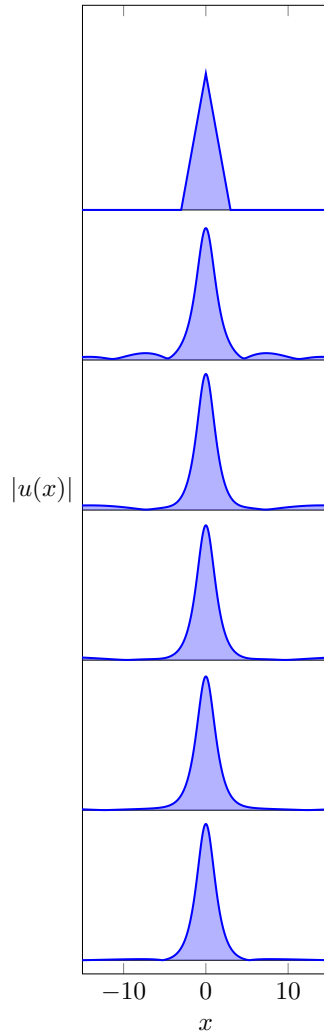


Figure II.6. Evolution of an initial triangular wave function (see figure II.5). From top to bottom, times are $t = 0, 2.5, 5, \dots, 12.5$.

Starting from an arbitrary initial condition $\psi(x, 0)$, it is not always easy to find the function at a later time t by numerical integration. But we can get round this difficulty by proceeding in three steps:

- We solve the eigenvalue problem for \hat{H} :

$$\hat{H}\phi_\lambda = E_\lambda \phi_\lambda. \quad (\text{II.12})$$

The eigenvalues E_λ can be discrete, corresponding to bound states in the potential $V(x)$, or they can be part of a continuum, corresponding to scattering states.

- The initial state $\psi(x, 0)$ is decomposed onto the eigenbasis $\{\phi_\lambda(x)\}$:

$$\psi(x, 0) = \sum_j c_{\lambda_j} \phi_{\lambda_j}(x) + \int c_\lambda \phi_\lambda(x) d\lambda. \quad (\text{II.13})$$

where we have explicitly separated the contributions of the discrete and continuous parts of the spectrum of \hat{H} .

- We obtain the wave function at any time using:

$$\psi(x, t) = \sum_j c_{\lambda_j} \phi_{\lambda_j}(x) e^{-i\lambda_j t/\hbar} + \int c_\lambda \phi_\lambda(x) e^{-i\lambda t/\hbar} d\lambda. \quad (\text{II.14})$$

If we want to determine the evolution of several initial conditions $\psi(x, 0)$, the first step only needs to be performed once, and the problem then boils down to determining the coefficients $\{c_\lambda\}$ for each of the initial conditions considered.

2-2 The Lax pair of operators

Let us consider the nonlinear Schrödinger equation in its dimensionless form for attractive interactions:

$$iu_t + u_{xx} + 2|u|^2u = 0 \quad (\text{II.15})$$

and start from an initial condition $u(x, 0)$ localized in space. The principle of the IST method is to replace the study of the nonlinear evolution of

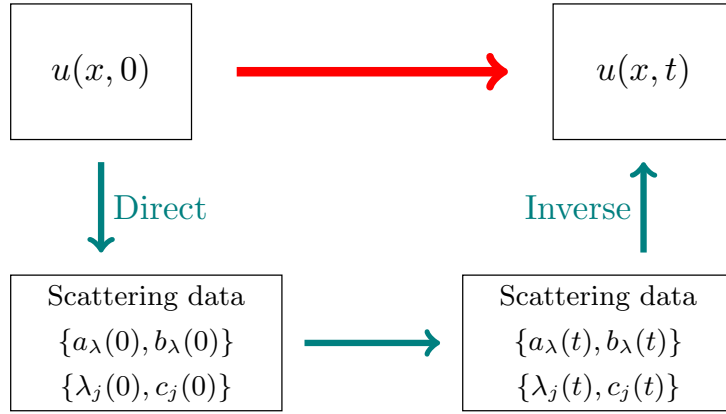


Figure II.7. Principle of the IST method. We replace the (numerical) calculation of the nonlinear evolution (red arrow) by three (a priori) easier, linear steps (green arrows).

$u(x, t)$ by a linear evolution in a different space, this evolution itself being treated as described in the previous paragraph (§2-1). This principle is summarized in figure II.7.

In Lax's method (Lax 1968), which implements this general idea, we associate a pair of linear operators \hat{L} and \hat{A} with the function $u(x, t)$ solution of the nonlinear equation under study. The operators \hat{L} and \hat{A} involve the function u and its spatial derivatives; they therefore implicitly depend on time, since $u(x, t)$ itself depends on time, but they do not involve ∂_t . The link between the equation verified by u and the pair $\{\hat{L}, \hat{A}\}$ is as follows:

$$u(x, t) \text{ solution of (II.15)} \Leftrightarrow \frac{d\hat{L}}{dt} = [\hat{A}, \hat{L}]. \quad (\text{II.16})$$

For a given integrable nonlinear equation, there is no uniqueness of the pair of Lax operators. In the case we are interested in here (eq. II.15), these operators act in the two-component spinor space (Zakharov & Shabat 1972)

$$\Phi(x) = \begin{pmatrix} \phi_a(x) \\ \phi_b(x) \end{pmatrix} \quad \phi_{a,b}(x) \in \mathbb{C} \quad (\text{II.17})$$

and a possible choice is

$$\hat{L} = i \begin{pmatrix} \partial_x & u \\ u^* & -\partial_x \end{pmatrix} \quad \hat{A} = i \begin{pmatrix} 2\partial_x^2 + |u|^2 & u_x + 2u\partial_x \\ u_x^* + 2u^*\partial_x & -2\partial_x^2 - |u|^2 \end{pmatrix} \quad (\text{II.18})$$

With this choice, we find:

$$\frac{d\hat{L}}{dt} = i \begin{pmatrix} 0 & u_t \\ u_t^* & 0 \end{pmatrix} \quad (\text{II.19})$$

and

$$[\hat{A}, \hat{L}] = \begin{pmatrix} 0 & -u_{xx} - 2|u|^2 u \\ u_{xx}^* + 2|u|^2 u^* & 0 \end{pmatrix} \quad (\text{II.20})$$

hence the equivalence given in (II.16).

Note that \hat{A} can also be written as a trinomial in \hat{L} , with coefficients that depend on x , but which do not involve the ∂_x operator:

$$\hat{A} = -2i \begin{pmatrix} 1 & 0 \\ 0 & -1 \end{pmatrix} \hat{L}^2 + 2 \begin{pmatrix} 0 & -u \\ u^* & 0 \end{pmatrix} \hat{L} + i \begin{pmatrix} |u|^2 & -u_x \\ -u_x^* & -|u|^2 \end{pmatrix}. \quad (\text{II.21})$$

This form is useful for formulating the Lax problem in a slightly different way (see appendix on the AKNS method).

The repulsive case. In the case of repulsive interactions, for which the nonlinear Schrödinger equation is $iu_t + u_{xx} - 2|u|^2 u = 0$, a possible Lax pair (\hat{L}, \hat{A}) is:

$$\hat{L} = i \begin{pmatrix} \partial_x & -u \\ u^* & -\partial_x \end{pmatrix} \quad \hat{A} = i \begin{pmatrix} 2\partial_x^2 - |u|^2 & -u_x - 2u\partial_x \\ u_x^* + 2u^*\partial_x & -2\partial_x^2 + |u|^2 \end{pmatrix}. \quad (\text{II.22})$$

Note that in this case, the operator \hat{L} is Hermitian and its spectrum consists solely of real numbers.

As we shall now see, the spectrum of \hat{L} given in (II.18) for the attractive case is not restricted to the real numbers, and this increase in the spectrum compared with the repulsive case is precisely due to the possibility of generating bright solitons, i.e. localized solutions $u(x, t)$ that do not deform nor expand with time.

2-3 Scattering data associated with \hat{L}

Once equivalence (II.16) has been established, we can replace the evolution under the effect of the nonlinear Schrödinger equation by the evolution of spinors under the effect of the linear operators \hat{A} and \hat{L} according to the scheme shown in figure II.7. More precisely, let us consider the eigenvalue problem for the operator \hat{L} at a given time t :

$$\hat{L}\Phi = \lambda\Phi \quad \text{with} \quad \Phi(x, t) = \begin{pmatrix} \phi_a(x, t) \\ \phi_b(x, t) \end{pmatrix} \quad (\text{II.23})$$

or its more explicit version:

$$i\partial_x\phi_a + iu\phi_b = \lambda\phi_a \quad (\text{II.24})$$

$$-i\partial_x\phi_b + iu^*\phi_a = \lambda\phi_b \quad (\text{II.25})$$

This system is close to an eigenvalue problem for a one-dimensional Schrödinger (or rather Dirac) equation, with the function $u(x)$ playing the role of a localized potential. In particular, outside the zone where $u(x)$ takes on significant values, this eigenvalue problem reduces to the solution of

$$\partial_x\phi_a = -i\lambda\phi_a \quad \partial_x\phi_b = i\lambda\phi_b \quad (\text{II.26})$$

which gives at lowest order in $u(x)$:

$$x \rightarrow \pm\infty: \quad \phi_a \propto e^{-i\lambda x} \quad \phi_b \propto e^{i\lambda x}. \quad (\text{II.27})$$

The analogy with the Schrödinger equation is not perfect, as \hat{L} is not self-adjoint and its eigenvalues λ can be complex. Furthermore, the function $u(x)$ that acts as a potential can also be complex. However, some general characteristics remain:

- At a given time t , the spectrum of \hat{L} consists of a continuum plus a set of discrete eigenvalues $\lambda_1, \dots, \lambda_n$.
- The continuous part of the spectrum corresponds to scattering states, propagating as $e^{\pm i\lambda x}$ to infinity. It corresponds to values of λ covering all real numbers. For each value of $\lambda \in \mathbb{R}$, the solutions of the system (II.24-II.25) form a space of dimension 2.

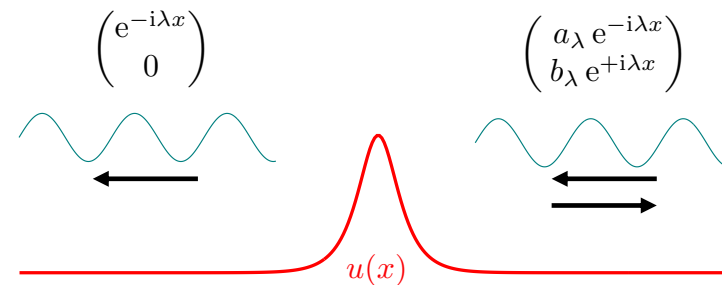


Figure II.8. The scattering states, eigenstates of the operator \hat{L} , associated to a real eigenvalue λ . The corresponding scattering data are the two coefficients a_λ and b_λ .

- Discrete eigenvalues are associated with eigenfunctions Φ that are localized where the function $u(x)$ itself takes significant values. To ensure localization, λ must have a nonzero imaginary part, $\lambda = \xi + i\eta$ with ξ and η real, to ensure that Φ decays as $e^{-|\eta x|}$ at infinity. Note that the existence of these bound states does not depend on the sign (or phase) of the "potential" $u(x)$. More precisely, if $(\phi_a, \phi_b)^T$ is a bound state in the potential $u(x)$ for the eigenvalue λ , then $(\phi_a, -\phi_b)^T$ will be a bound state in the potential $-u(x)$ for the same eigenvalue.

It is important to stress right away that we will not need to know the exact form of the eigenfunctions $\Phi(x)$ to carry out the IST program. This method relies solely on the spectrum of eigenvalues and on the asymptotic behavior of the eigenfunctions at $\pm\infty$.

More precisely, at a given point in time, for example the initial time $t = 0$, we will associate the function $u(x, 0)$ with a set of *scattering data*, such as the reflection coefficient associated with the "potential" $u(x, 0)$ and the behavior of the bound states in this "potential". We will then show that the time evolution of these scattering data is remarkably simple.

For the continuous part of the spectrum (real λ), we define the coeffi-

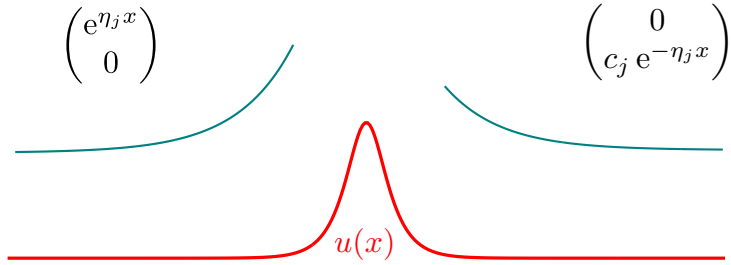


Figure II.9. Blue curve: A bound state, eigenstate of the operator \hat{L} with eigenvalue $\lambda_j = \xi_j + i\eta_j$, with here $\xi_j = 0$, $\eta_j > 0$. The corresponding scattering data are the eigenvalue λ_j and the coefficient c_j .

cients a_λ and b_λ characterizing the scattering states as (figure II.8)

$$x \rightarrow -\infty : \quad \Phi_\lambda(x) \sim \begin{pmatrix} 1 \\ 0 \end{pmatrix} e^{-i\lambda x} \quad (\text{II.28})$$

$$x \rightarrow +\infty : \quad \Phi_\lambda(x) \sim a_\lambda \begin{pmatrix} 1 \\ 0 \end{pmatrix} e^{-i\lambda x} + b_\lambda \begin{pmatrix} 0 \\ 1 \end{pmatrix} e^{+i\lambda x} \quad (\text{II.29})$$

For the discrete part of the spectrum, in addition to knowing the eigenvalues $\lambda_j = \xi_j + i\eta_j$, an important quantity is the ratio of the amplitudes on either side of where the u function is located (figure II.9):

$$x \rightarrow -\infty : \quad \Phi_j(x) \sim \begin{pmatrix} 1 \\ 0 \end{pmatrix} e^{\eta_j x} e^{-i\xi_j x} \quad (\text{II.30})$$

$$x \rightarrow +\infty : \quad \Phi_j(x) \sim c_j \begin{pmatrix} 0 \\ 1 \end{pmatrix} e^{-\eta_j x} e^{i\xi_j x} \quad (\text{II.31})$$

We have favored eigenfunctions proportional to the spinor $(1, 0)^T$ when $x \rightarrow -\infty$ [cf. (II.28) and (II.30)], which for bound states imposes a positive imaginary part for the eigenvalue λ . Eigenvalues with negative imaginary parts can also be obtained by considering the spinor $\bar{\Phi}$ conjugate to Φ :

$$\Phi = \begin{pmatrix} \phi_a \\ \phi_b \end{pmatrix} \quad \bar{\Phi} = \begin{pmatrix} \phi_b^* \\ -\phi_a^* \end{pmatrix}. \quad (\text{II.32})$$

Indeed, if the spinor Φ is an eigenstate of \hat{L} for the eigenvalue λ , the spinor $\bar{\Phi}$ is an eigenstate of \hat{L} for the eigenvalue λ^* . In what follows, we will restrict ourselves to describing the spectrum in the upper complex half-plane (including the real axis), with the $\lambda \leftrightarrow \lambda^*$ symmetry implicitly assumed.

For a given function $u(x, t)$, the spectrum of \hat{L} is therefore formed by:

- the set of real axes for scattering states,
- discrete eigenvalues outside the real axis, conjugated two by two, corresponding to localized states.

The first part of the program in figure II.7 therefore consists in associating these scattering data with the initial function $u(x, 0)$:

$$u(x, 0) \longrightarrow \text{scattering data: } \{a_\lambda(0), b_\lambda(0)\}, \{\lambda_j(0), c_j(0)\} \quad (\text{II.33})$$

2-4 The evolution of scattering data

A central point of the integrability criterion, linked to the existence of a pair of Lax operators, lies in the simplicity of the evolution over time of the scattering data.

Let us start by introducing the evolution operator $\hat{U}(t)$ between 0 and t defined by

$$\frac{d\hat{U}}{dt} = \hat{A}(t) \hat{U}(t) \quad \text{with} \quad \hat{U}(0) = \hat{1}. \quad (\text{II.34})$$

Note that unlike in quantum physics, where the role of \hat{A} is played by a Hermitian Hamiltonian and the evolution operator is therefore unitary, this property is not generally verified by the operator \hat{U} introduced here. However, this absence of the unitarity property will not be a hindrance in what follows.

The inverse operator \hat{U}^{-1} obeys the evolution equation:

$$\frac{d\hat{U}^{-1}}{dt} = -\hat{U}^{-1}(t) \hat{A}(t) \quad (\text{II.35})$$

as can be seen by calculating $\hat{U}(t + dt) \hat{U}^{-1}(t + dt)$ as a function of $\hat{U}(t) \hat{U}^{-1}(t)$ to order 1 in dt .

Once this evolution operator has been introduced, we can integrate the evolution equation for the operator \hat{L} :

$$\frac{d\hat{L}}{dt} = [\hat{A}(t), \hat{L}(t)] \Leftrightarrow \hat{L}(t) = \hat{U}(t)\hat{L}(0)\hat{U}^{-1}(t). \quad (\text{II.36})$$

Let us recast this relationship as

$$\hat{L}(t)\hat{U}(t) = \hat{U}(t)\hat{L}(0) \quad (\text{II.37})$$

and let it act on an eigenstate $\Phi_j(0)$ of the operator $\hat{L}(0)$ at the initial time, associated with the eigenvalue $\lambda_j(0)$:

$$\hat{L}(t) [\hat{U}(t)\Phi_j(0)] = \lambda_j(0) [\hat{U}(t)\Phi_j(0)]. \quad (\text{II.38})$$

We deduce that the eigenvalue $\lambda_j(0)$ at the initial time remains an eigenvalue over time and that the associated eigenvector is

$$\Phi_j(t) = \hat{U}(t)\Phi_j(0) \Leftrightarrow \frac{d\Phi_j}{dt} = \hat{A}(t)\Phi_j(t). \quad (\text{II.39})$$

The discrete part of the spectrum is therefore invariant during time evolution. We will see later that this discrete part is associated with solitons, and this invariance is therefore a signature of soliton robustness during evolution.

The evolution of the other scattering data can be deduced directly from the above. In the asymptotic region $x \rightarrow \pm\infty$, the function $u(x, t)$ takes on negligible values so that the operator \hat{A} there is given by [cf. (II.21)]:

$$x \rightarrow \pm\infty : \quad \hat{A} \approx -2i \begin{pmatrix} 1 & 0 \\ 0 & -1 \end{pmatrix} \hat{L}^2 \quad (\text{II.40})$$

which gives, when we make it act on an eigenstate of \hat{L} and take into account (II.39):

$$\frac{d\phi_a}{dt} = -2i\lambda^2\phi_a \quad \frac{d\phi_b}{dt} = 2i\lambda^2\phi_b. \quad (\text{II.41})$$

The system (II.28-II.29) becomes at time t

$$x \rightarrow -\infty : \quad \Phi_\lambda(x, t) \sim \begin{pmatrix} e^{-2i\lambda^2 t} \\ 0 \end{pmatrix} e^{-i\lambda x} \quad (\text{II.42})$$

$$x \rightarrow +\infty : \quad \Phi_\lambda(x, t) \sim a_\lambda \begin{pmatrix} e^{-2i\lambda^2 t} \\ 0 \end{pmatrix} e^{-i\lambda x} + b_\lambda \begin{pmatrix} 0 \\ e^{2i\lambda^2 t} \end{pmatrix} e^{+i\lambda x} \quad (\text{II.43})$$

Multiplying this set of equations by $e^{2i\lambda^2 t}$, we derive for the continuous part of the spectrum (scattering states, λ real):

$$a_\lambda(t) = a_\lambda(0) \quad b_\lambda(t) = b_\lambda(0) e^{4i\lambda^2 t} \quad (\text{II.44})$$

For the discrete part (bound states, λ with a non-zero imaginary part), an identical reasoning yields:

$$\lambda_j(t) = \lambda_j(0) \quad c_j(t) = c_j(0) e^{4i\lambda_j^2 t}. \quad (\text{II.45})$$

We have therefore completed the second part of the program in figure II.7:

$$\{a_\lambda(0), b_\lambda(0)\}, \{\lambda_j(0), c_j(0)\} \longrightarrow \{a_\lambda(t), b_\lambda(t)\}, \{\lambda_j(t), c_j(t)\}. \quad (\text{II.46})$$

2-5 Inversion of scattering data

The third and final part of the program in figure II.7 consists in inverting the scattering data: knowing the $\{a_\lambda(t), b_\lambda(t)\}, \{\lambda_j(t), c_j(t)\}$ at time t , can we reconstruct the "potential" associated with them, i.e., the function $u(x, t)$? This inversion is indeed possible, even if it can be numerically difficult to put into practice. Fortunately, even if we do not completely perform this last step, we can still deduce a number of interesting properties by considering the formal structure of the inversion process for scattering data.

Knowing the scattering data, we introduce the intermediate function defined at a given time t :

$$F(x, t) = \frac{1}{2\pi} \int_{-\infty}^{+\infty} \frac{b_\lambda(t)}{a_\lambda(t)} e^{i\lambda x} d\lambda + \sum_{j=1}^N c_j(t) e^{i\lambda_j x}. \quad (\text{II.47})$$

This function involves an integral over the continuous spectrum of the operator \hat{L} , with λ ranging from $-\infty$ to $+\infty$, as well as a sum over all discrete eigenvalues, of non-zero and positive imaginary part.

Once we know $F(x, t)$, we look for the solutions K_1 and K_2 of the pair

of integral equations (Marchenko equations)

$$0 = -K_1^*(x, y) + \int_x^{+\infty} K_2(x, s)F(y+s) ds + F(x+y) \quad (\text{II.48})$$

$$0 = K_2^*(x, y) + \int_x^{+\infty} K_1(x, s)F(y+s) ds \quad (\text{II.49})$$

where the dependence on t , which plays the role of a constant parameter in these two equations, is omitted for the different functions K_1 , K_2 and F . In the general case, this resolution is the step requiring the greatest numerical effort, but it remains a linear operation. Once this has been done, we obtain the function $u(x, t)$ as the solution to the original nonlinear equation:

$$u(x, t) = 2K_1(x, x, t) \quad \text{and} \quad \int_x^{+\infty} |u(x, t)|^2 dx = -2K_2(x, x, t). \quad (\text{II.50})$$

We will not go into the justification of this procedure here, but refer the reader to the seminal articles by Zakharov & Shabat (1972) and Ablowitz, Kaup, et al. (1974). Let us simply point out that it is based on the analysis of the large λ behavior of the solutions of the initial eigenvalue problem $\hat{L}\Phi = \lambda\Phi$, with the unknown function $u(x, t)$ appearing as the coefficient of the λ^{-1} term in the development of the eigenfunctions Φ .

Note. A notable simplification occurs for functions $u(x)$ such that the reflection coefficient $b(\lambda)$ cancels out for all values of λ , since only the discrete sum over the bound states in (II.47) then remains. It is in fact this case that we will discuss first in what follows, as it corresponds to the case of "pure" solitons.

3 The fundamental soliton

3-1 The fundamental soliton at rest

As a first example of the IST method, let us look at the fundamental soliton at rest. We take as our initial function

$$u(x, 0) = \frac{1}{\cosh x} \quad (\text{II.51})$$

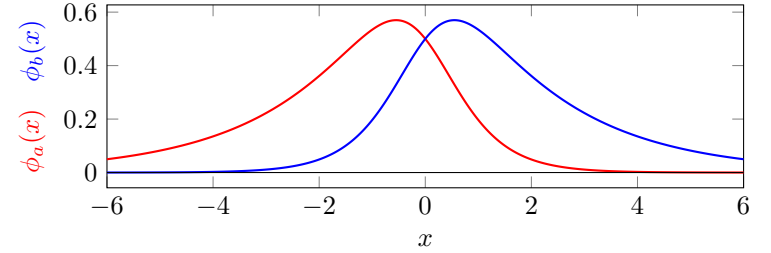


Figure II.10. Eigenfunction $\Phi_1 = (\phi_a, \phi_b)^T$ of the operator \hat{L} associated with the eigenvalue $\lambda_1 = i/2$ for the choice $u(x) = 1/\cosh(x)$.

for which we know it corresponds to an immobile soliton:

$$u(x, t) = \frac{e^{it}}{\cosh x}. \quad (\text{II.52})$$

Let us check that we can recover this result using the IST method by explicitly determining the scattering data, i.e. the reflection coefficients $b(\lambda)$ for the scattering states and the spectrum of bound states.

The calculation of the reflection coefficient $b(\lambda)$ involves the use of hypergeometric functions. The result is that for the choice (II.51), the reflection coefficient $b(\lambda)$ cancels for all scattering states (Satsuma & Yajima 1974):

$$\text{choice (II.51):} \quad b(\lambda) = 0 \quad \forall \lambda \in \mathbb{R} \quad (\text{II.53})$$

Consequently, only the discrete part of the spectrum of \hat{L} contributes in this case to the function $F(x)$ defined in (II.47).

Let us consider now this discrete part. Solving the eigenvalue equation

$$\hat{L}\Phi = \lambda\Phi \quad \Leftrightarrow \quad \begin{cases} \partial_x \phi_a + \frac{\phi_b}{\cosh x} = -i\lambda\phi_a \\ \partial_x \phi_b - \frac{\phi_a}{\cosh x} = i\lambda\phi_b \end{cases} \quad (\text{II.54})$$

also involves the use of hypergeometric functions. The result is that there is a single eigenvalue in the upper half of the complex plane³ outside the

³We remind that the eigenvalues of the discrete spectrum appear in pairs (λ_j, λ_j^*) . There is therefore also the eigenvalue $-i/2$ in the lower complex plane.

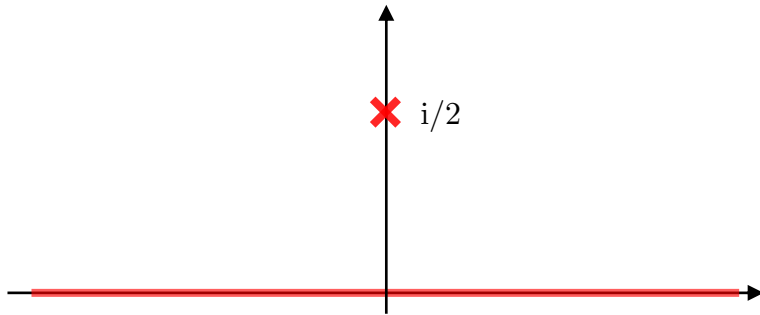


Figure II.11. Spectrum of the operator \hat{L} in the upper complex half-plane for the function $u(x) = 1/\cosh x$, i.e. a soliton at rest of mass 2. The spectrum is composed of the real axis and the point $\lambda_1 = i/2$.

real axis (Satsuma & Yajima 1974):

$$\lambda_1 = i/2 \quad \Phi_1(x) = \begin{pmatrix} e^{x/2}/(1 + e^{2x}) \\ e^{-x/2}/(1 + e^{-2x}) \end{pmatrix} \quad (\text{II.55})$$

so that $c_1(0) = 1$. These two components of the spinor Φ are plotted in figure II.10. The evolution of scattering data given in (II.45) therefore reduces to:

$$\lambda_1(t) = \frac{i}{2} \quad c_1(t) = e^{-it}. \quad (\text{II.56})$$

and the function $F(x)$ reads at time t :

$$F(x, t) = e^{-it} e^{-x/2}. \quad (\text{II.57})$$

This single eigenvalue in the upper complex half-plane (figure II.11) is the signature of the soliton chosen in (II.52), as we will now show.

For this function $F(x)$, solving the system (II.48-II.49) is very simple because we can look for solutions in the form

$$K_j(x, y, t) = L_j(x, t) e^{-y/2} \quad j = 1, 2. \quad (\text{II.58})$$

This system can then be written

$$\begin{aligned} 0 &= -L_1^* + e^{-it-x} L_2 + e^{-it-x/2} \\ 0 &= L_2^* + e^{-it-x} L_1 \end{aligned} \quad (\text{II.59})$$

and its solution is

$$L_1(x, t) = \frac{e^{it-x/2}}{1 + e^{-2x}} \quad L_2(x, t) = -\frac{e^{-3x/2}}{1 + e^{-2x}}. \quad (\text{II.60})$$

We can then use the general solution (II.50) and check that we recover the exact result that is already known (II.52). Of course, using all the formalism of the IST method for the simple case of the fundamental soliton at rest seems disproportionate, but it does allow us to check that the formalism we have presented is indeed under control. Furthermore, we will soon see how to use this same formalism to find much less obvious solutions.

3-2 Variants around the soliton at rest

Soliton displaced from $x = 0$. Choosing the initial function $u(x, 0) = 1/\cosh(x - x_0)$ does not change the coefficients $b(\lambda)$, which remain zero, nor the discrete eigenvalue $\lambda_1 = i/2$. We find the same system as in (II.54) after changing the variable $x \rightarrow x - x_0$, which has the effect of modifying the value of $c_1(0)$, which becomes

$$c_1(0) = e^{x_0} \quad (\text{II.61})$$

Solving (II.48-II.49) is done as in the case $x_0 = 0$ and leads to:

$$L_1(x, t) = \frac{e^{it} e^{-x/2} e^{x_0}}{1 + e^{-2(x-x_0)}} \quad L_2(x, t) = -\frac{e^{-3x/2} e^{2x_0}}{1 + e^{-2(x-x_0)}} \quad (\text{II.62})$$

We then deduce the solution of the Schrödinger equation at time t : $u(x, t) = e^{it}/\cosh(x - x_0)$.

Soliton of different mass. The soliton considered in (II.51) has a mass equal to 2:

$$\int |u(x, 0)|^2 dx = 2. \quad (\text{II.63})$$

Of course, other stationary solitons are also of interest:

$$u(x, 0) = \frac{\kappa}{\cosh(\kappa x)} \quad (\text{II.64})$$

with a mass and an energy given by:

$$M = \int |u(x, 0)|^2 dx = 2\kappa \quad E = \int (|\partial_x u|^2 - |u|^4) dx = -\frac{2}{3}\kappa^3. \quad (\text{II.65})$$

The above treatment remains valid whatever the value of κ . More precisely, (i) all reflection coefficients remain zero and (ii) the system (II.54) is solved identically by changing the variable $x' = \kappa x$, indicating that the eigenvalue associated with the soliton is now:

$$\lambda_1 = i\kappa/2. \quad (\text{II.66})$$

It therefore remains purely imaginary and at time t we find

$$u(x, t) = \frac{\kappa}{\cosh(\kappa x)} e^{i\kappa^2 t}. \quad (\text{II.67})$$

Soliton of different phase. If we change the phase of the initial condition (II.51) by taking $u(x, 0) = e^{i\varphi} / \cosh(x)$, we can easily see that we find the same system as in (II.54), with the substitution $\phi_b \rightarrow \phi_b e^{-i\varphi}$. The reflection coefficients $b(\lambda)$ are always zero, and we keep the same single pure imaginary eigenvalue $\lambda_1 = i/2$ in the upper complex half-plane. The only change concerns the coefficient $c_1(0)$, which becomes:

$$c_1(0) = e^{-i\varphi}. \quad (\text{II.68})$$

The function $F(x)$ then also acquires the phase $e^{-i\varphi}$, with the resolution of (II.48-II.49) remaining unchanged. We finally arrive at $u(x, t) = e^{-i(t+\varphi)} / \cosh(x)$, as expected.

Comparing (II.61) and (II.68) is instructive: changing the coefficient $c_1(0)$, other things being equal, allows us to account for a phase change or a translation of the initial function $u(x, 0)$ depending on whether we modify the phase or the modulus of c_1 .

3-3 The fundamental soliton in motion

Still in a one-soliton scheme, we can also take as our initial condition

$$u(x, 0) = \frac{e^{ikx}}{\cosh x}. \quad (\text{II.69})$$

We saw in the previous chapter that it represents a soliton whose envelope propagates at velocity $2k$. Let us check that we can recover this result using the IST method.

The eigenvalue equation (II.23) still admits one and only one solution for λ in the upper complex half-plane, but this eigenvalue now has a non-zero real part (figure II.12):

$$\lambda_1 = (i - k)/2 \quad \Phi_1(x) = \begin{pmatrix} e^{-i\lambda_1 x} / (1 + e^{2x}) \\ e^{+i\lambda_1 x} / (1 + e^{-2x}) \end{pmatrix} \quad (\text{II.70})$$

from which we deduce

$$c_1(0) = 1 \quad c_1(t) = e^{i(k^2-1)t} e^{2kt} \quad F(x, t) = c_1(t) e^{-x/2} e^{-ikx/2}. \quad (\text{II.71})$$

Solving the integral system (II.48-II.49) at a given time t can still be done by posing

$$K_j(x, y, t) = L_j(x, t) e^{(-1+ik)y/2} \quad (\text{II.72})$$

and we find

$$L_1(x, t) = \frac{e^{i(1-k^2)t} e^{i(k-1)x/2} e^{2kt}}{1 + e^{-2(x-vt)}} \quad \text{with } v = 2k \quad (\text{II.73})$$

and finally

$$u(x, t) = 2K_1(x, x, t) = \frac{e^{ikx} e^{i(1-k^2)t}}{\cosh(x - vt)}. \quad (\text{II.74})$$

Summarizing the previous two paragraphs, the fundamental soliton problem

$$u(x, 0) = \frac{\kappa e^{ikx}}{\cosh(\kappa x)} \quad \rightarrow \quad u(x, t) = \frac{\kappa e^{ikx}}{\cosh[\kappa(x - 2kt)]} e^{i(\kappa^2 - k^2)t} \quad (\text{II.75})$$

is characterized at any time t by :

- a null reflection coefficient $b(\lambda)$ for all real λ , i.e. for all scattering states resulting from the resolution of $\hat{L}\Phi = \lambda\Phi$;
- a single eigenvalue λ in the upper complex half-plane, and thus a single bound state:

$$\lambda_1 = \frac{1}{2}(i\kappa - k). \quad (\text{II.76})$$

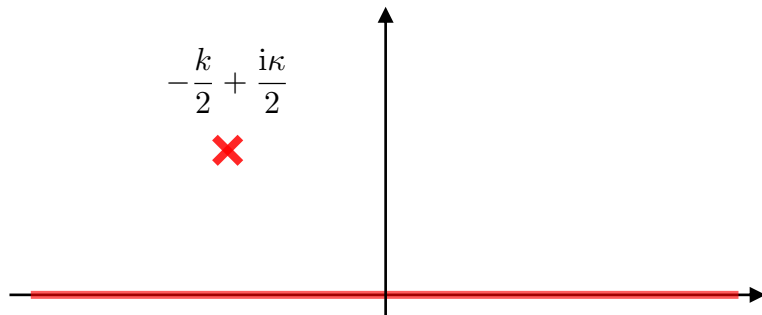


Figure II.12. Spectrum of the operator \hat{L} in the upper complex half-plane for a soliton of mass 2κ and velocity $2k$. This spectrum is composed of the real axis and the point $\lambda_1 = (-k + i\kappa)/2$.

This bound state is associated with the soliton, the imaginary part κ of the eigenvalue characterizes the mass of the soliton ($M = 2\kappa$) and the real part k characterizes the velocity of its envelope ($v = 2k$).

Summary. The results we have just obtained give a broader view of the robustness of the soliton discussed in §1. Let us first consider a function $u(x, 0)$ having exactly the form required to form a soliton. We know that the spectrum of \hat{L} will be composed of the set of real numbers and a pair of conjugate non-real eigenvalues. We also know that the reflection coefficients b_λ will all be zero.

Now let us suppose that we slightly distort this initial condition $u(x, 0)$. The nature of the spectrum will remain unchanged: it will always be composed of the real axis (scattering states) and a single pair of eigenvalues off the real axis (a bound state in the "potential" associated with $u(x, 0)$). On the other hand, the b_λ coefficients will probably become non-zero.

However, we know that the pair of non-real eigenvalues corresponds to a soliton. The imaginary part may differ from that of the desired soliton, which means that the number of particles will not be exactly that targeted, and the real part may also be different, corresponding to a velocity that is also slightly different from that desired. But the soliton will still be there!

The fact that the b_λ coefficients are nonzero indicates that the delocalized states will be populated, a necessary counterpart since the soliton will not have the initially expected number of atoms at long times.

If we modify the initial condition more drastically, the pair of complex eigenvalues may merge with the real axis and disappear: this means that we have not put in enough particles (given the initial size) to prevent the wave packet from expanding under the effect of kinetic energy. All the particles will disperse and no localized, stable collective structure will have been formed.

If the initial wave function is significantly different from the one initially targeted, other pairs of non-real eigenvalues may also appear. In this case, several solitons will be generated, a situation to which we will return in the next paragraph.

In any case, the first stage of the IST method, i.e. the diagonalization of the operator \hat{L} , can be seen as a "soliton detector", providing quantitative information on the final state that will be reached after evaporation of all surplus particles, by giving the number of solitons, their masses and their velocities.

4 Higher-order solitons

In this paragraph, we are interested in the situation where we have prepared an initial function $u(x, 0)$ and where the diagonalization of the corresponding operator \hat{L}

$$\hat{L} = i \begin{pmatrix} \partial_x & u(x, 0) \\ u^*(x, 0) & -\partial_x \end{pmatrix} \quad (\text{II.77})$$

leads (in addition to the real axis) to several eigenvalues $\{\lambda_j, j = 1, \dots, n\}$ in the upper complex half-plane, and of course their complex conjugates in the lower half-plane.

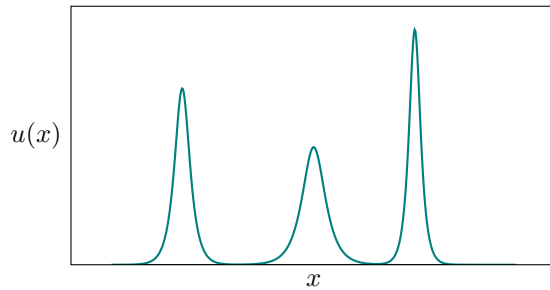


Figure II.13. Function $u(x)$ obtained by taking the sum of envelopes of fundamental solitons well separated from each other.

4-1 N solitons of different velocities

In this paragraph, we assume that the function $u(x, 0)$ is made up of n wave packets well separated from each other (figure II.13),

$$u(x, 0) = \sum_{j=1}^n u_j(x) \quad (\text{II.78})$$

where each function u_j corresponds exactly to a soliton located in x_j , with mass M_j and velocity v_j .

Let us take a look at the eigenvalue problem for \hat{L} and consider the scattering states first. We know that each of the "potentials" $u_j(x)$, taken alone, leads to a reflection coefficient b_λ that is strictly zero. If the envelopes of the functions u_j are well separated, the interferences between these different scattering centers can be neglected, leading to a zero reflection coefficient for each value of λ . In optical terms, a stack of surfaces, each with an anti-reflective coating, forms itself a non-reflective system.

We deduce from the general result (II.44) that the coefficients b_λ will remain zero over time, even if the solitons momentarily come into contact with each other. Therefore only discrete states will contribute to the function $F(x)$ given in (II.47) and the determination of $u(x, t)$ at any instant will not involve scattering states. In physical terms, we know from the outset that no particles will be evaporated during soliton collisions.

Let us now consider the bound states in the "potential" $u(x, 0)$. By construction, each $u_j(x)$ gives rise to a bound state localized in the vicinity of x_j , associated with the eigenvalue λ_j of \hat{L} . Assuming that the "potentials" $u_j(x)$ are very far apart, the diagonalization of \hat{L} will lead to n bound states very close to the bound states of each individual "potential" u_j . In a standard quantum formulation, this amounts to neglecting the tunnel coupling between potential wells arbitrarily far apart.

We also know that the spectrum $\{\lambda_j\}$ will remain constant [cf. (II.45)]. Once all the solitons have crossed, we will have the same eigenvalues λ_j as at the input. Remember that the real part of λ_j determines the mass of soliton j , and the imaginary part determines its velocity.

The general result (II.44-II.45) for the evolution of scattering data is therefore extremely powerful, since it allows us to account for the stability of solitons during a collision, whatever their number, masses and velocities. Solving the integral system (II.48-II.49) is only necessary if we wish to know the exact position of each soliton at a given instant t , this position resulting from the attractive or repulsive character of the interactions between solitons, itself dependent on their relative phase, and therefore on the coefficients c_j [cf. (II.68-II.61)].

4-2 Multi-solitons (or composite solitons)

In the previous paragraph, we assumed that there was an initial instant at which the n solitons were well separated from each other. We will now consider the opposite situation, where the solitons are initially superimposed on each other with the same velocity, which we will choose to be zero.

To further simplify the discussion, we will assume that the function u reads at initial time

$$u(x, 0) = \frac{A}{\cosh x}, \quad (\text{II.79})$$

corresponding to the following mass and energy:

$$M = \int |u|^2 dx = 2A^2 \quad E = \int (|\partial_x u|^2 - |u|^4) dx = -\frac{2}{3}A^2(2A^2 - 1). \quad (\text{II.80})$$

If we take $A = 1$, we recover the fundamental soliton studied in the previous section (§ 3). The question we wish to address concerns the evolution of the system for any value of A . To this end, we will use the results of Satsuma & Yajima (1974).

The eigenvalue problem for \hat{L} is solved by eliminating the function ϕ_b from the differential system (II.24-II.25) to obtain a second-order differential equation for the function ϕ_a only. This equation can be solved exactly and its solution can be written in terms of a hypergeometric function. The important result here concerns the discrete spectrum of \hat{L} , which we have seen to be a "soliton detector". This spectrum is plotted as a function of A on figure II.14 and has a very simple expression:

- For $A \leq 1/2$, there are no eigenvalues outside the real axis. There is therefore no soliton, and the initial wave packet will spread out indefinitely over time.
- For $A \in]1/2, 3/2]$, there is one and only one eigenvalue in the upper complex half-plane, and therefore only one soliton:

$$\lambda_1 = i \left(A - \frac{1}{2} \right) \quad (\text{II.81})$$

We return to the situation shown in figure II.2 and discussed at the end of section 3: apart from the $A = 1$ case, which constitutes the fundamental soliton ($\lambda_1 = i/2$), particles or radiation are emitted to asymptotically reach a soliton at rest, of mass $M_s = 2\kappa$ with $\lambda_1 = i\kappa/2$, i.e. $\kappa = 2A - 1$ and $M_s = 2(2A - 1)$. The difference between the starting mass $M = 2A^2$ and that of the soliton is $\Delta M = M - M_s = 2(A - 1)^2$. This is a strictly positive quantity, except for $A = 1$ since the initial state is then the fundamental soliton, as already mentioned.

When A tends towards the lower limit $A = 1/2$, the mass of the final soliton tends towards 0, corresponding to a wave packet of very low amplitude and large width. When A tends towards the upper limit $A = 3/2$, the mass of the soliton formed tends towards $M_s = 4$, whereas the initial mass is $M = 9/2$. The radiated mass is therefore $1/2$, the final solitonic wave packet $\kappa / \cosh(\kappa x)$ having a height greater than the initial height (2 instead of $3/2$) and a narrower width.

- For $A \in]3/2, 5/2]$, there are two discrete eigenvalues in the upper complex half-plane:

$$\lambda_1 = i \left(A - \frac{1}{2} \right) \quad \lambda_2 = i \left(A - \frac{3}{2} \right) \quad (\text{II.82})$$

We thus find a situation with two superimposed fundamental solitons, each at rest since the real part of these eigenvalues is zero. We will call this structure a "bi-soliton" and come back to it a little later to show that it gives rise to an oscillating structure (*breather*).

- More generally, for $A \in]n - 1/2, n + 1/2]$, there are n discrete eigenvalues in the upper complex half-plane:

$$\lambda_1 = i \left(A - \frac{1}{2} \right), \quad \dots, \quad \lambda_n = i \left(A - n + \frac{1}{2} \right). \quad (\text{II.83})$$

This structure corresponds to a multi-soliton, i.e. n superimposed fundamental solitons, all with zero velocity.

The reflection coefficients b_λ that characterize the continuous spectrum (real λ) also have a remarkable expression (Satsuma & Yajima 1974):

$$b_\lambda = i \frac{\sin(\pi A)}{\cosh(\pi \lambda)}. \quad (\text{II.84})$$

In particular, for integer values of A , i.e. A chosen at the center of the segments we have just identified, the reflection coefficients b_λ cancel out for all values of k . At these points, the continuous spectrum does not contribute to the expression of the function $F(x)$ defined in (II.47). Nor does it play a part in solving the system (II.48-II.49) that provides the function $u(x, t)$ at all times. For these integer values of A , no particles or radiation are emitted by the system during its evolution: all particles remain in the form of a multi-soliton.

This absence of evaporation can be verified for integer values $A = n$ by comparing the initial mass $M_{\text{ini}} = 2A^2 = 2n^2$ [cf. (II.80)] and the total mass of $A = n$ individual solitons associated with eigenvalues $\lambda_j = i(n - j + 1/2)$ [cf. (II.64-II.66)]. The amplitudes $\kappa_j = 2|\lambda_j|$ of these n solitons are the odd numbers $1, 3, \dots, (2n - 1)$ and the total mass is equal to

$$M_{\text{tot}} = 2 \sum_{j=1}^n (2j - 1) = 2n^2. \quad (\text{II.85})$$

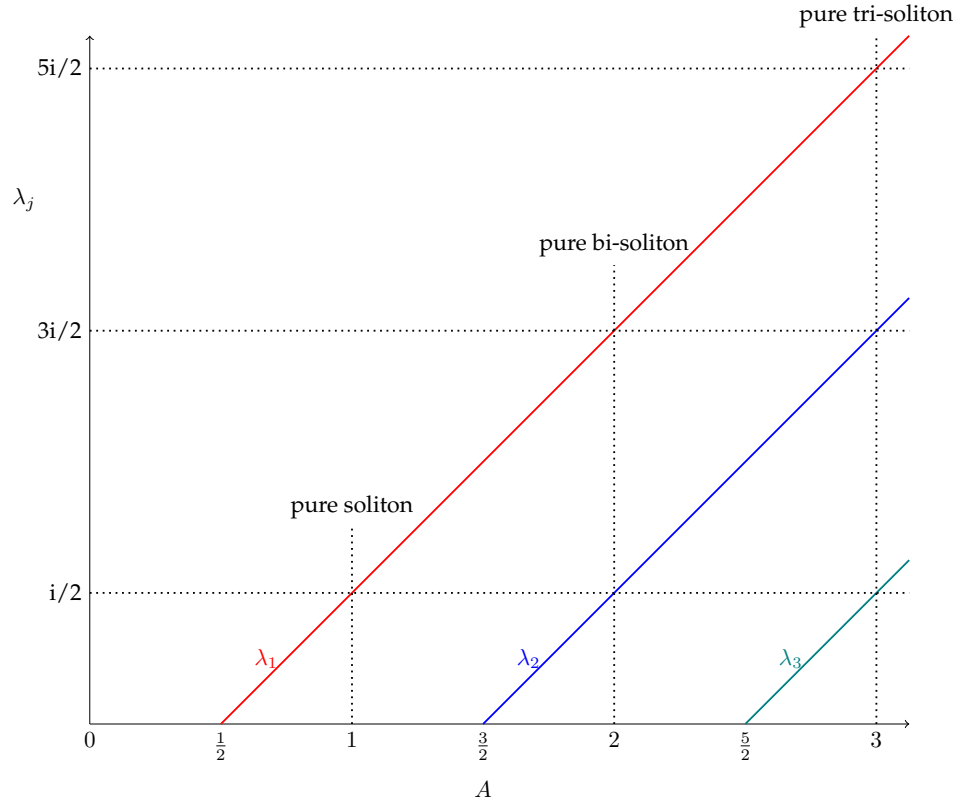


Figure II.14. Discrete eigenvalues of the operator \hat{L} for the choice $u(x) = A/\cosh x$.

The equality between the initial mass and the total mass of the n fundamental solitons confirms the absence of evaporation in the case where A is an integer.

4-3 Experimental observations

These multi-solitons were observed shortly after their prediction for light pulses propagating in optical fibers (Mollenauer, Stolen, et al. 1980). Here, we focus on their (much more recent) demonstration with matter waves by Di Carli, Colquhoun, et al. (2019) and Luo, Jin, et al. (2020).

Figure II.15 shows a series of results obtained by Luo, Jin, et al. (2020). The authors started with a fundamental soliton realized with $N = 50,000$ ^7Li atoms strongly confined along two axes ($\omega_{\perp}/2\pi = 300$ Hz), with much weaker confinement in the third direction, noted here z ($\omega_z/2\pi = 1$ Hz). At a given instant, they suddenly modify the strength g of the interactions by changing the scattering length using a Fano–Feshbach resonance. The change corresponds to $g \rightarrow A^2g$ with $A = 1.9(3)$ for the top of the figure, and $A = 2.6(4)$ for the bottom. We can check that this is equivalent to preparing the wave packet $A/\cosh x$ for the nonlinear Schrödinger equation in reduced coordinates that we have used in this chapter.

In the case $A = 1.9 \approx 2$, we obtain a composite object made up of the two elementary solitons of amplitudes 1 and 3, associated with eigenvalues $i/2$ and $3i/2$. The two coefficients $c_1(t)$ and $c_2(t)$ used to calculate the function $F(x)$ vary as $e^{4i\lambda_j^2 t}$ [cf. (II.45) and (II.47)], giving the beat frequency $\omega_B = 4(\frac{9}{4} - \frac{1}{4}) = 8$ in reduced units. We therefore expect to observe a periodic oscillation in the width of the wave packet and its central density at the frequency $\omega_B = 8$, or $\omega_B = \omega_{\perp} N^2 (a/2a_{\text{oh}})^2$ in dimensioned units where a denotes the scattering length after change.

Experimental data are in excellent agreement with this prediction. Satsuma & Yajima (1974) give the expression of the function $u(x, t)$ for this bi-soliton. We will not write it here as it is rather complicated, but we give the evolution of the central density $\rho_0(t) = |u(0, t)|^2$:

$$\rho_0(t) = \frac{8}{5 + 3 \cos(\omega_B t)} \rho_0(0) \quad (\text{II.86})$$

which leads to a variation of a factor of 4 over time. This prediction cor-

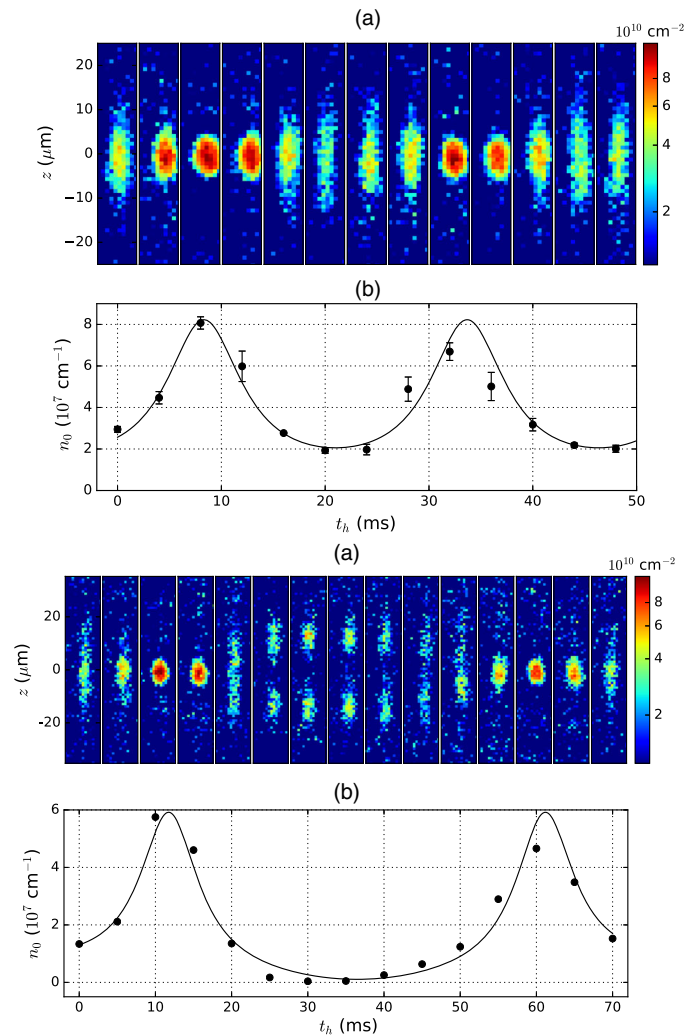


Figure II.15. Oscillations of a bi-soliton (top) and a tri-soliton (bottom) formed with lithium atoms in a harmonic trap. Figures taken from Luo, Jin, et al. (2020).

responds to the black curve shown in figure II.15 (with a shift in the time origin).

The data in the lower part of figure II.15 show the realization of a tri-soliton, i.e. an object composed of the three fundamental solitons of amplitudes 1, 3 and 5. Here too, the time evolution of the central density is a periodic function. It involves the "Bohr frequencies" $\omega_{ij} = 4|\lambda_i^2 - \lambda_j^2|$ and the experimental results are in good agreement with the predictions of the IST method.

4-4 Can a multi-soliton be decomposed?

A multi-soliton obtained by taking $A = n \in \mathbb{N}^*$ for the initial wave packet $u(x, 0) = A/\cosh x$ is a stable object. It results from the (nonlinear) combination of elementary solitons $u_j(x) = \kappa_j/\cosh(\kappa_j x)$ with amplitudes $\kappa_j = 1, 3, \dots, 2n - 1$, and its width and central density evolve periodically over time. However, this multi-soliton is not a bound state of n elementary solitons. To prove this point, we can just compare the energy of the initial wave packet [cf (II.80)]:

$$E_{\text{ini}} = -\frac{2}{3}n^2(2n^2 - 1) \quad (\text{II.87})$$

and the sum of the energies of the n constituents:

$$E_{\text{tot}} = -\sum_{j=1}^n \frac{2}{3}\kappa_j^3. \quad (\text{II.88})$$

The sum of the cubes of the first n odd numbers is precisely $n^2(2n^2 - 1)$, hence the equality between the two energies.

To decompose a multi-soliton into its elementary constituents, it is therefore sufficient in principle to introduce an element that breaks the integrability of the evolution equation. This is precisely what has been studied numerically by Marchukov, Malomed, et al. (2019). These authors calculated the behavior of a bi-soliton when a potential barrier in the form of a slightly off-center Dirac distribution is gradually applied to the system. A typical result is shown in figure II.16. It can be seen that, after the initial bi-soliton has oscillated for around 10 periods, its two components have separated, with one going to the left of the barrier and the other

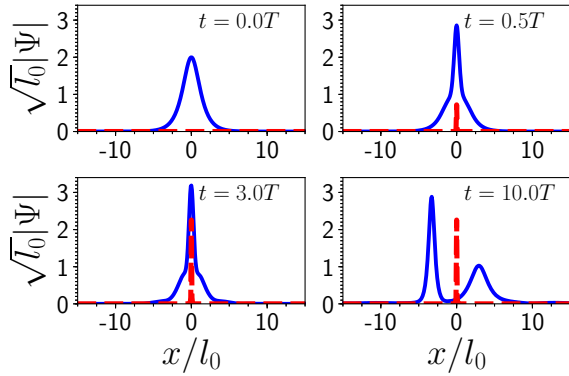


Figure II.16. Evolution of a bi-soliton when a potential barrier $V(x, t) = \epsilon f(t)\delta(x)$ is applied to the system. The barrier is slightly off-center with respect to the bi-soliton. The two components are then ejected on either side of the barrier. The time T represents the oscillation period of the bi-soliton. Figure taken from Marchukov, Malomed, et al. (2019).

to the right. One can check that the fission products are independent of the details of the barrier, i.e. its final height or decentering: the fragments are the fundamental constituents of the soliton, and the barrier is merely a "catalyst" for revealing them.

A similar result is obtained when a multi-soliton is sent over a potential barrier, with some elementary constituents being reflected while others are transmitted (Dunjko & Olshanii 2015).

Appendix: the AKNS approach

An equivalent version of the formulation adopted in this chapter is to switch from manipulating linear operators, such as \hat{L} and \hat{A} , to simple 2×2 matrices functions of x , which we will denote \hat{U} and \hat{V} (Ablowitz, Kaup, et al. 1974). The price to pay is the introduction of an additional parameter λ , which was an eigenvalue of \hat{L} in this chapter's treatment.

To present this approach for the nonlinear Schrödinger equation, let us

rewrite the system (II.24-II.25) in the form

$$\partial_x \Phi = \hat{U} \Phi \quad (\text{II.89})$$

with⁴

$$\hat{U} = \hat{U}_0 + \lambda \hat{U}_1 \quad \hat{U}_0 = \begin{pmatrix} 0 & -u \\ u^* & 0 \end{pmatrix} \quad \hat{U}_1 = \begin{pmatrix} -i & 0 \\ 0 & i \end{pmatrix}. \quad (\text{II.90})$$

Similarly, the combination of the evolution equation deduced from (II.34)

$$\Phi(t) = \hat{U}(t)\Phi(0) \quad (\text{II.91})$$

and the development (II.21) of \hat{A} into powers of λ leads to the equation

$$\partial_t \Phi = \hat{V} \Phi \quad (\text{II.92})$$

with

$$\hat{V} = \hat{V}_0 + \lambda \hat{V}_1 + \lambda^2 \hat{V}_2 \quad (\text{II.93})$$

and

$$\hat{V}_0 = i \begin{pmatrix} |u|^2 & -u_x \\ -u_x^* & -|u|^2 \end{pmatrix} \quad \hat{V}_1 = 2\hat{U}_0 \quad \hat{V}_2 = 2\hat{U}_1 \quad (\text{II.94})$$

In this point of view, λ is a time-independent parameter and the nonlinear Schrödinger equation is recovered by imposing that the two equations $\partial_x \Phi = \hat{U} \Phi$ and $\partial_t \Phi = \hat{V} \Phi$ are compatible with each other whatever λ . This compatibility condition can be deduced from

$$\partial_t (\partial_x \Phi) = \partial_x (\partial_t \Phi) \quad (\text{II.95})$$

or

$$\left(\partial_t \hat{U} - \partial_x \hat{V} + [\hat{U}, \hat{V}] \right) \Phi = 0. \quad (\text{II.96})$$

Remember that in this point of view, \hat{U} and \hat{V} are only functions of x (not operators). At any point where Φ does not cancel, we must therefore impose that the matrix acting on Φ is zero. We can check, for example by identifying the terms involving each power of λ , that this condition is satisfied if and only if $u(x, t)$ obeys the nonlinear Schrödinger equation:

$$\forall \lambda : \quad \partial_t \hat{U} - \partial_x \hat{V} + [\hat{U}, \hat{V}] = 0 \quad \Leftrightarrow \quad iu_t + u_{xx} + 2|u|^2 u = 0. \quad (\text{II.97})$$

⁴Do not confuse this matrix \hat{U} with the evolution operator \hat{U} introduced above!

The pair of matrices (\hat{U}, \hat{V}) is also called the Lax pair for this nonlinear equation.

The equation (II.96) is called *zero curvature condition* because it corresponds to the cancellation of the curvature tensor $F_{\mu,\nu} = [\partial_\mu - A_\mu, \partial_\nu - A_\nu]$.

Chapter III

Gray solitons

The first two chapters of this course were devoted to the study of condensates with attractive interactions, for which the soliton is the fundamental state of the system, at least in a one-dimensional geometry. We now turn to the case of repulsive interactions, still in a 1D or quasi-1D geometry. The solitonic structure then appears as a local depletion in a condensate of uniform or slowly varying density in space (Tsuzuki 1971). The depletion can be total, in which case we speak of a dark (or black) soliton, or partial, which is called a grey soliton. To a certain extent, these solitons can be seen as the 1D cousins of the vortices appearing in two- or three-dimensional quantum fluids.

The fact that grey solitons are generated in fluids which occupy a large region of space raises interesting questions about their theoretical description. The search for their dispersion relation, which links their energy and their momentum, is a tricky problem that we will tackle in two different geometries, that of a gas arranged on an infinite straight line and that of a gas on a ring.

Other interesting problems arise when the gas density is not uniform, but varies slowly in space. The soliton then behaves like a quasi-particle, whose equation of motion we will establish and compare with experimental observations. Finally, we will address the new questions that arise when we take into account the transverse extension of the gas, with the possibility of a grey soliton evolving into a vortex ring or a solitonic vortex.

For lack of space, we will not go through the IST approach here. Let

us simply mention that IST applies to the nonlinear Schrödinger equation in the repulsive case as well as in the attractive case explored in the previous chapter. On this subject, see the article by Del Vecchio Del Vecchio, Bastianello, et al. (2020) and its references: this article makes the link between the IST approach and generalized hydrodynamics for quantum 1D Bose gases¹, and shows how this type of system can be described in terms of a generalized Gibbs ensemble. The recent work of Bastianello, Tikan, et al. (2025) describes an implementation of this generalized Gibbs set concept on a photonic platform. In addition, see Saha & Dubessy (2025) for a study of integrable turbulence with a soliton gas, also using the IST method. We will not go into the subject of grey solitons in periodic lattices either, and refer readers interested in these problems to the review article by Frantzeskakis (2010).

1 The wave function of a grey soliton

1-1 The speed of sound in a uniform condensate

The solitons we will be considering in this chapter propagate in a condensate of uniform density ρ_0 and we will see that their speed is limited by the speed of sound waves in this condensate. In the first chapter of this lecture

¹The seminar by Jérôme Dubail on Friday March 28 was devoted to a description of this generalized hydrodynamic approach

series, we explained how to calculate this speed of sound. Let us take a brief look at the principle behind this calculation.

The dynamics of the condensate is described by the Gross–Pitaevskii equation

$$i\hbar \partial_t \psi = -\frac{\hbar^2}{2m} \partial_x^2 \psi + g|\psi|^2 \psi \quad (\text{III.1})$$

where $\psi(x, t)$ is a complex wave function. For repulsive interactions ($g > 0$), the ground state of the condensate corresponds to

$$\psi(x, t) = \sqrt{\rho_0} e^{-i\mu t/\hbar} \quad \text{with} \quad \mu = g\rho_0. \quad (\text{III.2})$$

We characterize the deviation from equilibrium by two complex numbers U and V of order 1 and a parameter $\varepsilon \ll 1$:

$$\psi(x, t) = \sqrt{\rho_0} \left\{ 1 + \varepsilon \left[U e^{i(kx-\omega t)} + V^* e^{-i(kx-\omega t)} \right] \right\} e^{-i\mu t/\hbar}. \quad (\text{III.3})$$

The dispersion relation linking k to ω is obtained by injecting this form for $\psi(x, t)$ into the Schrödinger equation and restricting ourselves to order 1 included in ε :

$$(\hbar\omega)^2 = 2\varepsilon_k g\rho_0 + \varepsilon_k^2 \quad \text{with} \quad \varepsilon_k \equiv \frac{\hbar^2 k^2}{2m}, \quad (\text{III.4})$$

which corresponds to the Bogoliubov dispersion relation.

We are interested here in the "phononic" limit of small k (long wavelength), so we can neglect the contribution of ε_k^2 and keep only $(\hbar\omega)^2 = 2\varepsilon_k g\rho_0$, which gives

$$\boxed{\omega = ck \quad \text{with} \quad c = \sqrt{g\rho_0/m}} \quad (\text{III.5})$$

Validity of the mean-field approach. Throughout this chapter, we will be using a macroscopic wavefunction $\psi(x, t)$ to describe the 1D gas. This approach is valid as long as quantum fluctuations play a negligible role, which is the case when the Lieb–Liniger parameter γ verifies:

$$\gamma \equiv \frac{gm}{\hbar^2 \rho_0} \ll 1. \quad (\text{III.6})$$

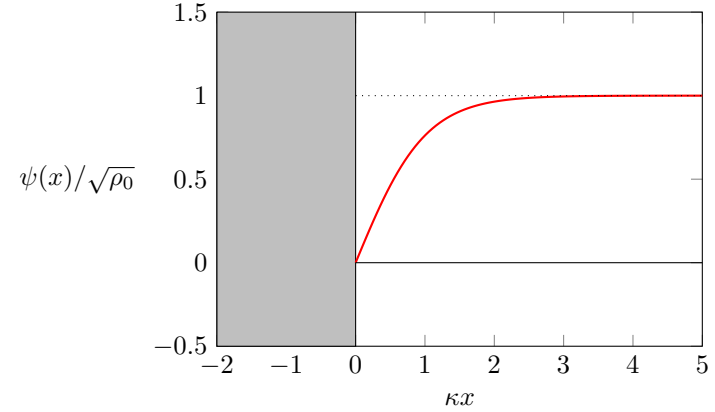


Figure III.1. Wave function $\psi(x) \propto \tanh(\kappa x)$ in the vicinity of a wall. The density $\rho(x) = |\psi(x)|^2$ becomes close to its asymptotic value ρ_0 for a distance from the wall of the order of the healing length $\xi = 1/(\kappa\sqrt{2})$.

1-2 The healing length

Before considering the case of a soliton, let us look at a 1D condensate in the presence of a wall located at $x = 0$, so that the fluid can only occupy the $x \geq 0$ part of space. We must therefore find the ground state of the fluid by imposing the wave function to cancel out on contact with the wall: $\psi(0) = 0$.

We can verify that the lowest-energy stationary solution is the wave function

$$\psi(x, t) = \sqrt{\rho_0} \tanh(\kappa x) e^{-i\mu t/\hbar} \quad (\text{III.7})$$

with

$$\boxed{\frac{\hbar^2 \kappa^2}{m} = \mu = mc^2 = g\rho_0} \quad (\text{III.8})$$

The wall thus creates a density hole over a typical length of the order of $1/\kappa$ (figure III.1). Traditionally, the *healing length* ξ is defined as

$$\xi \equiv \frac{\hbar}{\sqrt{2mg\rho_0}} \quad (\text{III.9})$$

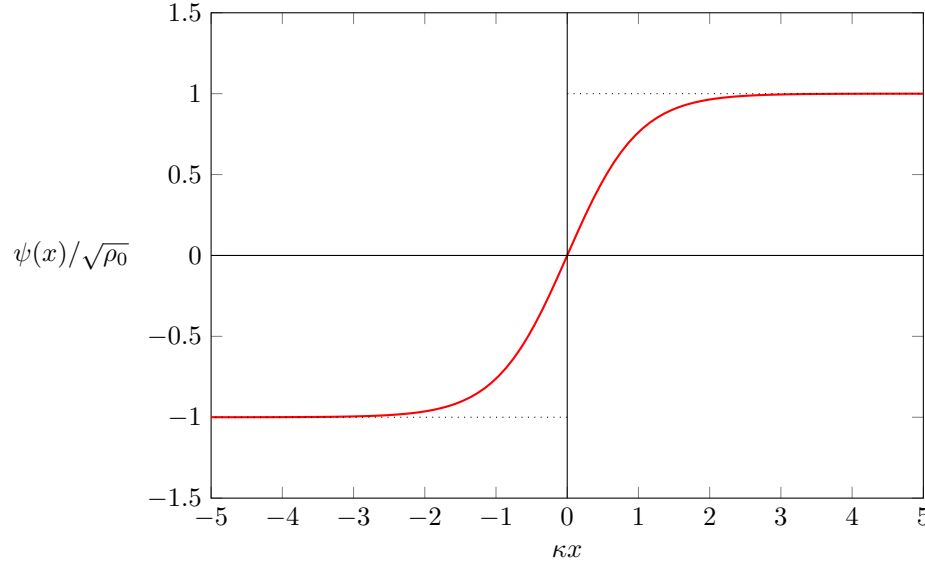


Figure III.2. Wave function $\psi(x,0)$ of a dark soliton centered in $x = 0$ [cf. eq. (III.10)].

i.e. $\xi = 1/(\kappa\sqrt{2})$. Note that the condition (III.6) on the Lieb-Lininger parameter reads $\rho\xi \gg 1$: there must be many atoms over the healing length ξ for the mean-field approximation to be valid.

1-3 Dark soliton (at rest)

The construction of a dark soliton in a condensate with repulsive interactions is straightforward once we know the result of the previous paragraph concerning the influence of a wall (figure III.2). We take the wave function

$$\psi(x,t) = \sqrt{\rho_0} \tanh(\kappa x) e^{-i\mu t/\hbar} \quad (\text{III.10})$$

over all accessible space, i.e. for x from $-\infty$ to $+\infty$. This is not the ground state of the system, which is given by the uniform wave function

$\sqrt{\rho_0} e^{-i\mu t/\hbar}$, but it is a steady state solution of the Gross-Pitaevskii equation. We can, of course, translate the position of the node of the soliton and replace the variable x by $x - x_0$, with x_0 arbitrary, in the expression of ψ .

The density associated with this wave function is written as

$$\rho(x) = \rho_0 \tanh^2(\kappa x) = \rho_0 - \frac{\rho_0}{\cosh^2(\kappa x)}. \quad (\text{III.11})$$

Its structure is therefore symmetrical with that of the bright solitons studied in the previous chapters, for which we had $\rho_{\text{bright}}(x) = \rho_0 / \cosh^2(\kappa x)$. The phase is discontinuous in $x = 0$, with a phase jump of $\pm\pi$ at this point corresponding to the change in sign of $\psi(x)$. Density and phase are plotted in figure III.3.

For the dimensionless version of the nonlinear Schrödinger equation in the repulsive case, $iu_t + u_{xx} - 2|u|^2u = 0$, the wave function corresponding to the dark soliton is

$$u(x,t) = \tanh x e^{-2it} \quad (\text{III.12})$$

1-4 The grey soliton (in motion)

In the case of bright solitons, we can pass from a soliton at rest to a soliton moving at speed v by a simple change of Galilean reference frame. The situation is different for a dark soliton, as the fluid that fills the entire space and in which the soliton is imprinted is at rest only in a particular reference frame.

We can nevertheless construct a solution to the Gross-Pitaevskii equation that corresponds to a soliton in motion, but its expression is a little more complicated than that of a soliton at rest. First, let us point out that the speed of a moving soliton cannot exceed the speed of sound: $|v| < c$. Under these conditions, it is useful to introduce the angle $\alpha \in]-\pi/2, \pi/2[$ such that

$$\alpha = \arcsin(v/c) : \quad \Rightarrow \quad \sin \alpha = \frac{v}{c} \quad \cos \alpha = \sqrt{1 - \frac{v^2}{c^2}}, \quad (\text{III.13})$$

the sign of α being the same as that of the velocity v . With this parameteri-

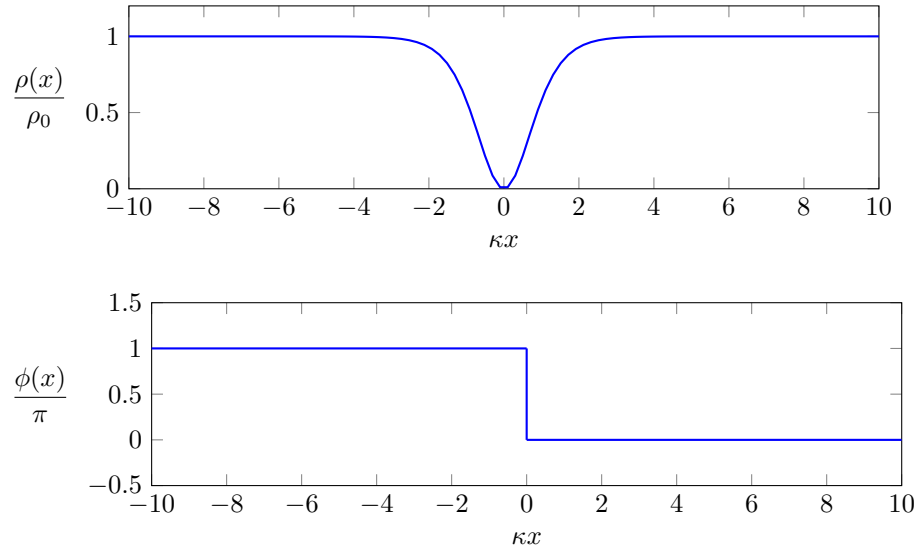


Figure III.3. Density and phase of a dark soliton centered in $x = 0$. The phase choice corresponds to $t = 0$ in (III.10).

zation, the solution we are looking for is written:

$$\psi(x, t) = \sqrt{\rho_0} \{ \cos \alpha \tanh[\kappa_v(x - vt)] + i \sin \alpha \} e^{-i\mu t/\hbar} \quad (\text{III.14})$$

with

$$\kappa_v = \kappa \sqrt{1 - \frac{v^2}{c^2}}. \quad (\text{III.15})$$

where κ is still defined by (III.8) and $\mu = g\rho_0$.

The density profile $\rho(x, t) = |\psi(x, t)|^2$ moves without deformation at speed v . For simplicity's sake, consider the time $t = 0$. We see that the density is minimal in $x = 0$, but no longer cancels out, unlike in the case of

the soliton at rest:

$$\rho(x, 0) = \rho_0 [\cos^2 \alpha \tanh^2(\kappa_v x) + \sin^2 \alpha] \quad (\text{III.16})$$

$$= \rho_0 \left[1 - \frac{\cos^2 \alpha}{\cosh^2(\kappa_v x)} \right]. \quad (\text{III.17})$$

The minimum density is $\rho_0 \times \frac{v^2}{c^2}$: the closer the soliton's velocity to the speed of sound, the smaller the density hole. The number of atoms contributing to the soliton is calculated from :

$$N_s = \int_{-\infty}^{+\infty} [|\psi(x, t)|^2 - 1] dx \quad (\text{III.18})$$

and we find:

$$N_s(\mu, v) = -2 \frac{\hbar}{g\sqrt{m}} (\mu - mv^2)^{1/2} \quad (\text{III.19})$$

also written as

$$N_s(\mu, v) = -2\sqrt{2} \rho_0 \xi \left(1 - \frac{v^2}{c^2} \right)^{1/2}. \quad (\text{III.20})$$

This number is negative, as the atoms are missing due to the density hole at the soliton. The corresponding density profile is plotted in figure III.4 (top) for $v = \pm c/2$.

For a non-zero v velocity, the phase profile shows no discontinuity (figure III.4, bottom). Again, let us take $t = 0$ in (III.14) and first choose $v > 0$. We find that

- When $x \rightarrow +\infty$, the wave function (III.14) tends towards $\rho_0 e^{i\alpha}$ and its phase $\phi(x)$ therefore tends towards the value α , which is between 0 and $\pi/2$ for $v > 0$.
- At $x = 0$, the wave function is $i\sqrt{\rho_0} \sin \alpha$. It is therefore pure imaginary and has phase $+\pi/2$ since $\sin \alpha > 0$.
- When $x \rightarrow -\infty$, the wave function (III.14) tends towards $-\rho_0 e^{-i\alpha} = \rho_0 e^{i(\pi-\alpha)}$ and its phase $\phi(x)$ tends towards the value $\pi - \alpha$, between $\pi/2$ and π .

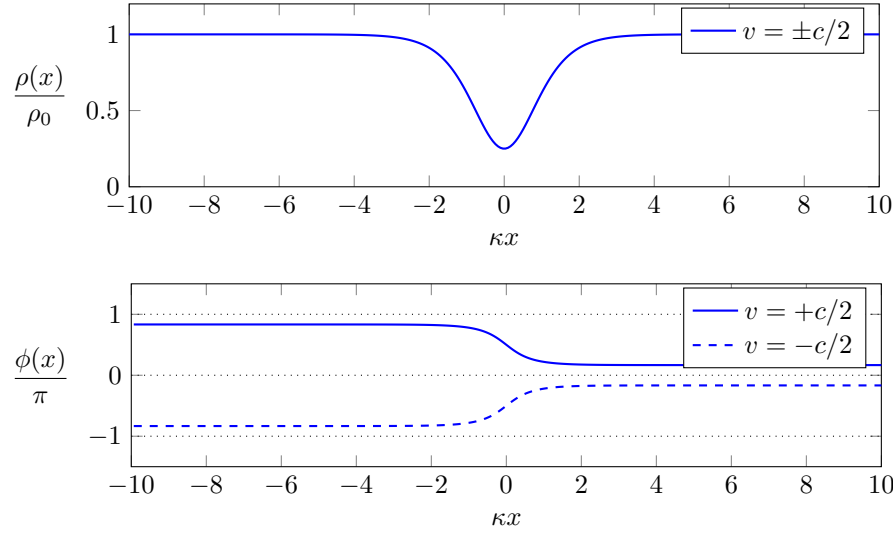


Figure III.4. Density and phase profiles for a grey soliton, here with $v = \pm c/2$. We have chosen the phase convention $\phi(0) = \pm\pi/2$.

Across the soliton and for $v > 0$, the phase variation of the wave function $\Delta\phi = \phi(+\infty) - \phi(-\infty)$ corresponds to the arc of circle from $\pi - \alpha$ to α , represented in figure III.5, top:

$$v > 0 : \quad \Delta\phi = \alpha - (\pi - \alpha) = -2 \arccos(v/c) \quad (\text{III.21})$$

where we used the fact that for x between -1 and 1 , $\arcsin x + \arccos x = \pi/2$.

Now let us take a negative velocity v (but smaller than c in absolute value), for which α is between $-\pi/2$ and 0 .

- For $x \rightarrow \infty$, we again find the value $\phi(+\infty) = \alpha$ for the phase of the wave function $\rho_0 e^{i\alpha}$.
- For $x = 0$, the wave function $i\sqrt{\rho_0} \sin \alpha$ has phase $-\pi/2$ since $\sin \alpha < 0$.
- For $x \rightarrow -\infty$, the wave function $-\rho_0 e^{-i\alpha}$ can be written $\rho_0 e^{-i(\pi+\alpha)}$, or $\phi(-\infty) = -\pi - \alpha$ if we choose this phase in the interval $]-\pi, -\pi/2[$.

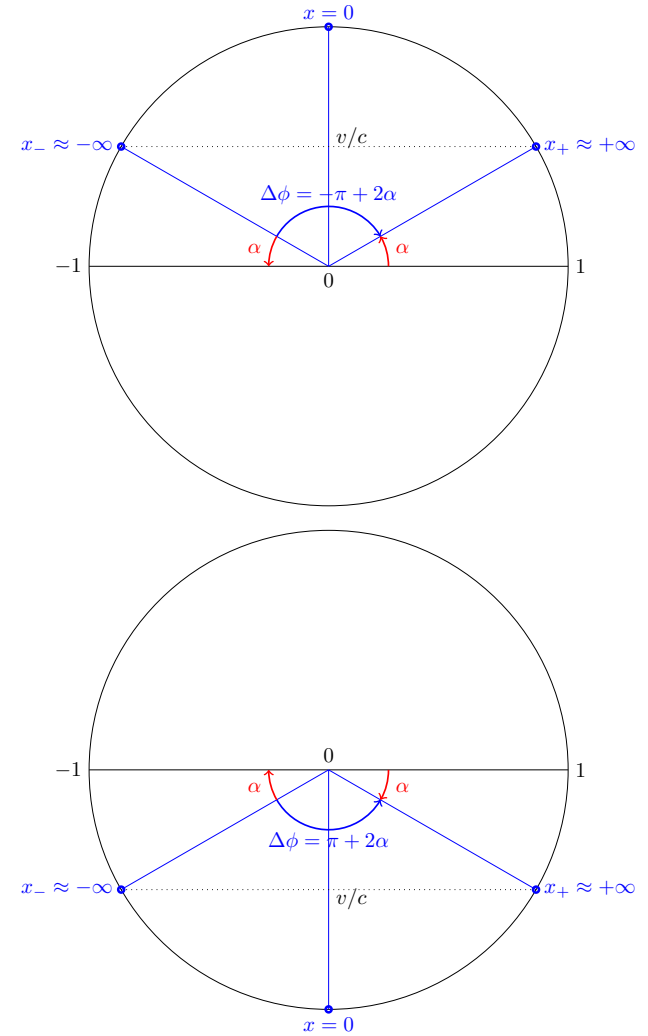


Figure III.5. Top: phase variation, here equal to the polar angle, for a grey soliton with velocity $v > 0$. By convention, we have assumed a phase of $\pi/2$ at the soliton's center, which amounts to positing $t = 0$ in (III.14). Bottom: ditto for $v < 0$. In both figures, we set $\alpha = \arcsin(v/c)$ as in (III.13), with $\alpha > 0$ for the top figure and $\alpha < 0$ for the bottom.

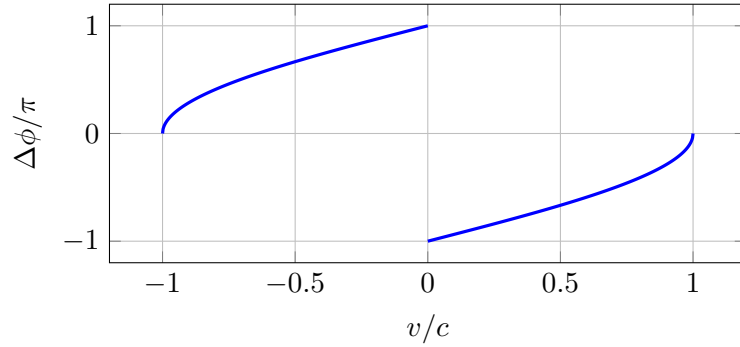


Figure III.6. Relationship between the velocity v and the phase difference $\Delta\phi$ across a moving soliton [Eqs. (III.21)-(III.22)].

When we go from $x = -\infty$ to $+\infty$, we describe the arc of a circle going from $-\pi - \alpha$ to α , represented in figure III.5, bottom:

$$\boxed{v < 0 : \quad \Delta\phi = \alpha - (-\pi - \alpha) = 2\pi - 2 \arccos(v/c)} \quad (\text{III.22})$$

With the phase convention adopted in (III.21)-(III.22), the phase variation $\Delta\phi$ tends towards 0 when the soliton velocity tends towards $\pm c$. It is discontinuous when v crosses the point of zero velocity: it tends towards $\mp\pi$ when $v \rightarrow 0_{\pm}$ (figure III.6).

Finally, let us note that in the $v \rightarrow \pm c$ limit, the soliton wave function (III.14) continuously approaches that of a uniform condensate: the number of missing atoms (III.19) tends towards 0, and the density and phase profiles become quasi-constant. This point will serve as a basis in the following paragraph for defining integration constants for velocity-dependent functions.

2 Energy and momentum of a grey soliton

2-1 Using the Gross-Pitaevskii functional

We now wish to calculate the energy required to go from a uniform condensate between $x = -\infty$ and $x = +\infty$, with density ρ_0 , to a condensate with a grey soliton of velocity v and the same asymptotic density ρ_0 . It should be noted at the outset that these two situations do not correspond to the same number of atoms, since the second is deduced from the first by digging a density hole in it. However, they do correspond to the same chemical potential $\mu = g\rho_0$.

We should therefore consider the energy functional best suited to a comparison in terms of chemical potential rather than number of atoms, i.e. the grand-potential (also known as Landau's free energy)

$$E'[\psi] = E[\psi] - \mu N[\psi] \quad (\text{III.23})$$

where $E[\psi]$ is the Gross-Pitaevskii energy functional we have already used:

$$E[\psi] = \frac{\hbar^2}{2m} \int |\partial_x \psi|^2 dx + \frac{g}{2} \int |\psi|^4 dx \quad (\text{III.24})$$

and

$$N[\psi] = \int |\psi|^2 dx. \quad (\text{III.25})$$

Since the density $\rho(x) = |\psi(x)|^2$ does not tend to 0 at infinity, some of the integrals written above are not convergent. However, the difference between solitonic and uniform solutions does converge. Using $\psi_0 = \sqrt{\rho_0}$ and $\mu = g\rho_0$, we find:

$$\begin{aligned} E_s(\mu, v) &= \{E[\psi] - \mu N[\psi]\} - \{E[\psi_0] - \mu N[\psi_0]\} \\ &= \left\{ \frac{\hbar^2}{2m} \int |\partial_x \psi|^2 + \frac{g}{2} \int |\psi|^4 - \mu \int |\psi|^2 \right\} - \left\{ \frac{g}{2} \int \rho_0^2 - \mu \int \rho_0 \right\} \\ &= \frac{\hbar^2}{2m} \int |\partial_x \psi|^2 dx + \frac{g}{2} \int (|\psi|^2 - \rho_0)^2 dx \end{aligned} \quad (\text{III.26})$$

which is indeed a convergent quantity.

We have written this free energy E_s , a function of chemical potential and soliton velocity, for a condensate of uniform density outside the soliton. However, this expression can be generalized to situations where the bath density ρ_0 (and therefore $\mu = g\rho_0$) varies with position, provided this variation remains small on the length scale κ^{-1} associated with the soliton (cf. §3-1).

Calculating $E_s(\mu, v)$ from the wave function (III.14) poses no major difficulties. We use the integral

$$\int_{-\infty}^{+\infty} \frac{dx}{\cosh^4 x} = \frac{4}{3} \quad (\text{III.27})$$

and we arrive at

$$E_s(\mu, v) = \frac{4}{3} \frac{\hbar}{g\sqrt{m}} (\mu - mv^2)^{3/2} \quad (\text{III.28})$$

Note the simple relationship between this energy and the number of atoms $N_s < 0$ calculated in (III.19):

$$E_s = -\frac{mg^2}{6\hbar^2} N_s^3 \quad (\text{III.29})$$

which is similar (except for a numerical factor) to that found for a bright soliton in Chapter 1.

Note that the number of atoms N_s can be found from the relation

$$N_s = -\left(\frac{\partial E_s}{\partial \mu}\right)_v \quad (\text{III.30})$$

See Pitaevskii (2016) for an in-depth discussion of this relationship, applied to more complex situations, in particular those involving quantum gas mixtures.

2-2 Local momentum vs. total momentum

In the first chapter of this lecture series, we indicated that for any wave function $\psi(x, t)$ solution of the Gross-Pitaevskii equation, the momentum

defined by

$$P[\psi] = -i\hbar \int \psi^* (\partial_x \psi) dx \quad (\text{III.31})$$

is a constant of motion.

For the solitons we have considered here, the wave function $\psi(x)$ varies significantly around the soliton node. We can give ourselves two points x_- and x_+ located on either side of this node, at a sufficiently large distance (several κ_v^{-1}) for the density to have resumed its asymptotic value ρ_0 . It is then tempting to write $P \approx P_{\text{loc}}$ with

$$P_{\text{loc}} = -i\hbar \int_{x_-}^{x_+} \psi^* (\partial_x \psi) dx, \quad (\text{III.32})$$

where "loc" stands for *local*. This quantity is zero for the uniform wave function $\psi_0 = \sqrt{\rho_0}$ and its value for the wave function (III.14) describing a grey soliton is:

$$P_{\text{loc}}(\rho_0, v) = -2\hbar\rho_0 \frac{v}{c} \left(1 - \frac{v^2}{c^2}\right)^{1/2} \quad (\text{III.33})$$

This momentum P_{loc} is plotted as a red dashed line on figure III.7. It cancels out when $v \rightarrow \pm c$, since in this limit we recover the wave function of a uniform condensate. It also cancels out at $v = 0$.

This local momentum can be written as a function of the number of missing atoms N_s calculated in (III.19):

$$P_{\text{loc}} = N_s m v \quad (\text{III.34})$$

which corresponds to the expected momentum for a hole of N_s missing particles, moving at speed v .

There is another way of calculating the momentum of a system, in the Lagrangian sense of the term, when we know the relationship between its energy and its velocity. We will call this momentum *total*, as opposed to the local momentum defined above. This total momentum is also called the *canonical momentum* and is the conjugate variable of velocity. The starting point is the relation

$$v = \left(\frac{\partial E_s}{\partial P}\right)_\mu \quad (\text{III.35})$$

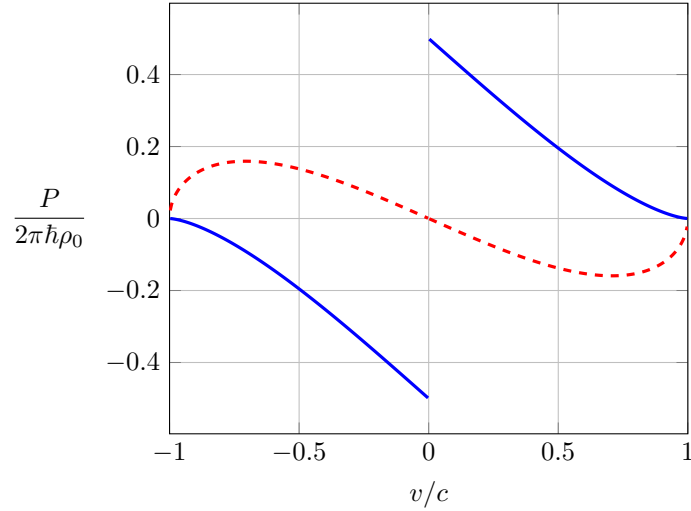


Figure III.7. Local momentum P_{loc} (red dashed curve) and total momentum P (blue solid curve) for a grey soliton as a function of its velocity v .

where the derivative is taken holding constant the other intensive parameters, in this case the chemical potential μ or equivalently the asymptotic density ρ_0 . This relationship is inverted to express P as a function of v and μ .

$$\text{with } \mu \text{ constant : } dP = \frac{dE_s}{v} = \left(\frac{\partial E_s}{\partial v} \right)_{\mu} \frac{dv}{v} \quad (\text{III.36})$$

which gives for a positive speed

$$v > 0 : \quad P(\mu, c) - P(\mu, v) = \int_v^c \left(\frac{\partial E_s}{\partial v} \right)_{\mu} \frac{dv'}{v'} \quad (\text{III.37})$$

The momentum $P(\mu, c)$ will be taken to be zero, since the soliton wave function tends towards that of a uniform condensate when $|v| \rightarrow c$. We then find

$$v > 0 : \quad P(\mu, v) = P_{\text{loc}}(\mu, v) + 2\hbar\rho_0 \arccos(v/c) \quad (\text{III.38})$$

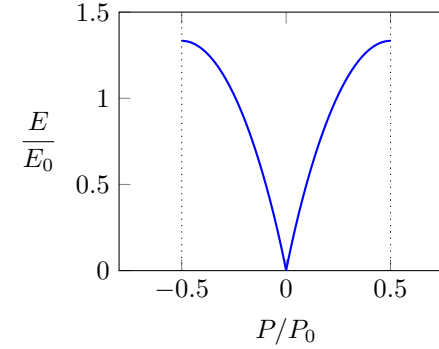


Figure III.8. Dispersion relation of a grey soliton: variation of energy E with momentum P . Units are $P_0 = 2\pi\hbar\rho_0$ and $E_0 = (\hbar^2 g \rho_0^3 / m)^{1/2}$.

The same reasoning can be used for a negative velocity v :

$$v < 0 : \quad P(\mu, v) - P(\mu, -c) = \int_{-c}^v \left(\frac{\partial E_s}{\partial v} \right)_{\mu} \frac{dv'}{v'} \quad (\text{III.39})$$

which gives, after setting $P(\mu, -c) = 0$ by continuity:

$$v < 0 : \quad P(\mu, v) = P_{\text{loc}}(\mu, v) + 2\hbar\rho_0 [\arccos(v/c) - \pi] \quad (\text{III.40})$$

We can combine the two results (III.38, III.40) in the form

$$P(\mu, v) = P_{\text{loc}}(\mu, v) - \hbar\rho_0 \Delta\phi \quad (\text{III.41})$$

where $\Delta\phi \equiv \phi(+\infty) - \phi(-\infty)$ represents the phase difference on either side of the soliton [see (III.21-III.22)].

The variation of the total momentum with soliton velocity is plotted in figure III.7 as a solid line (blue curve). It cancels out by construction at $v = \pm c$. It is discontinuous in $v = 0$:

$$v \rightarrow 0_{\pm} : \quad P(\mu, v) \rightarrow \pm\pi\hbar\rho_0. \quad (\text{III.42})$$

Similarly, we have plotted in figure III.8 the dispersion relation $E(P)$ for P varying between the two extreme values found above, $\pm\pi\hbar\rho_0$.

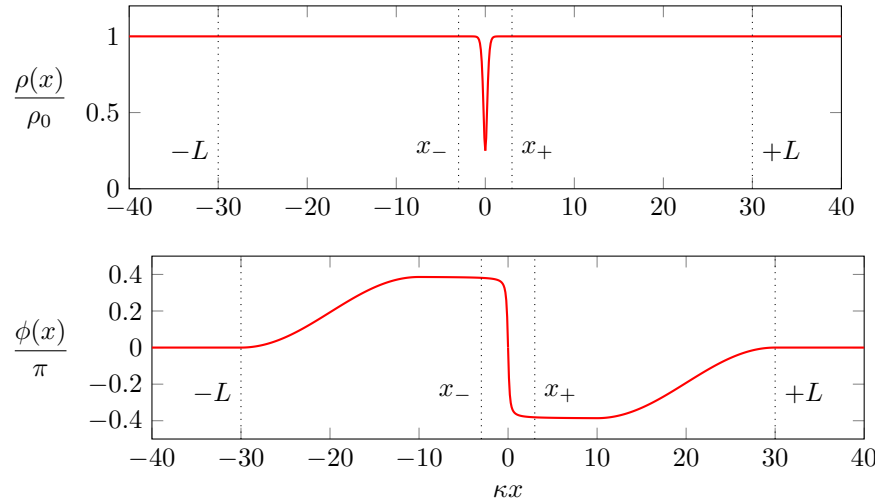


Figure III.9. A solitonic wavefunction "prepared" starting from a uniform condensate, by removing N_s particles in the vicinity of $x = 0$ and imparting the expected phase profile between x_- and x_+ . The preparation is local, in the sense that it has no effect on the fluid beyond the distance L .

2-3 Why two momenta? The case of a straight line

It is, of course, surprising to find two different results for the momentum, depending on whether it is calculated directly from the gradient of the wave function or using a Lagrangian approach, based on the relationship between energy and velocity.

This difference can be explained by considering how to prepare a soliton in a real experiment. Starting with a uniform condensate of density ρ_0 , we need to act on it to remove N_s atoms and "imprint" the desired density and phase profiles to prepare a soliton of velocity v , for example in the vicinity of the origin $x = 0$. But such an imprint cannot simultaneously affect all points on the x axis, which is assumed here to be infinite. It will concern a finite region of the axis, say between $-L$ and L , with the rest of the wave function remaining unchanged as shown in figure III.9. The

result is a density and phase profile like those shown in the figure. The soliton itself is concentrated in the $x_- < x < x_+$ zone, with $|x_{\pm}|$ of the order of a few κ_v^{-1} , and the $|x_{\pm}| < |x| < L$ zone is one of uniform density ρ_0 , in which the phase connects smoothly to 0 beyond $x = \pm L$.

It is easy to see, then, that the assumption we made when moving from (III.31) to (III.32), namely that $\psi(x)$ does not vary outside the interval $[x_-, x_+]$, is incorrect in this case. More precisely, let us evaluate the momentum to be supplied to the condensate to go from the uniform state to the profile shown in figure III.9. Let us start with the integral

$$\Delta P_{\text{supplied}} = -i\hbar \int_{-\infty}^{+\infty} \psi^* (\partial_x \psi) dx \quad (\text{III.43})$$

and separate the x axis into several regions:

- The parts $|x| < |x_{\pm}|$ are areas where the density and phase of the soliton vary significantly, and this variation is identical to that of the soliton considered in the previous section. The result for the integral $\int_{x_-}^{x_+}$ is therefore the same as that found for P_{loc} in (III.33).
- The zones $|x_{\pm}| < |x| < L$ are zones of uniform density and slowly varying $\phi(x)$ phase. Their contribution to the integral is

$$\hbar\rho_0 \left[\int_{-L}^{x_-} \partial_x \phi + \int_{x_+}^{+L} \partial_x \phi \right] = \hbar\rho_0 [\phi(x_-) - \phi(-L) + \phi(+L) - \phi(x_+)] \quad (\text{III.44})$$

The $\phi(\pm L)$ values are equal by construction, since the starting condensate, of uniform phase, has not been affected at these points. The quantity $\phi(x_+) - \phi(x_-)$ corresponds to the phase difference $\Delta\phi$ between the two sides of the soliton [cf. (III.21-III.22)].

- The parts $|x| > L$ do not contribute since the wave function has not been affected in these areas.

The momentum to be supplied to the system to go from a uniform condensate to the wave function represented in figure III.9 is therefore:

$$\Delta P_{\text{supplied}} = P_{\text{loc}} - \hbar\rho_0 \Delta\phi + 0. \quad (\text{III.45})$$

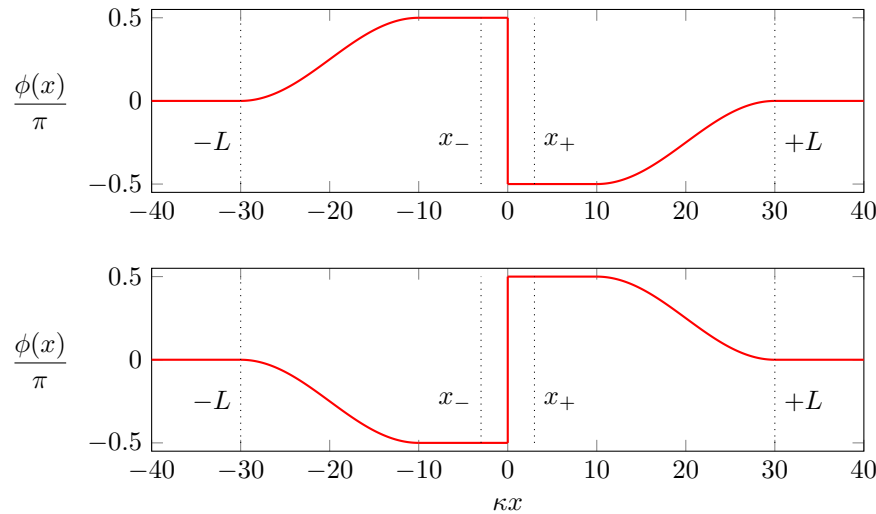


Figure III.10. Two phase profiles leading to a dark soliton (zero velocity) at $x = 0$. The total momentum transferred during the preparation is $+\pi\hbar\rho_0$ for the top profile and $-\pi\hbar\rho_0$ for the bottom profile.

This expression coincides with the total momentum expression given in (III.41). This is the Lagrangian expression to use when dealing with momentum exchange problems in the infinite gas in the presence of a soliton.

Note the rather unusual situation that arises for a soliton at rest. In this case, the two phase impressions shown in figure III.10 lead to the same result, i.e. the π phase jump at the density hole. However, the momenta supplied to the system are different: $+\pi\hbar\rho_0$ for the top choice and $-\pi\hbar\rho_0$ for the bottom choice.

2-4 Why two momenta? The case of a ring

Another way of approaching the problem, which leads to an equivalent result, is to place the gas on a ring, which means choosing periodic boundary conditions for the wave function $\psi(x)$, posing $\psi(-L/2) = \psi(L/2)$ for

a ring of perimeter L . This produces a phase profile of the type shown in figure III.11.

Calculating the momentum² required to prepare the fluid in this state is carried out in a similar way to that used above for an infinite straight line. Starting from

$$\Delta P_{\text{supplied}} = -i\hbar \int_{-L/2}^{+L/2} \psi^* (\partial_x \psi) dx, \quad (\text{III.46})$$

we can cut the integral into three pieces:

- The part $|x| < |x_{\pm}|$ gives the result P_{loc} found in (III.33).
- The two parts $|x_{\pm}| < |x| < L/2$ correspond to zones of uniform density, and contribute to $\Delta p_{\text{supplied}}$ because of the phase gradient required to maintain periodic boundary conditions. For the contribution of these two zones, we find:

$$\begin{aligned} \hbar\rho_0 \left[\int_{-L/2}^{x_-} \partial_x \phi + \int_{x_+}^{L/2} \partial_x \phi \right] &= \hbar\rho_0 [\phi(x_-) - \phi(-L/2) + \phi(L/2) - \phi(x_+)] \\ &= \hbar\rho_0 (-\Delta\phi + 2n\pi) \end{aligned} \quad (\text{III.47})$$

where $\Delta\phi = \phi(x_+) - \phi(x_-)$ and where $n \in \mathbb{Z}$ stands for the winding of the phase. Indeed periodic boundary conditions $e^{i\phi(L/2)} = e^{i\phi(-L/2)}$ entail that $\phi(-L/2) = \phi(L/2) + 2n\pi$.

The sum of these contributions shows that the momentum to be supplied is

$$P = P_{\text{loc}} - \hbar\rho_0 \Delta\phi + n 2\pi\hbar\rho_0 \quad n \in \mathbb{Z} \quad (\text{III.48})$$

The current flowing in the ring outside the soliton region is called the *back-flow current*. It carries the momentum

$$P_{\text{bf}} = -\hbar\rho_0 \Delta\phi + n 2\pi\hbar\rho_0 \quad (\text{III.49})$$

which is of the same order of magnitude as the local soliton momentum, at least for small values of n (see figure III.7 where these two momenta are plotted). The velocity v_{bf} of the backflow current can be deduced from

²In this ring geometry, it would be more appropriate to speak of angular momentum.

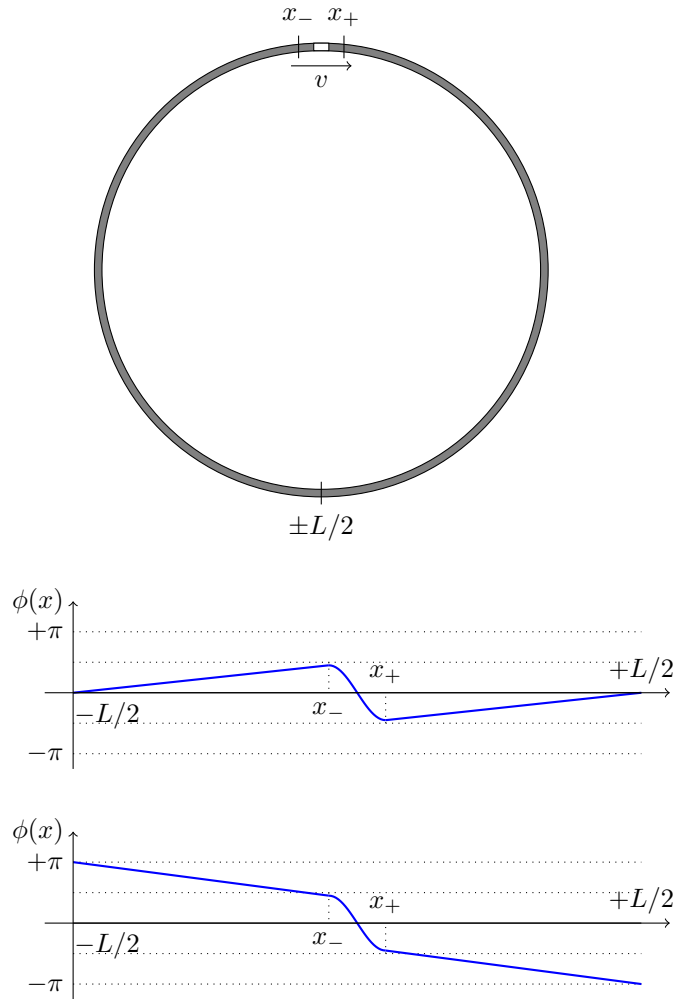


Figure III.11. Dark soliton on a closed ring. The two contributions to the total momentum result from (i) the current between x_- and x_+ corresponding to P_{loc} , (ii) the phase gradient over the rest of the ring $x_+ \rightarrow \pm L/2 \rightarrow x_-$. The two phase profiles shown here correspond to a winding number $n = 0$ and $n = 1$ in (III.47).

the above, using the fact that in the uniform density part ρ_0 , the velocity is equal to $\frac{\hbar}{m} \partial_x \phi$, which gives in the limit $|x_{\pm}| \ll L$:

$$v_{\text{bf}} = \frac{\hbar}{mL} (-\Delta\phi + 2n\pi). \quad (\text{III.50})$$

The variation of the phase change $\Delta\phi$ with the soliton velocity is plotted in figure III.6. Let us mention that Carr, Clark, et al. (2000) have searched for all *stationary* solutions of the Gross–Pitaevskii 1D equation in a ring, i.e. solutions such that the velocity of the backflow current exactly compensates for the natural velocity of the grey soliton.

Note. Even if the momentum associated with the backflow current is significant, its energy cancels out at the thermodynamic limit $L \rightarrow +\infty$ at constant ρ_0 . As the phase difference $\Delta\phi$ is distributed over the entire perimeter of the ring (outside the small arc x_-, x_+), the velocity associated with it in the zone of uniform density is $\sim \frac{\hbar}{mL} \Delta\phi$, which leads to the kinetic energy for the $N = \rho_0 L$ particles concerned:

$$\frac{1}{2} m N v^2 \sim \frac{\hbar^2 \rho_0}{2mL} (\Delta\phi)^2 \quad (\text{III.51})$$

which decreases as $1/L$ at the thermodynamic limit. The same applies to the velocity derived from the quantized component $n 2\pi\hbar\rho_0$, at least for small values of the integer n . We deduce that the dispersion relation $E(P)$ of a grey soliton in a ring at the thermodynamic limit is a periodic function of momentum, since we can add the quantum $2\pi\hbar\rho_0$ to P without changing the energy. The dispersion relation shown in figure III.8 can therefore be extended to give the one shown in figure III.12.

2-5 Effective soliton mass

We define the effective mass M_s of the soliton by

$$\frac{1}{M_s} = \left(\frac{\partial^2 E_s}{\partial P^2} \right)_{\mu} \quad (\text{III.52})$$

or

$$\frac{1}{M_s} = \left(\frac{\partial v}{\partial P} \right)_{\mu} \quad \text{since} \quad v = \left(\frac{\partial E_s}{\partial P} \right)_{\mu}. \quad (\text{III.53})$$

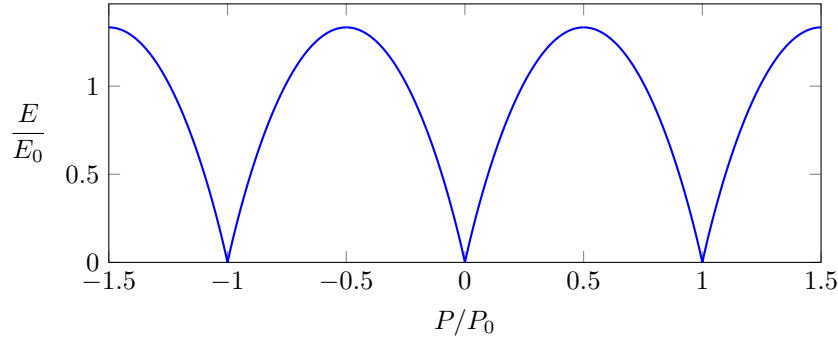


Figure III.12. Dispersion relation of a grey soliton in a ring of radius $R \rightarrow \infty$: variation of energy E with momentum P . The units are $P_0 = 2\pi\hbar\rho_0$ and $E_0 = (\hbar^2 g \rho_0^3 / m)^{1/2}$.

Using $E_s(\mu, P) = E_s[\mu, v(\mu, P)]$, we also have

$$\left(\frac{\partial E_s}{\partial P}\right)_\mu = \left(\frac{\partial E_s}{\partial v}\right)_\mu \left(\frac{\partial v}{\partial P}\right)_\mu \quad \Rightarrow \quad v = \left(\frac{\partial E_s}{\partial v}\right)_\mu \frac{1}{M_s}, \quad (\text{III.54})$$

which allows this effective mass to be put into the form:

$$M_s = \frac{1}{v} \left(\frac{\partial E_s}{\partial v}\right)_\mu. \quad (\text{III.55})$$

Using the explicit form $E_s(\mu, v)$ given in (III.28) and the expression (III.19) for N_s , we then find:

$$\boxed{M_s = 2mN_s} \quad (\text{III.56})$$

this mass being negative since N_s is negative.

The origin of the factor 2 in the above relationship is explained by the existence of the backflow current. For simplicity's sake, let us consider a gas with a soliton of zero initial velocity, and look for the momentum that needs to be applied to this gas to set the soliton in motion at velocity $\delta v \ll c$. The initial local momentum calculated from (III.33) is zero and the final local momentum is $\delta P_{\text{loc}} \approx -2\hbar\rho_0 \delta v/c$. The initial momentum due to the backflow current $P_{\text{bf}} = \pi\hbar\rho_0$ and its final value, deduced from (III.21)

and (III.49), is $P_{\text{cc}} \approx (\pi - 2\delta v/c)\hbar\rho_0$, i.e. a change $\delta P_{\text{cc}} \approx -2\hbar\rho_0 \delta v/c$. We therefore find that setting the soliton in motion requires the total momentum

$$\delta P = \delta P_{\text{loc}} + \delta P_{\text{bf}} \quad \text{with} \quad \delta P_{\text{loc}} \approx \delta P_{\text{bf}} \approx -2\hbar\rho_0 \frac{\delta v}{c}. \quad (\text{III.57})$$

The effective mass, deduced from $M_s = \delta P / \delta v$, therefore contains two contributions which are found to be equal in the case of zero initial velocity: $M_s \approx -4\hbar\rho_0/c$ to be compared with the number of atoms associated with the soliton deduced from (III.19): $mN_s \approx -2\hbar\rho_0/c$. In other words, the effective mass takes into account the fact that, in order to set the soliton in motion, it is necessary to count not only the momentum linked to the depletion motion, but also the change in momentum of the backflow current, both contributions being equal for a soliton initially at rest.

3 Gray soliton dynamics

3-1 The soliton seen as a quasi-particle

Consider a condensate at equilibrium in a potential $V(x)$, with chemical potential μ_0 . Let us further assume that a dark soliton profile has been imprinted in the vicinity of a point x in the condensate, and that the density of the condensate varies only slightly over the characteristic soliton length scale κ_v^{-1} , evaluated for the local density $\rho(x)$. In practice, this condition is satisfied if the condensate is in the Thomas-Fermi regime, discussed below. We can then treat the soliton as a quasiparticle and study its motion in the local density approximation. This approach is justified in detail by Konotop & Pitaevskii (2004) [see also Brazhnyi & Konotop (2003), Theocharis, Schmelcher, et al. (2005), and Brazhnyi, Konotop, et al. (2006)].

In this approach, we use the chemical potential at the soliton position

$$\mu(x) = \mu_0 - V(x) \quad (\text{III.58})$$

to deduce its energy $\mathcal{E}(x, v)$ as a function of its position x and velocity v . This energy is equal to the free energy calculated above for a soliton in a

uniform condensate [cf. (III.28)].

$$\mathcal{E}(x, v) \equiv E_s[\mu(x), v] = \frac{4\hbar}{3g\sqrt{m}} [\mu(x) - mv^2]^{3/2} \quad (\text{III.59})$$

and the soliton's equation of motion can be obtained directly by writing that $\mathcal{E}(x, v)$ is a constant of motion as the soliton's position x and velocity v change over time. We then write:

$$0 = \frac{d\mathcal{E}}{dt} = \left(\frac{\partial E_s}{\partial \mu} \right)_v \frac{d\mu}{dx} \frac{dx}{dt} + \left(\frac{\partial E_s}{\partial v} \right)_\mu \frac{dv}{dt}. \quad (\text{III.60})$$

A simple calculation using the explicit relation (III.28) giving E_s as a function of μ and v then leads to:

$$\boxed{2m \frac{dv}{dt} = f(x)} \quad (\text{III.61})$$

where the force $f(x)$ derives from the potential $V(x)$:

$$f(x) = -\frac{dV}{dx} = \frac{d\mu}{dx}. \quad (\text{III.62})$$

So it is as if the soliton were a particle of mass $2m$ feeling the same force as the atoms in the condensate.

In general, the relation (III.60) expressing the conservation of energy $E_s[\mu - V(x), v]$ is written as³

$$0 = -N_s f(x) v + M_s v \frac{dv}{dt} \quad \Rightarrow \quad \boxed{M_s \frac{dv}{dt} = N_s f(x)} \quad (\text{III.63})$$

with the relationships already mentioned in (III.30) and (III.55):

$$N_s = -\left(\frac{\partial E_s}{\partial \mu} \right)_v \quad M_s v = -\left(\frac{\partial E_s}{\partial v} \right)_\mu, \quad (\text{III.64})$$

³We can also work with the variables (μ, P) rather than (μ, v) . We then have

$$0 = -N'_s f(x) v + v \frac{dP}{dt} \quad \Rightarrow \quad \frac{dP}{dt} = N'_s f(x)$$

with

$$N'_s = -\left(\frac{\partial E_s}{\partial \mu} \right)_P \quad v = \left(\frac{\partial E_s}{\partial P} \right)_\mu.$$

in accordance with (III.61) after multiplication of both equation members by N_s and the relationship $M_s = 2mN_s$ found in (III.56). This form can be interpreted as the equation of motion of an object of negative mass M_s under the effect of the "collective" force $N_s f$, with N_s also negative. From this point of view, the fact that the soliton is accelerated in the same direction as the atoms in the condensate results from the compensation between these two negative signs.

Remarkably, the soliton's motion occurs without any change of shape, even if the bath is not of constant density. To demonstrate this, we can first note that the relationship between the energy and the number of missing atoms, $\mathcal{E} = -\frac{mg^2}{6\hbar^2} N_s^3$, implies that N_s is constant since \mathcal{E} is. More precisely, the profile of the density hole itself remains unchanged, as can be seen from the wave function (III.14). The position-dependent part, i.e. the real part of the brace, can be written:

$$\frac{1}{\sqrt{g}} (\mu - mv^2)^{1/2} \tanh \left[\frac{\sqrt{m}}{\hbar} (\mu - mv^2)^{1/2} x(t) \right] \quad (\text{III.65})$$

so that the amplitude and width of this density hole remain constant, since $\mu - mv^2$ is independent of time. Only the position of the soliton x and the amplitude $\frac{v}{c} \sqrt{\rho}$ of the imaginary part of the brace, i.e. the residual density at the center of the soliton, vary with time.

Figure III.13 shows the numerical calculation of the evolution of a soliton initially at rest, i.e. dark, prepared at the center of a condensate confined in a segment and subjected to a constant force f , i.e. a linear potential $V(x) = -fx$. The total number of atoms is sufficiently large for the spatial profile of the condensate to be given as a good approximation by the Thomas-Fermi approximation⁴:

$$g\rho(x) + V(x) = \mu_0 \quad \Rightarrow \quad \rho(x) = \frac{\mu_0}{g} + \frac{fx}{g} \quad (\text{III.66})$$

The condensate state is prepared by performing an imaginary-time evolution of the Gross-Pitaevskii equation, with the constraint $\psi(x) = 0$ at the

⁴This approximation amounts to neglecting the kinetic energy term in the Gross-Pitaevskii equation giving the equilibrium form of the condensate:

$$-\frac{\hbar^2}{2m} \partial_x^2 \psi + [g|\psi(x)|^2 + V(x)] \psi(x) = \mu_0 \psi(x).$$

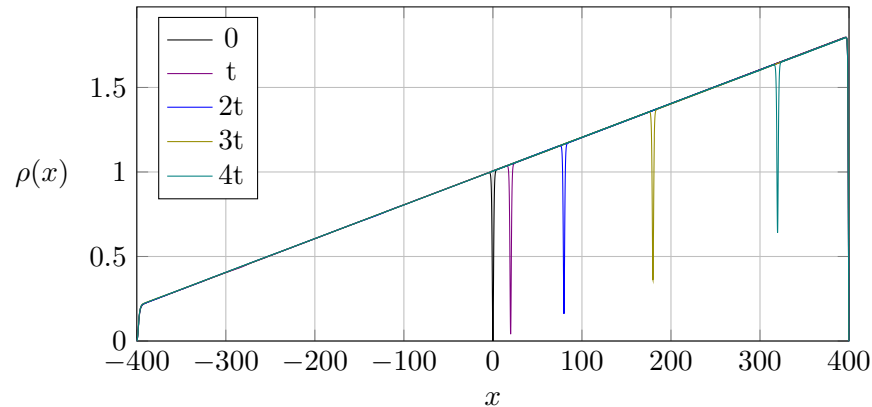


Figure III.13. Evolution of a dark soliton under the effect of a force directed to the right. The motion of the soliton center is in excellent agreement with $x = ft^2/4m$, i.e. an acceleration $a = f/2m$ (calculated with a grid of 8192 points).

center of the segment. This constraint is then removed for the real-time evolution shown in figure III.13 and we see that the soliton moves in the direction of the force with a uniformly accelerated motion, and an acceleration equal to $f/2m$ as expected from (III.61).

3-2 Oscillation in a harmonic trap

The results of the previous paragraph, obtained for a uniform force, can be generalized to any type of potential $V(x)$ provided that the approximation allowing the soliton to be treated as a quasiparticle is valid. A remarkable situation is obtained for harmonic confinement along the x axis: $V(x) = m\omega^2 x^2/2$ (Busch & Anglin 2000). In this case, the force $f(x)$ is equal to $-m\omega^2 x$, so the equation of motion (III.61) is written:

$$\frac{d^2x}{dt^2} + \frac{\omega^2}{2}x = 0 \quad (\text{III.67})$$

which indicates that the soliton oscillates with frequency $\omega/\sqrt{2}$.

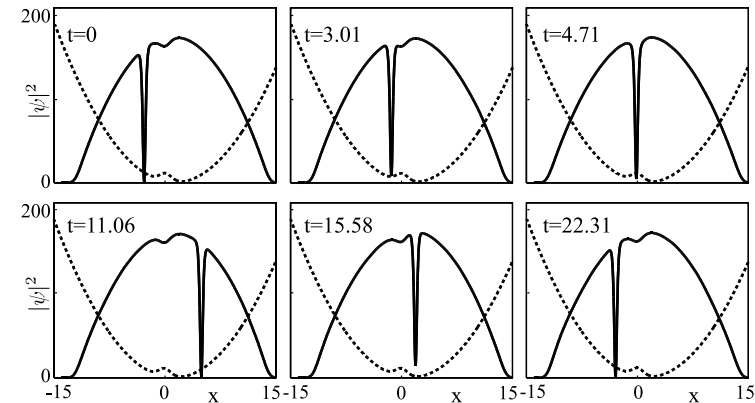


Figure III.14. Motion of a soliton in a 1D condensate confined in a (nearly) harmonic potential of frequency ω (the authors have added a slight potential bump near the center). The number of atoms is sufficiently large for the equilibrium form of the condensate (apart from the soliton) to be well described by the Thomas-Fermi approximation. The frequency of the oscillating motion is close to $\omega/\sqrt{2}$. Figure taken from Busch & Anglin (2000).

This prediction is verified numerically (see figure III.14) and remains valid even if the amplitude of the soliton's oscillation is not small compared to the size of the condensate. The turning points of the soliton's oscillating motion (where its velocity cancels out) correspond to complete depletion. The soliton's oscillation can be superimposed on an oscillation of the condensate's center of mass in the harmonic trap.

The simplicity of the equation of motion (III.67) can be deceptive. It is only valid in an ideal system, i.e. a perfectly condensed gas described by the Gross-Pitaevskii equation, i.e. at zero temperature. If the temperature is non-zero, energy dissipation towards already populated phonon modes may occur. More precisely, for an ordinary oscillator, energy dissipation has the effect of driving the oscillator towards the center of the trap with zero velocity (we are neglecting quantum effects here). But for our soliton,

the energy (III.28) is written:

$$E_s(x, v) = \frac{4}{3} \frac{\hbar}{g\sqrt{m}} \left(\mu_0 - \frac{1}{2} m\omega^2 x^2 - mv^2 \right)^2. \quad (\text{III.68})$$

In a 3D gas, for which the Gross-Pitaevskii equation is not integrable, a dissipative mechanism linked to phonon scattering can irreversibly increase the quantity $\frac{1}{2}m\omega^2 x^2 + mv^2$, thus accelerating the soliton towards the edge of the condensate, which then makes it disappear. This is a thermodynamic instability, which translates into the existence of excitations with negative energy. Muryshev, Shlyapnikov, et al. (2002) show that the typical lifetime of the soliton then decreases as $1/T$ in the regime where the temperature T is greater than μ_0/k_B .

Another type of instability, called *dynamic instability* (like that encountered in Chapter 1), results in the existence of excitations with complex energy, leading to an exponential growth of seeds coming from initial noise. This type of instability is absent in the strictly 1D case studied here. On the other hand, for a soliton in an elongated 3D trap, dynamic instability can arise when the chemical potential μ_0 becomes comparable to or greater than the characteristic energy of the transverse confinement $\hbar\omega_\perp$. We will come back to this in § 4.

Quantum treatment of soliton motion. In this chapter, we have used a classical field equation, the Gross-Pitaevskii equation, to treat the motion of a grey soliton. These solitons can be found also in the quantum treatment of a 1D gas, and they then appear as wave packets formed from type II Lieb excitations [see articles by Wadkin-Snaith & Gangardt (2012) and Del Vecchio Del Vecchio, Bastianello, et al. (2020) and their references]. In this quantum treatment, solitons acquire a finite lifetime, even in a strictly 1D geometry and at zero temperature, as soon as they evolve in a bath of variable density $\rho(x)$ (this is enough to break the integrability of the problem). Moving solitons radiate phonons in a process formally analogous to the electromagnetic radiation of an accelerated charged particle. Wadkin-Snaith & Gangardt (2012) evaluate the corresponding lifetime, which remains large in front of the oscillation period as long as the amplitude of the soliton's motion remains significantly smaller than the extension of the condensate.

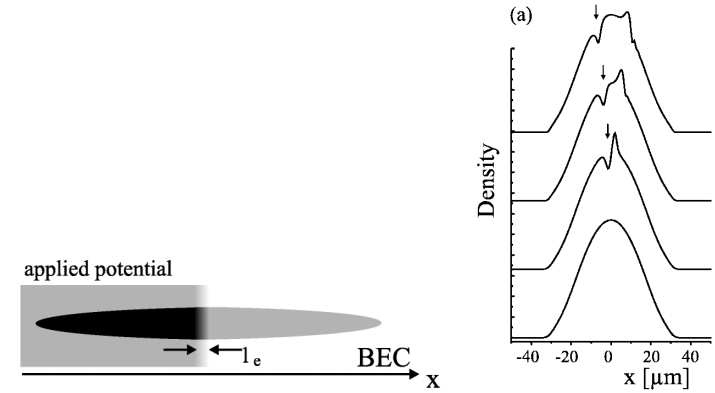


Figure III.15. Left: principle of the phase impression of a soliton on an elongated condensate. Right: numerical solution of the Gross-Pitaevskii equation, showing the creation of a density wave leaving behind a depleted zone of low velocity, corresponding to a grey soliton with $\Delta\phi = 2\pi/3$. The evolution times are (from bottom to top): 0, 1, 3, 5 ms. Figure taken from Burger, Bongs, et al. (1999).

3-3 Experimental observations

The first grey solitons in Bose-Einstein condensates were produced experimentally by Burger, Bongs, et al. (1999) and Denschlag, Simsarian, et al. (2000). In both experiments, the soliton is produced by phase printing. One half of the condensate is illuminated by a non-resonant laser beam for a short time τ (figure III.15, left). The illuminated part acquires a phase ϕ proportional to the light intensity and duration τ , which is adjusted to $\phi \sim \pi$. At the boundary between light and dark, the strong phase gradient induces a current that sets a density wave in motion (figure III.15, right). This movement leaves behind a density hole corresponding (roughly) to the desired soliton.

In these early experiments and those that immediately followed, such as Anderson, Haljan, et al. (2001) and Ginsberg, Brand, et al. (2005), the soliton's lifetime was short, less than ten milliseconds. This was due both to dynamic instabilities of the soliton when the trap shape was too far from the ideal 1D situation, and to thermodynamic instabilities when the ther-

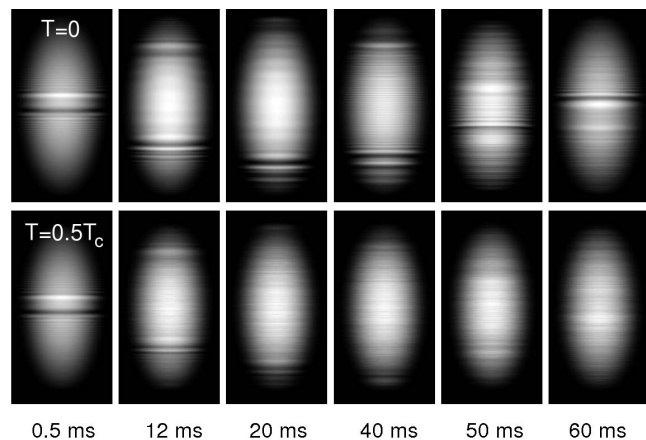


Figure III.16. Simulation of Burger, Bongs, et al. (1999)'s experiment, showing the effect of a thermodynamic instability when $T = T_c/2$. Figure taken from Jackson, Proukakis, et al. (2007).

mal fraction of the gas was not negligible compared with the condensed fraction.

Concerning this second type of instability, the simulation carried out by Jackson, Proukakis, et al. (2007) for the parameters of the experiment of Burger, Bongs, et al. (1999) and shown in figure III.16 is enlightening: while at zero temperature, the soliton oscillates as expected in the trap, it misses its first turning point if the temperature exceeds $0.5 T_c$ (where T_c is the critical Bose–Einstein condensation temperature) and disappears at the edge of the condensate.

Since 2008, very low-temperature experiments with soliton lifetimes in excess of one second have been performed, enabling one to demonstrate the soliton dynamics described by (III.61) (Becker, Stellmer, et al. 2008; Weller, Ronzheimer, et al. 2008). Figure 2 shows the evolution of a soliton prepared by phase printing, performing a complete oscillation in a condensate confined in a harmonic trap with longitudinal frequency $\nu_x = 5.9$ Hz. The measured frequency of the oscillation is $3.8(1)$ Hz, in good agreement with the $\nu_x/\sqrt{2}$ prediction.

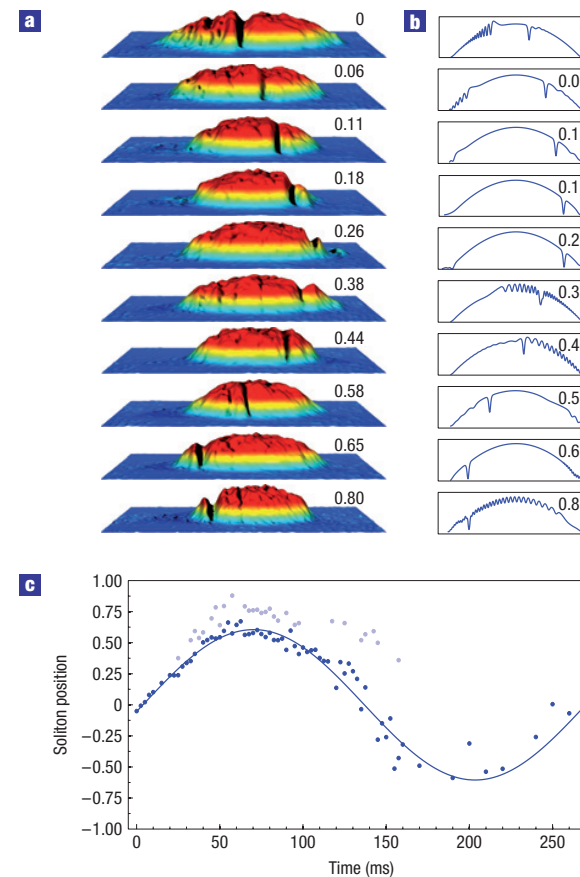


Figure III.17. a) Oscillations of a grey soliton in a condensate of 50 000 ^{87}Rb atoms, confined in a trap of frequencies $5.9 \times 85 \times 133$ Hz. The chemical potential μ_0 is of the order of $h \times 400$ Hz, placing this system at the frontier of the dynamic stability zone with respect to the transverse motion. The phase impression time is $40 \mu\text{s}$, which is very short compared with other time scales in the problem. b) Numerical solution of the 1D Gross-Pitaevskii equation. c) Position of the main soliton (dark dots) and a secondary soliton (light dots) as a function of time. Data fitting leads to a soliton oscillation frequency of $3.8(1)$ Hz. Figure taken from Becker, Stellmer, et al. (2008).

3-4 Collision between two grey solitons

The 1D nonlinear Schrödinger equation is integrable in both the attractive ($g < 0$) and repulsive ($g > 0$) cases. We explained in previous chapters that for the attractive case, this means that the collision between two bright solitons is elastic: both solitons emerge from the collision unchanged, with the same number of atoms and the same velocity as on entry. The only control parameter is their relative phase, which determines whether the effective interaction between solitons is attractive or repulsive.

In the repulsive case of interest here, integrability again means that the collision between two grey solitons is elastic, with both solitons emerging with a depletion (and hence a velocity) identical to their initial depletion. Note that the phase is now fixed, as it is given by the extended condensate. It is therefore no longer a control parameter, and one can show that the interaction between solitons is always repulsive⁵ for the nonlinear Schrödinger equation [see for example Kivshar & Królikowski (1995) and refs. in].

Elastic collisions between grey solitons have been observed by several groups. Here we describe the experiment by Weller, Ronzheimer, et al. (2008), which led to the spectacular images shown in figure III.18. The two solitons were created by a collision between two condensates sharing the same phase. To achieve this, the authors used an elongated trap with a central barrier, i.e. a double potential well. The height of the barrier, created with a focused light beam, was adjusted to maintain the coherence of the whole gas, while creating a significant density hole in the center. When the barrier is switched off, the two condensates came into contact with each other and a pair of solitons was created (Reinhardt & Clark 1997).

In the experiment by Weller, Ronzheimer, et al. (2008), the sample contains around $N = 1500$ atoms and the two clouds are initially separated by 5 micrometers. The temperature is ~ 10 nK, well below the critical temperature (110 nK), which ensures that the solitons have a long lifetime. Solitons oscillate in the trap at a frequency close to $\omega/\sqrt{2}$. Every half-period, they collide with each other at the center of the trap (experimental resolution is insufficient to observe the repulsive nature of soliton interaction).

⁵For non-local particle interactions, i.e. beyond the Gross-Pitaevskii equation, one can observe an attraction between grey solitons (Dreisruh, Neshev, et al. 2006).

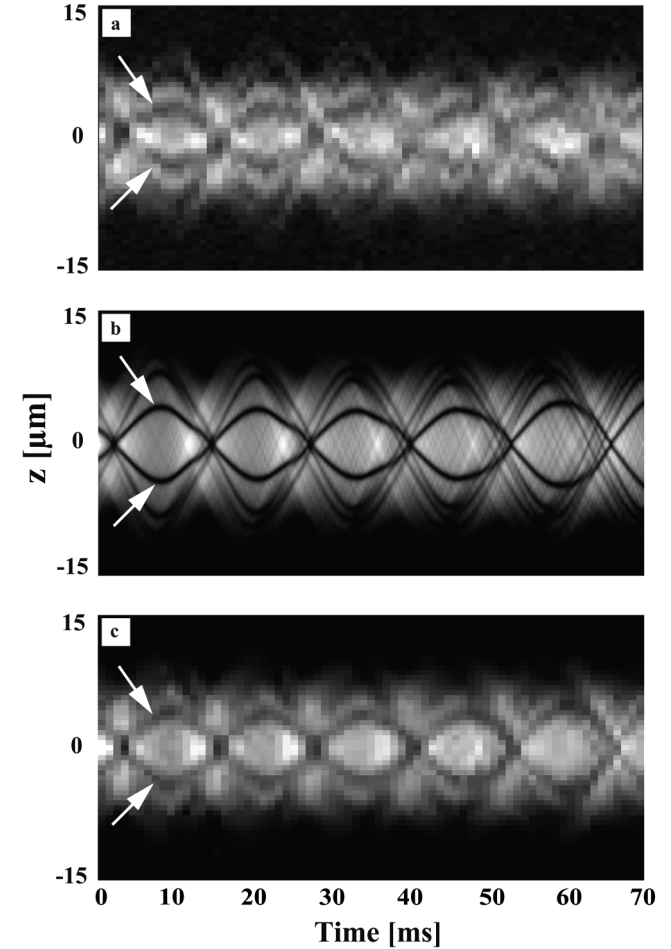


Figure III.18. Top: experimental observation of the time evolution of two dark solitons in a harmonic trap, with an elastic collision at each half-period of the oscillation. Middle: numerical simulation of the experiment. Bottom: same numerical simulation, taking into account the experiment's temporal and spatial resolution. Figure taken from Weller, Ronzheimer, et al. (2008).

3-5 Does a quantum soliton stay dark?

The Gross-Pitaevskii equation is a classical field equation for which a soliton represents a stationary state. A much-debated question concerns the quantum version of the problem: does an initially dark soliton stay dark, or is it destabilized by quantum fluctuations?

When one analyzes these fluctuations using Bogoliubov's method and calculate the average spatial density, one finds that the density hole corresponding to the soliton fills up due to the contribution of particles from the non-condensed fraction (Dziarmaga 2004). However, this filling of the one-body density function may well mask the following phenomenon: the soliton remains completely dark, but its center moves randomly from one realization of the experiment to another, so that the average of the density profiles sees its depletion reduced.

To predict unambiguously whether a given measurement of a soliton's density profile corresponds to full depletion, one needs to calculate the system's N -body correlation function. Equivalently, one can simulate the successive detection of the positions of N particles during a given run of the experiment; to do this, after each detection, that of particle j for example, one needs to project the state vector onto the subspace \mathcal{E}_j corresponding to the measurement result x_j , then move on to the detection of the position of particle $j + 1$. One then constructs a set $\{x_1, x_2, \dots, x_N\}$ of positions and one can check whether this set of positions is compatible with a completely dark soliton.

This procedure has been implemented by several authors, starting from different initial N -body states. Here we present the results obtained by Delande & Sacha (2014) who started from the N -body quantum state of a 1D gas of $N = 180$ bosons in repulsive interaction, confined on a segment with open boundary conditions. The state of the system is represented almost exactly by a matrix product state (MPS). This state is obtained by first imposing a barrier at the center of the segment, so as to create a hole of density very similar to that expected for a dark soliton. The central barrier is then removed, a π phase is printed on one half of the segment, and the evolution of the system is studied by numerically solving the N -body Schrödinger equation.

The evolution of the average spatial density confirms the disappearance

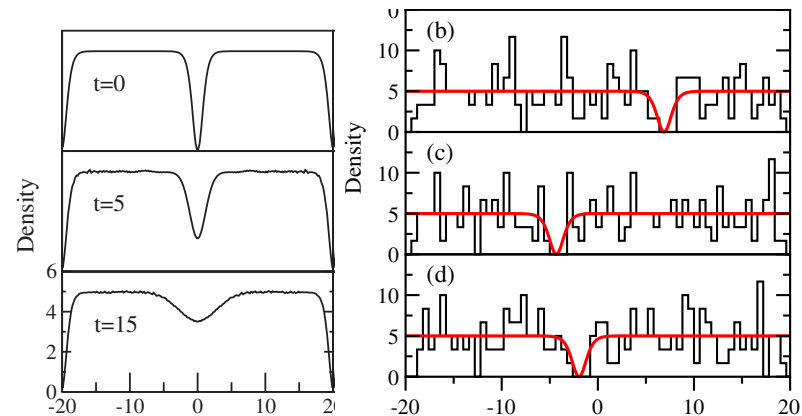


Figure III.19. Left: evolution of the average spatial density for a $N = 180$ particle quantum state initially reproducing a dark soliton. Right: histogram of N particle position measurements for three realizations of the experiment at $t = 25$ (position and time units: κ^{-1} and \hbar/μ). Figure taken from Delande & Sacha (2014).

of the density hole after a time of the order of tens of \hbar/μ (figure III.19, left). But each realization of the experiment leads to a marked hole in the distribution of positions, with the position of this hole fluctuating from one realization of the experiment to the next (figure III.19, right).

For a given realization, the center q of the depletion can be determined by fitting the density distribution with a solitonic profile, and all the density distributions can then be superimposed by translating them so that all the centers are superimposed on one another. The result obtained for 10^5 realizations is shown in figure III.20. We can see that the profile averaged in this way does not evolve and remains that of a perfectly dark soliton, at least on the time scale considered in this work. This study also enabled the authors to determine the time evolution of the distribution of the individual centers q . Delande & Sacha (2014) showed that the variance of this distribution increases as t^2 , compatible with a ballistic propagation from an initial velocity distribution.

This method of studying quantum solitons based on N -body correlations has been generalized to other initial states, see for example Shamailov & Brand (2019) and Syrwid (2021) and refs. in.

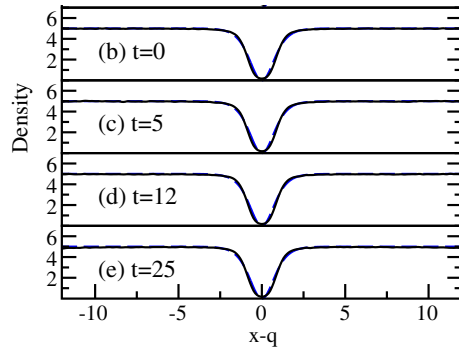


Figure III.20. Superposition of 10^5 position histograms, after recentering by the fitted displacement q , for different evolution times. The profile obtained remains virtually identical to that of a dark soliton. Figure taken from Delande & Sacha (2014).

4 Transitions to other states

Up to now, we have assumed that the gas, confined in an elongated trap of axis x , is well described by a 1D equation, i.e. that the transverse degrees of freedom are frozen. This assumption is legitimate if the quantum of energy $\hbar\omega_{\perp}$ corresponding to the excitation of these transverse degrees of freedom is large in front of the other energy scales of the problem, in particular the chemical potential $\mu = g\rho_0$.

When μ becomes comparable to or greater than $\hbar\omega_{\perp}$, the grey soliton is no longer necessarily a stable object. As it propagates, its initially flat surface can deform and the soliton transforms into other structures, such as a vorticity ring with an axis aligned with that of the trap, or a solitonic vortex.

4-1 The instability of the nodal plane

Muryshev, Heuvel, et al. (1999) have investigated the possibility of a nodal plane instability for a dark soliton in a three-dimensional condensate. To do this, they first considered a homogeneous gas filling the whole 3D space

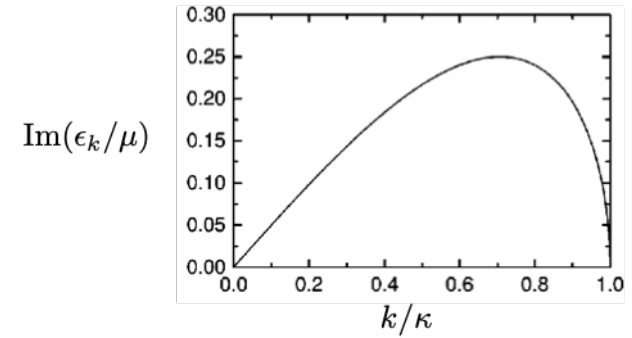


Figure III.21. Dispersion relation of transverse excitations of a wave vector k of a 3D condensate with a nodal plane corresponding to a soliton. Figure adapted from Muryshev, Heuvel, et al. (1999).

with the asymptotic spatial density ρ_0 and with a node in the $x = 0$ plane, i.e. a wave function $\psi(x) = \sqrt{\rho_0} \tanh(\kappa x)$. The chemical potential is $\mu = g\rho_0$ where g is now defined for a 3D gas ($g = 4\pi\hbar^2 a/m$ where a is the scattering length). We still have the link between μ and the speed of sound $\mu = mc^2 = \hbar^2\kappa^2/m$ and therefore $\kappa = mc/\hbar$.

Muryshev, Heuvel, et al. (1999) then used Bogoliubov's method to find the dispersion relation of waves propagating with a wave vector k perpendicular to the x axis and located in the vicinity of the nodal plane $x = 0$. They showed that for $k < \kappa$, these modes had an imaginary energy ϵ_k , and were therefore dynamically unstable (figure III.21): it is not possible to indefinitely maintain a soliton with a flat nodal surface in a homogeneous 3D gas. The most unstable mode corresponds to a wave vector $k = \kappa/\sqrt{2}$.

The same authors then considered the case of a gas in a harmonic trap with rotational symmetry around the x axis and oscillation frequencies ω_x and ω_{\perp} (figure III.22). The stability of the soliton prepared in the $x = 0$ plane then depends on two parameters: the ratios ω_{\perp}/ω_x and $\mu/\hbar\omega_{\perp}$. Muryshev, Heuvel, et al. (1999) have shown that for a very elongated trap ($\omega_{\perp}/\omega_x \gg 1$), it is enough to ensure that the chemical potential μ remains below $\sim 2.4\hbar\omega_{\perp}$ for the planar nodal surface to remain stable. However, when one switches to spherical or oblate traps ($\omega_{\perp}/\omega_x \lesssim 1$), the planar nodal surface is destabilized, whatever the value of μ .

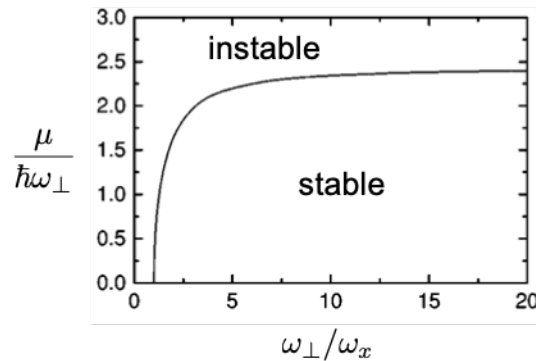


Figure III.22. Stable and unstable zones of the nodal plane of a dark soliton in the $x = 0$ plane, at the center of a harmonic trap with frequencies ω_x and ω_\perp . Figure adapted from Muryshev, Heuvell, et al. (1999).

4-2 The different possible stationary states

The instability found by Muryshev, Heuvell, et al. (1999) indicates that the nodal surface will deform, with exponential growth of certain imaginary-frequency modes at short times. However, it provides no information on the nature of the structures that will subsequently appear. This study was the subject of numerous publications, both theoretical and experimental, in the years following the observation of the first dark condensates. Theoretical publications include Brand & Reinhardt (2002) and Komineas & Papanicolaou (2003). On the experimental side, ripple instability of the soliton nodal plane was observed by Denschlag, Simsarian, et al. (2000), the emergence of vorticity rings by Anderson, Haljan, et al. (2001) and Dutton, Budde, et al. (2001), and more recently solitonic vortices by Becker, Sengstock, et al. (2013) and Donadello, Serafini, et al. (2014) in Bose-Einstein condensates and by Yefsah, Sommer, et al. (2013) and Ku, Ji, et al. (2014) in a strongly interacting Fermi gas.

Figure III.23, taken from the article by Muñoz Mateo & Brand (2014), shows a series of stationary structures, obtained by a systematic search for solutions of the nonlinear Schrödinger equation in a cylindrical geometry. The authors also indicate the range of $\mu/\hbar\omega_\perp$ values for which these struc-

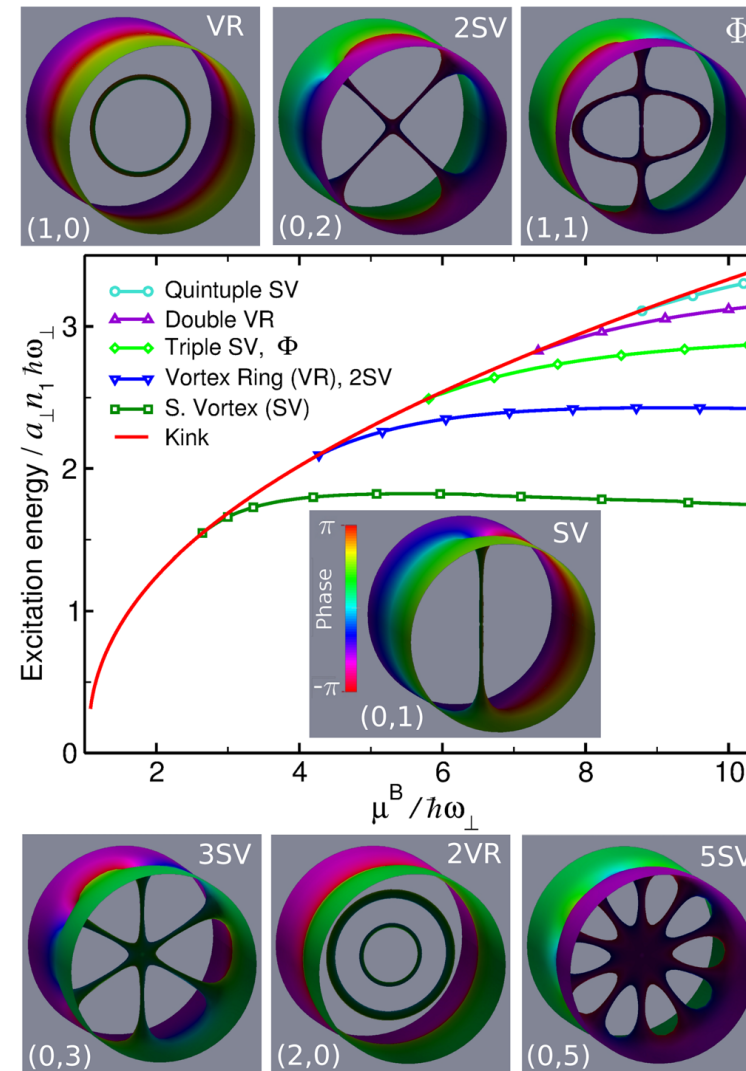


Figure III.23. Different possible stationary solutions of a condensate confined in a transverse harmonic trap of frequency ω_\perp , as a function of the ratio $\mu/\hbar\omega_\perp$. The iso-density surface corresponding to $\rho(\mathbf{r}) = \rho_{\max}/20$ is shown here. Figure taken from Muñoz Mateo & Brand (2014).

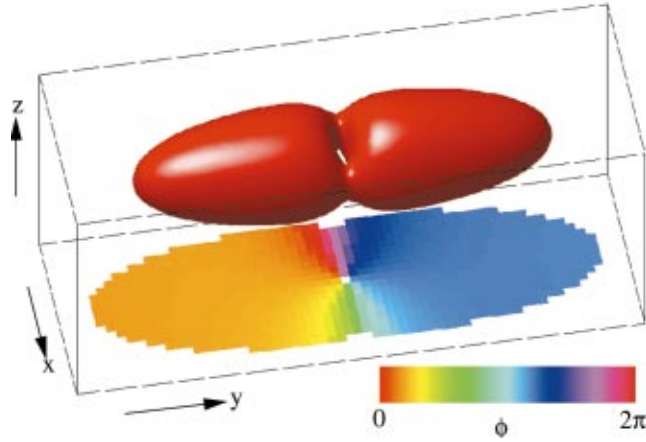


Figure III.24. Equi-density surface and phase of a condensate containing a solitonic vortex. Figure taken from Brand & Reinhardt (2002).

tures are observable.

This figure III.23 shows the structures mentioned above. The solitonic vortex (SV) consists of a straight vortex line, perpendicular to the x axis of the cylinder. Another representation of a solitonic vortex is shown in figure III.24 for a condensate confined in an elongated 3D harmonic trap. The phase winding around the vortex line is 2π (see Aftalion & Sandier (2023) and Aftalion, Gravejat, et al. (2024) for a detailed mathematical analysis of this structure in a two-dimensional band geometry).

In figure III.23, the VR sign corresponds to a vortex ring, similar to a smoke ring. Solutions corresponding to more complex configurations can be formed, such as solitonic vortices of various directions, crossing each other on the condensate axis, or double vortex rings, or even a combination SV-VR, displaying the letter Φ .

As we saw on figure III.21 in the limit $\omega_x \rightarrow 0$, i.e. $\omega_\perp/\omega_x \rightarrow +\infty$, these structures can only appear if $\mu/\hbar\omega_\perp \gtrsim 2.4$. When this is the case, we see that the single solitonic vortex corresponds to the minimum-energy structure, but this does not tell us anything about the dynamics of the system to reach this structure, as we will see in the next paragraph.

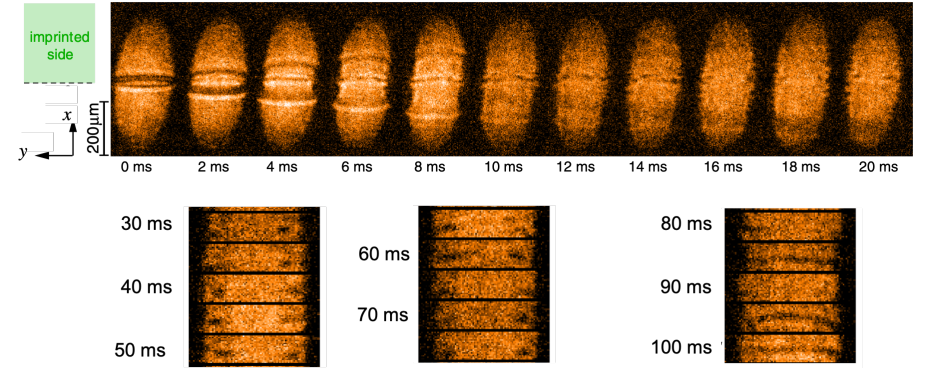


Figure III.25. Cascade of transitions observed in an unpolarized gas of spin 1/2 fermions close to the unitary limit, starting from a soliton with a nodal plane at $x = 0$, passing through a vortex ring between 20 and 80 ms, then a solitonic vortex from 100 ms. Imaging is performed on a thin slice between z and $z + \delta z$. Figure taken from Ku, Mukherjee, et al. (2016).

4-3 Observations on a superfluid Fermi gas

Here we describe an experiment carried out at MIT in Zwierlein's group, which demonstrated a cascade of transitions from the planar soliton to the solitonic vortex (Ku, Mukherjee, et al. 2016). Unlike the setups described above, the authors are not working here with a Bose-Einstein condensate, but with a Fermi gas in the unitary regime. This system can be described approximately by a mean-field method, based on the Bogoliubov-de Gennes formalism, so that the ideas developed in this chapter remain relevant, subject to the modification of certain numerical parameters [see Scott, Dalfovo, et al. (2011)].

The experiment corresponds to the following sequence:

- At the initial instant, the π phase jump is imparted to generate a zero-velocity soliton in a gas of 1.4×10^6 ${}^6\text{Li}$ atoms, confined in an elongated harmonic trap of frequencies $11 \times 70 \times 70$ Hz. The gas contains equal parts of two spin states and it is prepared in the vicinity of a Fano-

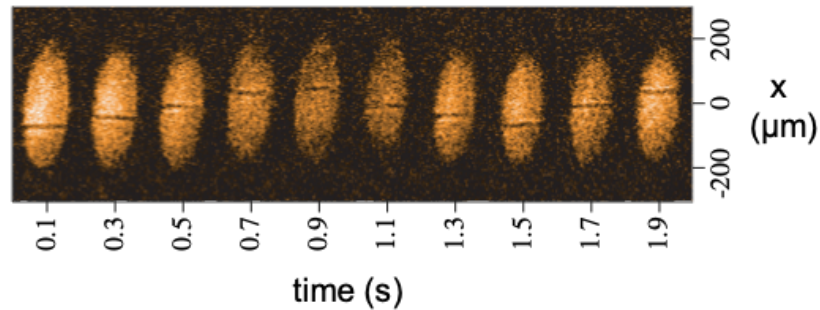


Figure III.26. Oscillation of a solitonic vortex in an unpolarized gas of spin 1/2 fermions close to the unitary limit. Figure taken from Ku, Ji, et al. (2014).

Feshbach resonance for the interaction between these two states⁶ (unitary regime).

- In the first few milliseconds, a nodal plane appears at the center of the trap, characteristic of the soliton.
- This plane deforms rapidly, revealing its instability. The fastest-growing mode is the one whose wavelength is equal to the Thomas-Fermi diameter.
- After ~ 20 ms, one no longer observes the nodal plane of the soliton on a cross-section of the soliton in the xy plane, but simply two dark points. This corresponds to a vortex ring, with axis x .
- Around 80 ms, a structure reminiscent of the Φ shape of figure III.23 is revealed by a tomographic analysis of the gas.
- After ~ 100 ms, a solitonic vortex is observed that persists for a long time. This solitonic vortex oscillates in the superfluid with a very long period compared to $2\pi/\omega_x$ (figure III.26). In the experiment, the two transverse frequencies ω_y and ω_z are not strictly equal, and the vortex axis aligns along the axis corresponding to the higher frequency. Ku,

⁶Remember that in this low-temperature domain, two fermions in the same spin state do not interact with each other

Ji, et al. (2014) presented a model of the oscillation in good agreement with these experimental observations.

Chapter IV

Magnetic solitons and Bloch oscillations

The first chapters of this course were devoted to the solitons that can be generated in a one-component fluid. Depending on the attractive or repulsive nature of the interactions in this fluid, we found bright or dark solitons.

This final chapter is devoted to a brief overview of more complex solitonic structures that can be generated in mixtures of Bose-Einstein condensates. This is an extremely rich field, and there is no question of covering it exhaustively. We will concentrate here on a type of soliton that appears in a ferromagnetic material and can be reproduced almost identically in a binary condensate mixture.

More specifically, we will study the case of a slightly immiscible mixture, for which the solitons that appear are equivalent to those of an "easy-axis" ferromagnet. We will also describe the demonstration of a phenomenon predicted for magnetic solitons a long time ago, and recently observed with a mixture of condensates: the Bloch oscillation of a soliton subjected to a constant force.

For lack of space, we will not describe other types of structure that appear in two-component mixtures, such as dark-bright solitons (Busch & Anglin 2001; Becker, Stellmer, et al. 2008; Hamner, Chang, et al. 2011; Danaila, Khamehchi, et al. 2016; Katsimiga, Mistakidis, et al. 2020; Meng, Luo, et al. 2025) or structures obtained from three-component mixtures (Bersano, Gokhroo, et al. 2018; Lannig, Schmied, et al. 2020; Yu & Blakie 2022; Siovitz, Lannig, et al. 2023). We refer interested readers to the re-

cent article by Mossman, Katsimiga, et al. (2024), which provides a fairly comprehensive review of work in this field.

1 The ferromagnetic chain

1-1 The relevant energy scales

In this section, we will develop a simple model of a one-dimensional chain of magnetic moments μ_j ($j \in \mathbb{Z}$), all with the same modulus μ (figure IV.1). This chain can be seen as a line extracted from a ferromagnetic crystal, a one-dimensional approximation that is valid for a whole class of materials (see, for example, Mikeska & Steiner (1991) and Dauxois & Peyrard (2006) and refs. in). We now write the equation of motion of a magnetic moment μ_j under the effect of the three dominant terms:

- Each magnetic moment interacts with its neighbors. This is essentially an exchange interaction¹, which we will model by

$$-J \sum_j \mu_j \cdot \mu_{j+1} . \quad (\text{IV.1})$$

¹We neglect here the dipole-dipole interaction of magnetic origin, which is much weaker than the exchange interaction, which is of electrostatic origin.

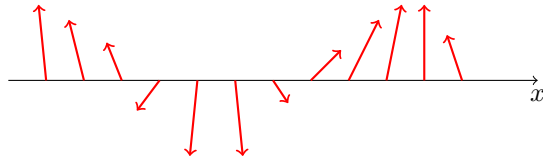


Figure IV.1. One-dimensional chain of magnetic moments, all with the same modulus μ .

The constant J , called the exchange integral, is chosen to be positive so that the magnetic moments minimize their energy by aligning with each other, as expected for a ferromagnetic material. This interaction is isotropic: the common direction chosen by the magnetic moments to minimize this energy is random if this interaction is the only one present. In its quantum version, (IV.1) is the Heisenberg Hamiltonian.

- The second term in the energy is a small correction to the previous term, resulting from the fact that 3D ferromagnetic crystals are generally not perfectly isotropic. An important class concerns uniaxial materials for which one axis (noted here as z) leads to a different interaction from that for the other two axes (x and y). To take this effect into account, we add the energy²:

$$-J' \sum_j \mu_j^{(z)} \mu_{j+1}^{(z)}. \quad (\text{IV.2})$$

If $J' > 0$, the anisotropic interaction favors the emergence of a magnetization along the z axis (in positive or negative directions) and we then speak of a *easy-axis* material. If $J' < 0$, the system minimizes its energy with magnetization in the xy plane, and is referred to as an *easy-plane* material.

- The chain can be placed in an external magnetic field leading to the

²We have adopted here the modeling of Kosevich, Ivanov, et al. (1990). We will see later [cf. (IV.13)] that the contribution of this term is limited to its lowest order, for which we can replace μ_{j+1} by μ_j (Dauxois & Peyrard 2006).

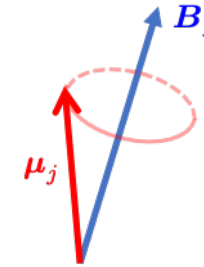


Figure IV.2. The precession motion of the magnetic moment μ_j under the effect of the local magnetic field B_j according to the equation of motion (IV.8).

energy

$$-\sum_j \mu_j \cdot B_{\text{ext}}. \quad (\text{IV.3})$$

Like the term (IV.2) proportional to J' , the presence of this external field breaks the invariance by rotation. If J' plays a negligible role, then the preferred direction of magnetization is that of the external field.

1-2 Dynamics of a magnetic moment

Let us consider a magnetic moment μ_j and study its equation of motion. We know that an angular momentum is associated with this magnetic moment. We denote this angular momentum s_j , and the link between μ_j and s_j is provided by the gyromagnetic ratio γ :

$$\mu_j = \gamma s_j. \quad (\text{IV.4})$$

The evolution of the angular momentum s_j is

$$\frac{ds_j}{dt} = \Gamma_j \quad (\text{IV.5})$$

where Γ_j is the torque acting on this moment. For the magnetic moment μ_j , this torque is written as

$$\Gamma_j = \mu_j \times B_j, \quad (\text{IV.6})$$

where \mathbf{B}_j is the effective magnetic field at site j , deduced from the three interaction terms (IV.1,IV.2,IV.3) described above:

$$\mathbf{B}_j = J(\boldsymbol{\mu}_{j-1} + \boldsymbol{\mu}_{j+1}) + J'(\mu_{j-1}^{(z)} + \mu_{j+1}^{(z)})\hat{\mathbf{z}} + \mathbf{B}_{\text{ext}} \quad (\text{IV.7})$$

where $\hat{\mathbf{z}}$ denotes the unit vector aligned along z . By multiplying the two members of the equation (IV.5) by the gyromagnetic ratio γ , we obtain the desired equation of motion (see figure IV.2):

$$\frac{d\boldsymbol{\mu}_j}{dt} = \gamma \boldsymbol{\mu}_j \times \mathbf{B}_j. \quad (\text{IV.8})$$

The evolution equation of each $\boldsymbol{\mu}_j$ is coupled to that of its neighbors, which makes solving this system tricky. To make progress, we are going to move to a continuous limit to transform this discrete differential system into a partial differential equation.

Note. We have adopted a classical approach here, but a quantum treatment leads to an identical result. We start from the Heisenberg equation for angular momentum $\hat{\mathbf{s}}_j$:

$$i\hbar \frac{d\hat{\mathbf{s}}_j}{dt} = [\hat{\mathbf{s}}_j, \hat{H}] \quad (\text{IV.9})$$

and consider the terms in the Hamiltonian that are not commuting with $\hat{\mathbf{s}}_j$:

$$-J\gamma^2(\hat{\mathbf{s}}_{j+1} + \hat{\mathbf{s}}_{j-1}) \cdot \hat{\mathbf{s}}_j - J'\gamma^2(\hat{s}_{j+1}^{(z)} + \hat{s}_{j-1}^{(z)})\hat{s}_j^{(z)} - \gamma\mathbf{B}_{\text{ext}} \cdot \hat{\mathbf{s}}_j. \quad (\text{IV.10})$$

We use the canonical commutation relations for angular momentum $[\hat{s}^{(x)}, \hat{s}^{(y)}] = i\hbar \hat{s}^{(z)}$ and we reach, for the operators $\hat{\mathbf{s}}_j$ or $\hat{\boldsymbol{\mu}}_j$, a result identical to (IV.7-IV.8). For a 1/2 spin chain, this model is exactly solvable by a Bethe ansatz [Des Cloizeaux & Gaudin (1966) and refs. in], as is the classical moment chain considered above.

1-3 Switching to a continuous description

We are now going to look at the situation, realistic in practice, where the orientation of any magnetic moment $\boldsymbol{\mu}_j$ is close to those of its neighbors

$\boldsymbol{\mu}_{j\pm 1}$. Variations in magnetization orientation are possible, but on a length scale much greater than the spatial period of the chain, which we will denote by a .

We now turn to a continuous description of the chain of magnetic moments³:

$$\boldsymbol{\mu}_j(t) \longrightarrow \boldsymbol{\mu}(x_j, t) \quad \text{with} \quad x_j = ja \quad (\text{IV.11})$$

and establish the equation of motion of $\boldsymbol{\mu}(x, t)$ deduced from (IV.8). To do this, let us take up one by one the three contributions to the field \mathbf{B}_{eff} involved in this equation of motion:

- The first contribution is $J(\boldsymbol{\mu}_{j-1} + \boldsymbol{\mu}_{j+1})$ which we develop up to order 2 in a :

$$\boldsymbol{\mu}(x_{j-1}) + \boldsymbol{\mu}(x_{j+1}) = 2\boldsymbol{\mu}(x_j) + a^2 \frac{\partial^2 \boldsymbol{\mu}}{\partial x^2} + \mathcal{O}(a^4). \quad (\text{IV.12})$$

The zero-order term $2\boldsymbol{\mu}(x_j)$, although dominant, has a zero effect on the evolution equation as it intervenes in (IV.8) via $\boldsymbol{\mu}(x_j) \times \boldsymbol{\mu}(x_j) = 0$. This is why it is essential to push the above development to order 2.

- For the term related to the anisotropy J' of the material, we can restrict ourselves to the zero order term in a :

$$\mu^{(z)}(x_{j-1}) + \mu^{(z)}(x_{j+1}) = 2\mu^{(z)}(x_j) + \mathcal{O}(a^2). \quad (\text{IV.13})$$

Since $J' \ll J$, there is no inconsistency in limiting our expansion to this order while pushing the expansion (IV.12) to order 2 in a .

- The external field term remains unchanged.

We then arrive at the evolution equation for the vector field $\boldsymbol{\mu}(x, t)$ (Landau & Lifshitz 1935):

$$\frac{\partial \boldsymbol{\mu}}{\partial t} = \gamma \boldsymbol{\mu} \times \mathbf{B} \quad \text{with} \quad \mathbf{B} = Ja^2 \frac{\partial^2 \boldsymbol{\mu}}{\partial x^2} + 2J'\mu^{(z)}\hat{\mathbf{z}} + \mathbf{B}_{\text{ext}}. \quad (\text{IV.14})$$

³As in the previous chapters, we use the variable x to identify the spatial position. It is important to note that the corresponding direction is *a priori* decorrelated from the x, y, z axes defining the magnetic moment Hamiltonian.

As we did for the nonlinear Schrödinger equation, we can simplify this equation by writing it in a dimensionless form:

$$\boxed{\frac{\partial \mathbf{m}}{\partial \tilde{t}} = \mathbf{m} \times \mathbf{b} \quad \text{with} \quad \mathbf{b} = \frac{\partial^2 \mathbf{m}}{\partial \tilde{x}^2} \pm m^{(z)} \hat{\mathbf{z}} + \mathbf{b}_{\text{ext}}} \quad (\text{IV.15})$$

where the vector field $\mathbf{m}(\tilde{x}, \tilde{t})$ is of modulus 1 at any point ($|\mathbf{m}(\tilde{x}, \tilde{t})| = 1$), and where the following time and length scales have been introduced:

$$\tilde{t} = \frac{t}{t_0} \quad \tilde{x} = \frac{x}{x_0} \quad \text{with} \quad t_0 = \frac{1}{2\gamma\mu|J'|} \quad x_0 = a\sqrt{\frac{J}{2|J'|}} \quad (\text{IV.16})$$

and

$$\mathbf{b}_{\text{ext}} = \frac{\mathbf{B}_{\text{ext}}}{2\mu|J'|}. \quad (\text{IV.17})$$

In equation (IV.15), the + sign corresponds to the *easy-axis* case ($J' > 0$) and the – sign to the *easy-plane* case ($J' < 0$). Note that the natural length scale x_0 is very large compared with the spatial period a of the chain, since we have assumed that $J \gg |J'|$. Structures of characteristic size of the order of 1 in reduced units can therefore be correctly described by this continuous approach, as they extend over many sites of the discrete chain. In what follows, we will omit the symbol $\tilde{\cdot}$ on the variables x and t to lighten the notations, the context indicating whether to adopt the reduced or the physical units.

Angular representation around the z axis. Since the vector fields $\boldsymbol{\mu}(x, t)$ or $\mathbf{m}(x, t)$ have a constant modulus, they can be parameterized by the two angles in spherical coordinates $\theta(x, t)$ and $\varphi(x, t)$ (see figure IV.3):

$$m^{(x)} + im^{(y)} = \sin \theta e^{i\varphi} \quad m^{(z)} = \cos \theta. \quad (\text{IV.18})$$

The evolution equation (IV.15) is rewritten for these two angles (Kosevich, Ivanov, et al. 1990):

$$\boxed{\begin{cases} \theta_t &= -2\theta_x \varphi_x \cos \theta - \varphi_{xx} \sin \theta \\ \varphi_t &= -\cos \theta (\varphi_x^2 \pm 1) + \frac{\theta_{xx}}{\sin \theta} \end{cases}} \quad (\text{IV.19})$$

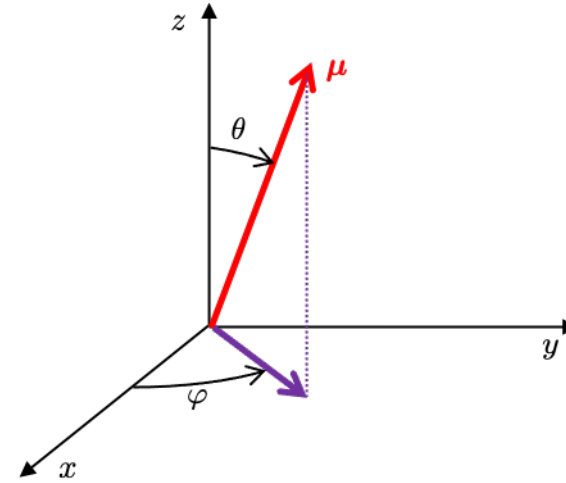


Figure IV.3. Parameterization of $\boldsymbol{\mu}(x, t)$ by the two angles $\theta(x, t)$ and $\varphi(x, t)$.

where we have taken $\mathbf{b}_{\text{ext}} = 0$ to simplify. We will see later how these two equations appear identically for the description of a binary condensate mixture in the regime where the three interaction constants g_{ij} ($i, j = 1, 2$) are close to each other (Manakov regime). This makes it possible to study the physics of magnetic solitons using quantum fluids.

1-4 Lagrangian approach

The equations of motion for the two fields $\theta(x, t)$ and $\varphi(x, t)$ can be obtained from a Lagrangian approach, with the Lagrangian density $\mathcal{L}[\theta, \theta_t, \theta_x, \varphi, \varphi_t, \varphi_x]$ given by:

$$\mathcal{L} = \mathcal{L}_{\text{cin}} - \mathcal{V} \quad (\text{IV.20})$$

with (Kosevich, Ivanov, et al. 1990):

$$\mathcal{L}_{\text{cin}} = -\frac{1}{2}(1 - \cos \theta)\varphi_t \quad \mathcal{V} = \frac{1}{4} [\theta_x^2 + (\varphi_x^2 \pm 1) \sin^2 \theta]. \quad (\text{IV.21})$$

To do this, we use the Euler-Lagrange equation for the field θ :

$$\frac{\partial \mathcal{L}}{\partial \theta} = \frac{\partial}{\partial x} \left(\frac{\partial \mathcal{L}}{\partial \theta_x} \right) + \frac{\partial}{\partial t} \left(\frac{\partial \mathcal{L}}{\partial \theta_t} \right) \quad (\text{IV.22})$$

and its analog for the field φ .

We define the "mass" M (or rather the polarization in this context) which is a conserved quantity:

$$M = \frac{1}{2} \int_{-\infty}^{+\infty} (1 - \cos \theta) \, dx, \quad (\text{IV.23})$$

where we assume that $\theta \rightarrow 0$ at infinity for the integral to be convergent (this will be the case for the solutions considered in this chapter). Moreover, time and space invariances imply the conservation of the system's energy E and momentum P , with

$$E = \frac{1}{4} \int_{-\infty}^{+\infty} [\theta_x^2 + (\phi_x^2 \pm 1) \sin^2 \theta] \, dx \quad (\text{IV.24})$$

$$P = \frac{1}{2} \int_{-\infty}^{+\infty} (1 - \cos \theta) \varphi_x \, dx. \quad (\text{IV.25})$$

Note. In the case where the anisotropy characterized by J' is absent, we can also write a system of coupled equations for θ and φ . We arrive at a system similar to that written above, but without the ± 1 (Lakshmanan, Ruijgrok, et al. 1976) term. The length and time scales (IV.16) must be modified accordingly.

1-5 Link with the nonlinear Schrödinger equation

It is possible to establish a formal link, called gauge equivalence, between the Landau-Lifshitz equation and the nonlinear Schrödinger equation for a one-component gas. This link was first proposed regardless of the sign of J' by Nakamura & Sasada (1982), but the proof in the case $J' < 0$ (easy-plane) was criticized by Kundu & Pshaev (1983). On the other hand, in the case $J' > 0$ (easy-axis), gauge equivalence with the attractive nonlinear Schrödinger equation is valid.

We will not go into this general connection here, but it is possible to show how the attractive nonlinear Schrödinger equation emerges in a simple limiting case of the Landau-Lifshitz equation. Let us place ourselves in the case $J' > 0$ (easy-axis) and assume that the direction of magnetization is at all points close to \mathbf{u}_z , i.e. the polar angle θ close to 0:

$$|m^{(x)}|, |m^{(y)}| \ll m^{(z)} \approx 1. \quad (\text{IV.26})$$

We will also restrict ourselves to solutions with a large spatial scale compared to the natural scale x_0 , i.e.

$$\left| \frac{\partial^2 m^{(\alpha)}}{\partial x^2} \right| \ll \left| \frac{\partial m^{(\alpha)}}{\partial x} \right| \ll |m^{(\alpha)}|, \quad \alpha = x, y. \quad (\text{IV.27})$$

Now let us introduce the complex quantity :

$$\psi = \left(m^{(x)} + im^{(y)} \right) e^{it} \quad (\text{IV.28})$$

whose evolution equation deduced from (IV.15) is

$$i \frac{\partial \psi}{\partial t} = \psi \left(b^{(z)} - 1 \right) - m^{(z)} b^{(+)} \quad \text{with} \quad b^{(+)} = \left(b^{(x)} + ib^{(y)} \right) e^{it}. \quad (\text{IV.29})$$

Assuming that no external field is applied, we have

$$b^{(z)} = \frac{\partial^2 m^{(z)}}{\partial x^2} + m^{(z)} \approx m^{(z)} \quad (\text{IV.30})$$

where we have neglected the second derivative because its contribution to (IV.29) would have been negligible once multiplied by ψ . Let us also perform an expansion to order 2 included in ψ for $m^{(z)}$:

$$b^{(z)} \approx 1 - \frac{|\psi|^2}{2}. \quad (\text{IV.31})$$

The quantity $b^{(+)}$ is multiplied by $m^{(z)} \approx 1$ in (IV.29), so the second derivative must be kept at this level of the calculation:

$$b^{(+)} = \frac{\partial^2 (m^{(x)} + im^{(y)})}{\partial x^2} e^{it} \quad (\text{IV.32})$$

so that we arrive at:

$$\boxed{\frac{\partial \psi}{\partial t} \approx -\frac{\partial^2 \psi}{\partial x^2} - \frac{1}{2} |\psi|^2 \psi}, \quad (\text{IV.33})$$

i.e. the attractive nonlinear Schrödinger equation.

Link with the sine–Gordon equation. The Landau Lifshitz equation admits another important limit, the sine–Gordon equation, also much studied in the context of solitons, as it gives rise to topological solitons. We place ourselves in the opposite situation to the previous paragraph, choosing $J' < 0$ (easy-plane). The energy-minimizing macroscopic polarization is then oriented in the xy plane.

We also assume that a weak external field is applied along the x axis, $\mathbf{b}_{\text{ext}} = b_0 \hat{\mathbf{x}}$ with $b \ll 1$. The presence of this field leads us to add the terms $b_0 \sin \varphi$ and $b_0 \cot \theta \cos \varphi$ to the two equations of the system (IV.19). Restricting ourselves, as in the previous paragraph, to solutions varying slowly on the scale of x_0 , and taking $|\theta - \frac{\pi}{2}| \ll 1$, we can simplify the system (IV.19) and obtain:

$$\begin{cases} \theta_t \approx -\varphi_{xx} + b_0 \sin \varphi \\ \varphi_t \approx \cos \theta \end{cases} \quad (\text{IV.34})$$

We eliminate the variable θ by taking the derivative with respect to time of the second equation, $\varphi_{tt} \approx -\theta_t \sin \theta \approx -\theta_t$, which finally gives:

$$\boxed{\varphi_{tt} - \varphi_{xx} + b_0 \sin \varphi = 0} \quad (\text{IV.35})$$

We will not comment further on this limit here, and refer readers to the detailed discussion in Dauxois & Peyrard (2006), as well as Schweigler, Kasper, et al. (2017) and Wybo, Bastianello, et al. (2023) for realizations in the context of ultra-cold atom gases.

2 A binary mixture of condensates

2-1 Coupled Gross-Pitaevskii equations

We now consider a mixture of two Bose gases at zero temperature, which we assume to be well described in the Gross–Pitaevskii approach by the macroscopic wave functions $\psi_1(\mathbf{r})$ and $\psi_2(\mathbf{r})$. For simplicity, we will assume that the atoms of both gases have the same mass m , which corresponds to the case of two fluids of the same atomic species, prepared in two different internal states.

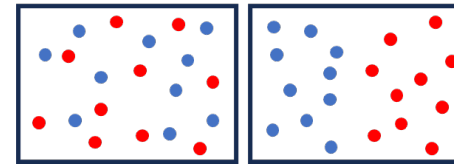


Figure IV.4. Two possible configurations depending on whether a mixture is miscible (left) or immiscible (right).

We will assume that the interactions can be described by a contact potential, with the three couplings g_{11} , g_{22} and g_{12} . The first two describe intra-species interactions and the third describes inter-species interaction. The Gross–Pitaevskii energy functional is then written in dimension D :

$$\begin{aligned} E[\psi_1, \psi_2] &= \frac{\hbar^2}{2m} \int (|\nabla \psi_1|^2 + |\nabla \psi_2|^2) \, d^D r \\ &+ \frac{1}{2} \int [g_{11} \rho_1^2(\mathbf{r}) + 2g_{12} \rho_1(\mathbf{r})\rho_2(\mathbf{r}) + g_{22} \rho_2^2(\mathbf{r})] \, d^D r \end{aligned}$$

with $\rho_j = |\psi_j|^2$, $j = 1, 2$. In what follows, we will assume that all coefficients g_{ij} are positive to avoid any risk of one of the fluids collapsing. We will not consider the case where a coherent coupling is set up between the two condensates. Such a coupling would be taken into account by an additional term $\int \psi_1^* \psi_2 + \psi_2^* \psi_1$ [see for example Qu, Tylutki, et al. (2017)].

The equation for the evolution of ψ_1 and ψ_2 can be deduced from the energy functional given above:

$$i\hbar \partial_t \psi_i = -\frac{\hbar^2}{2m} \nabla^2 \psi_i + (g_{ii} \rho_i + g_{ij} \rho_j) \psi_i \quad (\text{IV.36})$$

with $i, j = 1, 2$ and $j \neq i$. Each fluid thus evolves under the effect of its own mean field as well as that created by the other component. For each fluid, we have the continuity equation:

$$\partial_t \rho_j + \nabla \cdot (\rho_j \mathbf{v}_j) = 0 \quad \text{with} \quad \rho_j \mathbf{v}_j = \frac{\hbar}{m} \text{Im} (\psi_j^* \nabla \psi_j) \quad (\text{IV.37})$$

since there is no transfer of matter from one fluid to the other.

Miscibility criterion. We will briefly recall the nature of the mixture – miscible or immiscible – according to the values of the coefficients g_{ij} . Our reasoning will be based solely on the interaction energies involved in $E[\psi_1, \psi_2]$ and will neglect kinetic energy terms. Our result applies equally well to a mixture of classical fluids, insofar as surface effects are negligible compared with volume effects.

Let us denote N_1 and N_2 the number of particles in each fluid and consider the two situations shown in figure IV.4 :

- The two fluids occupy the entire volume V available to form a homogeneous mixture, so the interaction energy is equal to

$$E_{\text{hom}} = \frac{1}{2V} (g_{11}N_1^2 + 2g_{12}N_1N_2 + g_{22}N_2^2). \quad (\text{IV.38})$$

- The two fluids are spatially separated and occupy volumes V_1 and V_2 with $V = V_1 + V_2$, which leads to the interaction energy:

$$E_{\text{sep}} = \frac{g_{11}N_1^2}{2V_1} + \frac{g_{22}N_2^2}{2V_2}. \quad (\text{IV.39})$$

In the second case, the volumes V_1 and V_2 adjust (under the constraint $V_1 + V_2 = V$) to minimize energy. This happens for

$$V_1 = V \frac{\sqrt{g_{11}}N_1}{\sqrt{g_{11}}N_1 + \sqrt{g_{22}}N_2} \quad V_2 = V - V_1, \quad (\text{IV.40})$$

which leads to

$$E_{\text{sep}} = \frac{1}{2V} (g_{11}N_1^2 + 2\sqrt{g_{11}g_{22}}N_1N_2 + g_{22}N_2^2). \quad (\text{IV.41})$$

Comparing (IV.38) and (IV.41) gives the desired result:

$$\boxed{\text{miscible mixture} \quad \Leftrightarrow \quad g_{12} < \sqrt{g_{11}g_{22}}} \quad (\text{IV.42})$$

2-2 Manakov regime

Generally speaking, the description of two coupled quantum fluids requires two complex fields, ψ_1 and ψ_2 , or equivalently four real fields, the

two densities $\rho_{1,2}$ and the two phases $\varphi_{1,2}$ with $\psi_j = \sqrt{\rho_j} e^{i\varphi_j}$. The state of the system is then described by the spinor

$$\begin{pmatrix} \psi_1 \\ \psi_2 \end{pmatrix} = \begin{pmatrix} \sqrt{\rho_1} e^{i\varphi_1} \\ \sqrt{\rho_2} e^{i\varphi_2} \end{pmatrix}. \quad (\text{IV.43})$$

We consider in the following the situation where all three coefficients g_{ij} are positive and close to each other⁴, a situation called the *Manakov regime*. To simplify calculations, we will assume more precisely that

$$g_{11} = g_{22} \quad (\text{IV.44})$$

and introduce the difference

$$g_s = g_{12} - g \quad \text{with} \quad |g_s| \ll g, \quad (\text{IV.45})$$

the subscript "s" referring to spin excitations, as we will see in a moment. With this assumption, the miscible and immiscible regimes found in (IV.42) correspond to $g_s < 0$ and $g_s > 0$ respectively.

In practice, the equality $g_{11} = g_{22}$ can be realized for atomic species whose ground electronic level has angular momentum $F = 1$, as is the case for ${}^7\text{Li}$, ${}^{23}\text{Na}$, ${}^{39}\text{K}$, ${}^{41}\text{K}$, ${}^{87}\text{Rb}$. All we need to do is work with the two states $|F = 1, m_F = \pm 1\rangle$, and the equality $g_{11} = g_{22}$ then results from rotational symmetry. For ${}^{87}\text{Rb}$, the assumption $|g_s| \ll g$ is very well verified: $g_s/g \sim 10^{-2}$.

In this situation, decoupling occurs between two types of excitation of the binary system (Kamchatnov, Kartashov, et al. 2014; Qu, Pitaevskii, et al. 2016; Congy, Kamchatnov, et al. 2016):

- Low-energy excitations take place at constant total density $\rho_1 + \rho_2$; they involve only the polarization $\rho_1 - \rho_2$ and the coupling coefficient g_s .
- High-energy excitations, on the other hand, are associated with a modulation of the total density $\rho_1 + \rho_2$ and involve the coupling g .

⁴This regime is very different from the one studied in Course 2021-22, IV.3, where we considered a mixture with $g_{11}, g_{22} > 0$, and the third parameter g_{12} chosen to be negative and close to $-\sqrt{g_{11}g_{22}}$. This situation gives rise to quantum droplets in a 3D geometry and bright solitons in a quasi-1D geometry, as shown experimentally by Cheiney, Cabrera, et al. (2018).

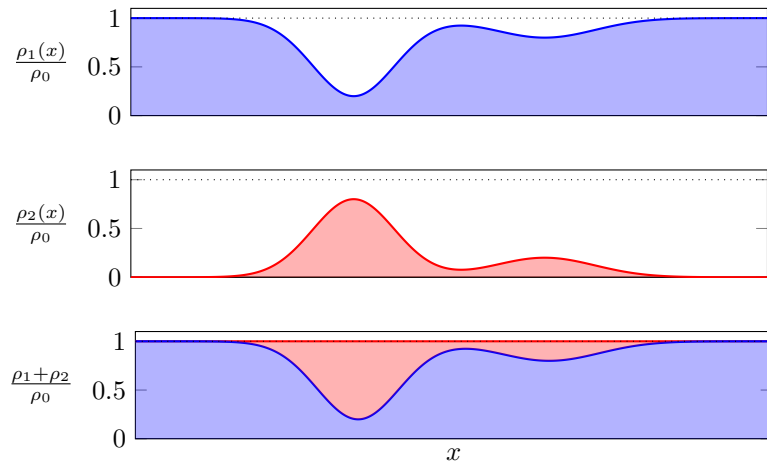


Figure IV.5. Spatial variation of densities $\rho_1(x)$ and $\rho_2(x)$ with constant total density condition $\rho_1(x, t) + \rho_2(x, t) = \rho_0$.

In the following, we will consider a one-dimensional problem, focus on low-energy excitations, and approximate

$$\rho_1(x, t) + \rho_2(x, t) = \rho_0 \quad (\text{IV.46})$$

where ρ_0 is a constant, at any point x and any time t (figure IV.5). The sum of the two continuity equations (IV.37) then leads to

$$\partial_x J = 0 \quad \text{with} \quad J = \rho_1 v_1 + \rho_2 v_2. \quad (\text{IV.47})$$

The total current of particles is therefore uniform in space.

In this constant-density regime, the spinor parameterization describing the gas is reduced to three real fields $\theta(x, t)$, $\Phi(x, t)$ and $\varphi(x, t)$:

$$\begin{pmatrix} \psi_1 \\ \psi_2 \end{pmatrix} = \sqrt{\rho_0} e^{i\Phi/2} \begin{pmatrix} \cos(\theta/2) e^{-i\varphi/2} \\ \sin(\theta/2) e^{+i\varphi/2} \end{pmatrix} \quad (\text{IV.48})$$

where Φ and φ denote the overall phase and relative phase of the two components respectively:

$$\Phi(x, t) = \varphi_1(x, t) + \varphi_2(x, t) \quad \varphi(x, t) = \varphi_2(x, t) - \varphi_1(x, t) \quad (\text{IV.49})$$

The fluid velocities v_j defined in (IV.37) are given by

$$v_1 = \frac{\hbar}{2m} (\Phi_x - \varphi_x) \quad v_2 = \frac{\hbar}{2m} (\Phi_x + \varphi_x) \quad (\text{IV.50})$$

so that the relationship $\partial_x J = 0$ becomes:

$$\partial_x (\Phi_x - \cos \theta \varphi_x) = 0. \quad (\text{IV.51})$$

This relationship, a direct consequence of the assumption of constant total density, partially links the global phase Φ , the relative phase φ and the mixing angle θ . It integrates to give

$$\boxed{\Phi_x - \cos \theta \varphi_x = 2k(t)} \quad (\text{IV.52})$$

where k is at this stage an arbitrary function of time.

In the following, we will consider situations where component 2 is located in a reduced area of space compared to the extension of component 1, which we will call a "bath". In this case, far from the minority component, we have $\theta \approx 0$ and therefore

$$\text{area such that } \rho_2 \approx 0 : \quad k \approx \frac{1}{2} (\Phi_x - \varphi_x) = \frac{mv_1}{\hbar}. \quad (\text{IV.53})$$

The quantity k thus represents the bath wave number in zones where this bath is essentially pure.

2-3 Bath at rest: the magnetic chain regained

In this paragraph, we consider the case where the bath is immobile, for example because it is confined to a segment, with an infinite barrier at each end. In this case, we can set $k(t) = 0$ at any instant t and eliminate the phase Φ in favor of φ thanks to :

$$\boxed{\text{Bath at rest: } \Phi_x = \cos \theta \varphi_x} \quad (\text{IV.54})$$

As long as we restrict ourselves to low-energy excitations and assume a constant density, the state of the binary mixture is described by the two

fields $\theta(x, t)$ and $\varphi(x, t)$. Rewriting the equations (IV.36) in terms of θ and φ gives

$$\begin{cases} \frac{2m}{\hbar}\theta_t &= -2\theta_x\varphi_x \cos\theta - \varphi_{xx} \sin\theta \\ \frac{2m}{\hbar}\varphi_t &= -\cos\theta \left(\varphi_x^2 + \frac{2mg_s\rho_0}{\hbar^2} \right) + \frac{\theta_{xx}}{\sin\theta} \end{cases} \quad (\text{IV.55})$$

Let us choose the unit of length x_0 such that

$$x_0 = \frac{\hbar}{\sqrt{2m|g_s|\rho_0}} \quad (\text{IV.56})$$

and the associated t_0 unit of time

$$t_0 = \frac{2mx_0^2}{\hbar} = \frac{\hbar}{|g_s|\rho_0} \quad (\text{IV.57})$$

which gives the same system as that found for the magnetic chain in (IV.19):

$$\begin{cases} \theta_t &= -2\theta_x\varphi_x \cos\theta - \varphi_{xx} \sin\theta \\ \varphi_t &= -\cos\theta (\varphi_x^2 \pm 1) + \frac{\theta_{xx}}{\sin\theta} \end{cases} \quad (\text{IV.58})$$

where $+$ now refers to the immiscible case and $-$ to the miscible case.

For a bath at rest and with the assumption of a constant total density, there is therefore a perfect correspondence between the equations of motion of a chain of magnetic moments and those of a binary mixture of condensates with:

$$\begin{aligned} \text{"easy-axis" ferromagnet} &\Leftrightarrow \text{immiscible mixture} \\ \text{"easy-plane" ferromagnet} &\Leftrightarrow \text{miscible mixture.} \end{aligned}$$

In particular, the Lagrangian approach presented in §1-4 remains unchanged (Congy, Kamchatnov, et al. 2016).

We thus recover the three conserved quantities mentioned above, starting with the mass (IV.23), written here as $N_2/\rho_0 x_0$, i.e. the population of the minority component (in reduced units):

$$\text{Bath at rest:} \quad N_2 = \frac{\rho_0}{2} \int (1 - \cos\theta) dx \quad (\text{IV.59})$$

where the integral is taken over the entire length of the bath, but where only regions where ψ_2 takes significant values actually contribute. The expressions (IV.24) and (IV.25) for the energy and for the momentum are also unchanged, the corresponding units being⁵:

$$\text{Energy unit: } E_0 = \frac{\hbar}{t_0} \rho_0 x_0 \quad \text{Momentum unit: } P_0 = \hbar \rho_0. \quad (\text{IV.60})$$

In physical units

$$\text{Bath at rest:} \quad E_{\text{rest}} = \frac{1}{4} E_0 x_0 \int \left[\theta_x^2 + \left(\phi_x^2 \pm \frac{1}{x_0^2} \right) \sin^2\theta \right] dx \quad (\text{IV.61})$$

The expression (IV.25) for the momentum can also be simplified considerably by using the relation $\Phi_x = \varphi_x \cos\theta$ which leads to

$$\text{Bath at rest:} \quad P_{\text{rest}} = \frac{\hbar\rho_0}{2} \int (\varphi_x - \Phi_x) dx = -\hbar\rho_0 \int \varphi_{1,x} dx \quad (\text{IV.62})$$

or, returning to physical units:

$$\text{Bath at rest:} \quad P_{\text{rest}} = -\hbar\rho_0 [\varphi_1(x_+) - \varphi_1(x_-)] \quad (\text{IV.63})$$

where x_{\pm} are located on either side of the zone where ψ_2 takes significant values, and where the bath phase φ_1 can vary (see figure IV.6, top).

Note. The reader might be concerned about the discontinuity that appears in (IV.58) at the miscible-unmiscible transition. The important point to note is that the length scale x_0 diverges at this point. For a finite sample size L , this length scale loses its interest if $x_0 > L$ and it is better to work with the dimensioned system of equations (IV.55), which is not singular in the limit $|g_s| \rightarrow 0$.

2-4 Unconstrained bath

We now consider a gas that can move freely on a ring, with periodic boundary conditions for the wave functions ψ_1 and ψ_2 . In this case, there is no

⁵Note that these units involve the dimensionless quantity $\rho_0 x_0$, so it is not possible to restore the correct units by just a dimensional analysis. The choice made here ensures $E_0 = P_0 v_0$, where the unit of velocity v_0 is given by $v_0 = x_0/t_0$.

reason to assume that the bath is at rest at all times, especially when an external force is applied to the system, as will be the case in §4. The special relationship (IV.54) must therefore be replaced by the more general one written in (IV.52). Still assuming a constant total density equal to ρ_0 , we now find for the evolution of the fields θ and φ :

$$\begin{cases} \theta_t &= -2\theta_x \varphi_x \cos \theta - \varphi_{xx} \sin \theta - 2k\theta_x \\ \varphi_t &= -\cos \theta (\varphi_x^2 \pm 1) + \frac{\theta_{xx}}{\sin \theta} - 2k\varphi_x \end{cases} \quad (\text{IV.64})$$

where the wavenumber k is expressed in units of $1/x_0$. We will see later that k is directly proportional to the momentum of the system [eq. (IV.73)] and is therefore independent of time as long as no external force is acting on either fluid.

Again, these equations can be obtained from a Lagrangian approach, now involving the three fields θ, Φ, φ and their first derivatives with respect to time and space. This Lagrangian is calculated from the one governing the evolution of the two coupled nonlinear Schrödinger equations:

$$\mathcal{L}_{\text{NLS}} = \sum_{j=1,2} \left(i\hbar \psi_j^* \psi_{j,t} - \frac{\hbar^2}{2m} |\psi_{j,x}|^2 - \frac{g}{2} |\psi_j|^4 \right) - g_{12} |\psi_1|^2 |\psi_2|^2. \quad (\text{IV.65})$$

We inject the form (IV.48) of the spinor (ψ_1, ψ_2) and find

$$\mathcal{L} = \mathcal{L}_{\text{kin}} - \mathcal{V} \quad (\text{IV.66})$$

with

$$\mathcal{L}_{\text{cin}} = \frac{1}{2} (\varphi_t \cos \theta - \Phi_t) \quad (\text{IV.67})$$

and

$$\mathcal{V} = \frac{1}{4} (\theta_x^2 + \varphi_x^2 + \Phi_x^2) - \frac{1}{2} \Phi_x \varphi_x \cos \theta \pm \frac{1}{4} \sin^2 \theta. \quad (\text{IV.68})$$

The Lagrange equation for Φ provides the general link (IV.52) between Φ , φ and θ , and those for θ and φ lead to (IV.64).

Here again, we find three conserved quantities:

- The number of atoms in the minority component

$$\text{Unconstrained bath: } N_2 = \frac{\rho_0}{2} \int (1 - \cos \theta) dx \quad (\text{IV.69})$$

which takes on the same value whether the bath is in free motion or forced to remain at rest as in §2-3.

- Energy (in physical units):

$$\text{Unconstrained bath: } E_{\text{unc.}} = \frac{1}{4} E_0 x_0 \int \left[\theta_x^2 + (\varphi_x^2 \pm \frac{1}{x_0^2}) \sin^2 \theta + 4k^2 \right] dx \quad (\text{IV.70})$$

In comparison with the case of the bath at rest (IV.61), for a ring of length L we note the addition of the term

$$E_0 x_0 L k^2 = \frac{\hbar^2 k^2}{2m} \rho_0 L \quad (\text{IV.71})$$

which simply corresponds to the kinetic energy of $\rho_0 L$ atoms moving at speed $\hbar k/m$.

- The momentum (in physical units):

$$P_{\text{unc.}} = \frac{\hbar \rho_0}{2} \int (\Phi_x - \varphi_x \cos \theta) dx \quad (\text{IV.72})$$

Exploiting the link (IV.52) between Φ_x and φ_x , this momentum can also be written for a ring of length L :

$$\text{Unconstrained bath: } P_{\text{unc.}} = \hbar k \rho_0 L \quad (\text{IV.73})$$

Link between P_{rest} and $P_{\text{unc.}}$. The difference (IV.71) between the energy of the "bath at rest" and "unconstrained bath" cases can be understood simply in terms of the bath's kinetic energy. On the other hand, the difference between the momenta (IV.63) for the bath at rest and (IV.73) for the bath moving freely on a ring deserves comment.

Figure IV.6 shows a phase profile of the bath in each case. We will not describe here what happens in the shaded area where the minority component is present, as this will be the subject of the next section for the special case of a soliton. We simply assume that the mixing of the two components produces the same phase difference $\Delta\varphi_1 = \varphi_1(x_+) - \varphi_1(x_-)$ on either side of this zone, whether the bath is at rest on a segment or free in a ring. We

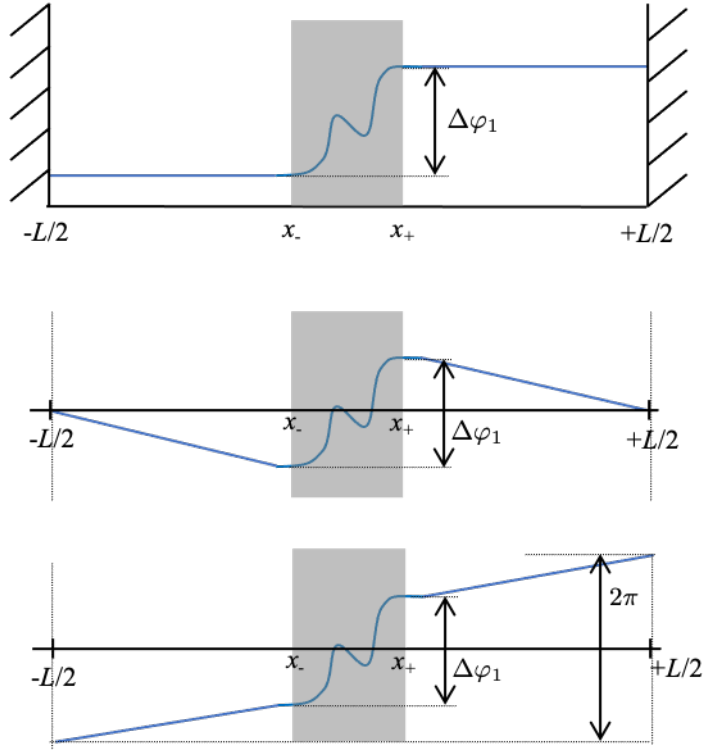


Figure IV.6. Possible profiles for the phase $\varphi_1(x)$ of the bath. The minority component 2 is assumed to be located in the shaded area, and its presence results in a phase variation $\Delta\varphi_1$ between points x_- and x_+ . Top: Confinement on a segment, imposing an immobile bath and therefore a uniform phase φ_1 outside the shaded zone. Middle and bottom: case of a bath freely moving on a ring, with periodic boundary conditions $\psi_1(L/2) = \psi_1(-L/2)$, so $\varphi_1(L/2) = \varphi_1(-L/2) + 2\pi n$ with $n \in \mathbb{Z}$. We have taken $n = 0$ for the middle figure (no phase winding) and $n = 1$ for the bottom figure.

also assume that the extension of the shaded area is very small compared to the total length L of the bath.

In the case of the bath at rest, we saw in (IV.63) that the momentum is simply equal to $-\hbar\rho_0\Delta\varphi_1$ (figure IV.6, top). In the case of the bath moving freely on a ring, the bath wave function ψ_1 must be mono-valued, which requires the phase to take the same value (modulo 2π) in $\pm L/2$. Let us first consider the case without phase winding (figure IV.6, middle): when we traverse the bath from point x_+ to point x_- (i.e. without passing through the shaded area), we have a phase gradient, and therefore a wavenumber, given by $k = -\Delta\varphi_1/L$. The result (IV.73) $P_{\text{unc.}} = \hbar k\rho_0 L$ is therefore rewritten $P_{\text{unc.}} = -\hbar\rho_0\Delta\varphi_1$, which coincides with the case of a bath at rest. If a phase winding is present in the ring, the phase difference between x_+ and x_- is equal to $-\Delta\varphi_1 + 2n\pi$ with $n \in \mathbb{Z}$ (figure IV.6, low for $n = 1$), which provides the general relationship between P_{rest} and $P_{\text{unc.}}$:

$$P_{\text{unc.}} = P_{\text{rest.}} + n 2\pi\hbar\rho_0. \quad (\text{IV.74})$$

3 The magnetic soliton

The realization of magnetic solitons from condensate mixtures is a subject that has been explored by several groups over the last ten years, both theoretically and experimentally⁶. These studies initially focused on the miscible case, corresponding to the *easy-plane* case for the magnetic chain. See Qu, Pitaevskii, et al. (2016), Ivanov, Kamchatnov, et al. (2017), Qu, Tylutki, et al. (2017), and Pitaevskii (2019) for the theory and Farolfi, Trypogeorgos, et al. (2020) and Chai, Lao, et al. (2020) for the first two experimental realizations.

In what follows, we will focus on the immiscible case, i.e. the *easy-axis* case for the ferromagnetic equivalent. More precisely, we consider a finite number of atoms of species 2 immersed in a long bath formed by species 1. In this section, we will be investigating the shape this cloud of particles 2 must take if it is to move at a constant speed v without undergoing

⁶"Real" magnetic solitons in solid materials have been observed for many years, in connection with interfaces between two zones of different magnetization. See Kosevich, Ivanov, et al. (1990) for historical references, and Togawa, Koyama, et al. (2012) and Caretta, Oh, et al. (2020) for recent achievements.

deformation, which is the definition of a soliton.

3-1 General structure of the solution

We are interested in a state of the mixture such that the fluid is composed exclusively of particles of type 1 when $x \rightarrow \pm\infty$. This imposes:

$$x \rightarrow \pm\infty : \quad \theta \rightarrow 0 \pmod{2\pi}. \quad (\text{IV.75})$$

We impose no constraint between the bath phase on either side of the soliton, which amounts to placing ourselves on an (arbitrarily long) segment.

We consider here the case of a bath at rest⁷, and look for the solitonic solutions of the system (IV.58) in the form of

$$\begin{cases} \theta(x, t) = \theta(x - vt) \\ \varphi(x, t) = \Omega t + \phi(x - vt) \end{cases} \quad (\text{IV.76})$$

A soliton is thus characterized by two parameters, its velocity v and the parameter Ω . We shall see later that it is essential to introduce this second parameter Ω to obtain interesting solutions⁸. A similar constraint had arisen for bright solitons, for which the phase of the wave function did not evolve with the same argument $x - vt$ as its modulus.

When we inject this solution structure into the equations of motion (IV.58), we obtain the following differential system for one-variable functions θ and ϕ (Long & Bishop 1979):

$$\begin{cases} -v\theta' &= -2\theta'\phi' \cos\theta - \phi'' \sin\theta \\ \Omega - v\phi' &= -\cos\theta [(\phi')^2 + 1] + \frac{\theta''}{\sin\theta} \end{cases} \quad (\text{IV.77})$$

Recall that to obtain this system, we expressed position and time in units of x_0 and t_0 defined as (IV.56-IV.57), with velocity in units of x_0/t_0 . We will now solve this system in the special case $v = 0$, and then move on to a soliton of any velocity.

⁷The case of a bath with wave number k and velocity $v_b = \hbar k/m$, described by the equations (IV.64), can be deduced by replacing v by $v - v_b$ in the following.

⁸The article by Chai, You, et al. (2022) implicitly posits $\Omega = 0$ and finds only a subset of the solitonic solutions discussed here.

3-2 The magnetic soliton at rest

For a soliton with zero velocity, the first equation of (IV.77) gives

$$\frac{d}{dx} (\phi' \sin^2 \theta) = 0. \quad (\text{IV.78})$$

As θ tends to 0 at infinity, we deduce that $\phi' = 0$ except at a point x_s where $\sin\theta = 0$ and where we can have $\phi'(x)$ proportional to the Dirac distribution $\delta(x - x_s)$. The ϕ phase is therefore uniform, with a possible discontinuity at a point where $\theta = 0$ or $\theta = \pi$ (total depletion of one or other of the components):

$$\text{Point } x_s \text{ where } \sin[\theta(x)] = 0 : \quad \phi(x) = \phi_0 + \phi_1 Y(x - x_s) \quad (\text{IV.79})$$

where $Y(x)$ represents the Heaviside function.

The second equation of (IV.77) then becomes:

$$\theta'' = \Omega \sin\theta + \frac{1}{2} \sin(2\theta). \quad (\text{IV.80})$$

Solving this differential equation is relatively technical, so we will confine ourselves to indicating the main conclusions for solutions centered at $x = 0$ (the problem is translation-invariant):

- The parameter Ω must be such that

$$\boxed{\Omega > -1} \quad (\text{IV.81})$$

- When this condition is verified, the solution is written:

$$\boxed{\frac{\rho_2(x)}{\rho_0} = \sin^2 \frac{\theta}{2} = \frac{2 + 2\Omega}{2 + \Omega + |\Omega| \cosh(2\kappa x)}} \quad (\text{IV.82})$$

with

$$\boxed{\kappa = \sqrt{1 + \Omega}} \quad (\text{IV.83})$$

This solution is maximal at $x = 0$ and decreases exponentially fast at infinity.

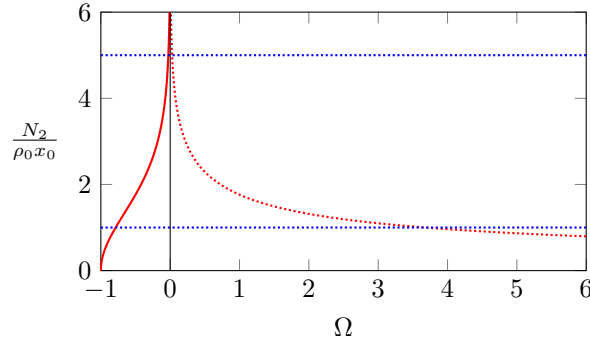


Figure IV.7. Graphical solution of the relationship between the parameter Ω and the number of atoms N_2 in the minority component. The two blue dotted lines correspond to the number of atoms in the minority component $\tilde{N}_2 \equiv N_2/\rho_0 x_0 = 1$ and $\tilde{N}_2 = 5$. The corresponding profiles are plotted in figure IV.8 and IV.9, respectively. For $\tilde{N}_2 = 1$, the solutions are $\Omega \approx -0.78$ (solid red) and $\Omega \approx 3.68$ (dotted red). For $\tilde{N}_2 = 5$, the solutions are $\Omega \approx -2.66 \cdot 10^{-2}$ (solid red) and $\Omega \approx 2.73 \cdot 10^{-2}$ (dotted red).

- The number of particles N_2 in the minority component is given by (IV.59) and we find

$$N_2 = \rho_0 x_0 \ln \left(\frac{2 + \Omega + 2\kappa}{|\Omega|} \right) \quad (\text{IV.84})$$

We show in figure IV.7 the principle of a graphical solution of this equation, allowing us to find the value(s) of Ω corresponding to a given number N_2 of particles in the minority component. For each N_2 , we find two values of Ω , one negative between $\Omega = -1$ and $\Omega = 0$ (continuous branch), the other positive (dotted branch). There are therefore two possible expressions for a soliton at rest for each value of N_2 . The energy of these solutions calculated using (IV.61) is $E = 2\kappa = 2\sqrt{1 + \Omega}$. The solution obtained for $\Omega < 0$ therefore has a lower energy than that corresponding to $\Omega > 0$.

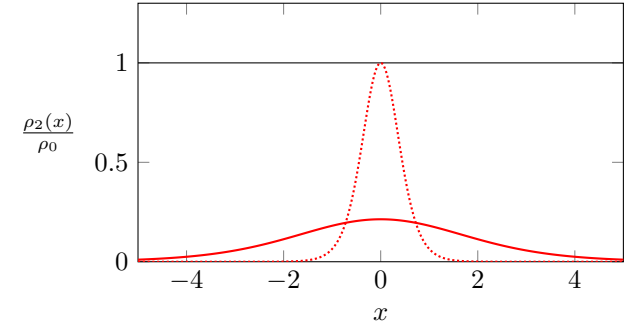


Figure IV.8. The two density profiles of the minority component for $N_2/\rho_0 x_0 = 1$ for a zero-velocity magnetic soliton.

Small numbers N_2 . In the case where $N_2/\rho_0 x_0 \lesssim 1$, the two solutions obtained are very different from each other, as shown in figure IV.8. One of the solutions (solid red line on this figure) corresponds to $\Omega \approx -1$, for which (IV.82) simplifies to

$$\frac{\rho_2(x)}{\rho_0} \approx \frac{\kappa^2}{\cosh^2(\kappa x)} \quad (\text{IV.85})$$

with $\kappa = \sqrt{1 + \Omega} \ll 1$. We find the characteristic structure of a bright soliton of low amplitude, with a width large in front of x_0 . This type of solution was to be expected, as we had found in §1-5 that the Landau-Lifshitz equation reduces to the nonlinear Schrödinger equation in the regime where θ remains close to 0, i.e. the low-depletion regime.

The other solution for the same value of N_2 (dotted red line in the figure) corresponds to $\Omega \gg 1$, and therefore $\kappa \gg 1$. It is much narrower, with complete depletion of component 1. Note that the emergence of a narrow structure is necessarily associated with high kinetic energy; the assumption of separation of the energy scales linked to spin and total density excitations must therefore be carefully re-examined for this type of solution: the spin structure that appears here costs a lot of energy and may couple with a density excitation.

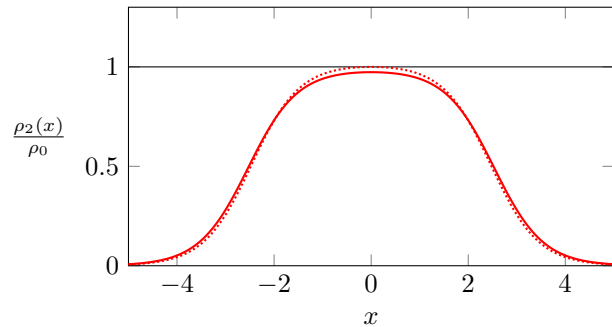


Figure IV.9. The two density profiles of the minority component for $N_2/\rho_0 x_0 = 5$ for a zero-velocity magnetic soliton.

Large numbers N_2 . In the case where $N_2/\rho_0 x_0 \gg 1$, the values Ω found by solving (IV.84) are close to $\Omega = 0$ and opposite to each other. They lead to very similar spatial profiles:

$$\frac{\rho_2(x)}{\rho_0} \approx \frac{1}{1 + \frac{|\Omega|}{2} \cosh(2x)}, \quad (\text{IV.86})$$

shown with solid and dotted lines in figure IV.9 for $N_2/\rho_0 x_0 = 5$. These profiles are \approx flat and close to 1 on a segment of length $\ln(4/|\Omega|) \approx N_2/\rho_0 x_0$ centered on $x = 0$. They decrease towards 0 on the length scale x_0 since $\kappa \approx 1$ in this case. This structure corresponds to a spin domain in the ferromagnetic case, or a quasi-pure bubble of condensate 2 of density ρ_0 , immersed in condensate 1.

Possible phase jumps. We indicated in (IV.79) the possibility of a jump of the phase φ (of unknown amplitude at this stage) at a point x_s where $\sin[\theta(x_s)] = 0$, i.e., where $\theta = 0$ or $\theta = \pi$. Let us briefly revisit this point for the two categories of solutions considered, and see what it means for the phases of the two condensates. First, let us note that the solution given in (IV.82) for $\sin(\theta/2)$ never cancels out, whatever the sign of Ω . This rules out finding a point x where $\theta(x) = 0$. A possible zero of $\sin[\theta(x)]$ must therefore correspond to $\theta(x) = \pi$, i.e. a point x for which $\sin[\theta(x)/2] = 1$ corresponding to the total depletion of the bath.

We can see from (IV.82) that the condition $\sin(\theta/2) = 1$ is indeed fulfilled at $x = 0$ for the solutions with $\Omega > 0$. The phases ϕ and φ can therefore be discontinuous at this point. The phases φ_1 and φ_2 of the two condensates can then be deduced from (IV.49-IV.52)

$$\partial_x \varphi_1 = -\sin^2(\theta/2) \partial_x \varphi \quad \partial_x \varphi_2 = \cos^2(\theta/2) \partial_x \varphi. \quad (\text{IV.87})$$

At a point x_s where $\theta(x_s) = \pi$, the discontinuity of φ is transferred (up to a \pm sign) to the bath phase φ_1 . More precisely, if we return to the wave function of the bath $\psi_1(x)$, it can be written (up a global phase) as

$$\Omega > 0, v = 0: \quad \psi_1(x) = \sqrt{\rho_0} \frac{\sqrt{\Omega} \sinh(\kappa x)}{[1 + \Omega \cosh^2(\kappa x)]^{1/2}}, \quad (\text{IV.88})$$

thus a phase jump of $\pm\pi$ in $x = 0$. On the other hand, there is no phase discontinuity for the wave function of the minority component at this point.

On the other hand, solutions corresponding to $\Omega < 0$ never reach the value 1, so the bath depletion is never total for them. We deduce that the phase $\varphi(x)$ is uniform throughout space for these solutions, and the same applies to the individual phases of the two condensates φ_1 and φ_2 . From (IV.82), we find for the bath wave function (still up to a global phase):

$$\Omega < 0, v = 0: \quad \psi_1(x) = \sqrt{\rho_0} \frac{\sqrt{|\Omega|} \cosh(\kappa x)}{[1 + |\Omega| \sinh^2(\kappa x)]^{1/2}} \quad (\text{IV.89})$$

and for the wave function of the minority component

$$\Omega < 0, v = 0: \quad \psi_2(x) = \sqrt{\rho_0} \frac{(1 - |\Omega|)^{1/2}}{[1 + |\Omega| \sinh^2(\kappa x)]^{1/2}}. \quad (\text{IV.90})$$

3-3 Experimental realization of a soliton at rest

The Collège de France group recently carried out an experiment in which a magnetic soliton at rest was produced and characterized in a two-component mixture (figure IV.10). The starting point is a flat-bottom box-shaped optical trap along the x axis with a length $L_x = 60 \mu\text{m}$. The other degrees of freedom are tightly confined, with width $L_y = 3 \mu\text{m}$ and thickness $L_z \sim 0.3 \mu\text{m}$. A uniform condensed gas of $N_1 \approx 20\,000$ rubidium

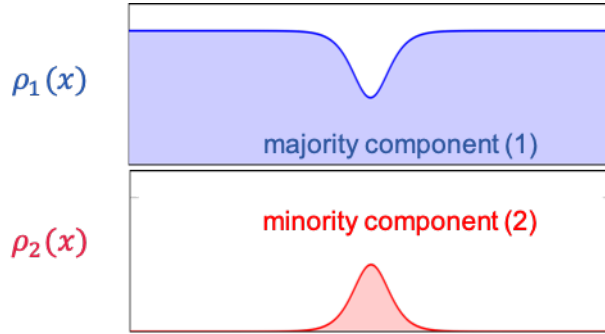


Figure IV.10. Magnetic soliton in a two-component mixture.

atoms (i.e. $\rho_0 = 370$ atoms/ μm) is prepared at very low temperature. Spin dynamics are frozen along the y and z directions, so that the gas is initially described to a good approximation by the one-dimensional wave function $\psi(x) = \sqrt{\rho_0}$. Atoms are prepared in the electronic ground state and in the hyperfine sublevel $|F = 1, m_F = -1\rangle$.

Using a transition involving an infrared photon of wavelength ~ 790 nm and a microwave photon, we transfer a fraction of the atoms from $|F = 1, m_F = -1\rangle$ to $|F = 1, m_F = +1\rangle$. The infrared beam is spatially shaped by a system of micro-mirrors so that the x dependence of the transferred fraction reproduces the function $\sin^2(\theta/2)$ given in (IV.82). During the transfer, the total density remains equal to ρ_0 at any point x . Furthermore, we aim for a solution $\Omega < 0$ so that the wave functions $\psi_{1,2}$ have a uniform phase: there is therefore no manipulation required to obtain the right phase profile, unlike in experiments with dark solitons.

In practice, we are interested in situations of low depletion, where the density of the minority component varies approximately as $1/\cosh^2(\kappa x)$ [cf. (IV.85)]. This simple profile is "printed" by choosing a given value of κ , in this case $\kappa^{-1} = 5.5 \mu\text{m}$. The number of atoms transferred is varied by changing the intensity of the light beam. We then measure whether the resulting structure contracts, expands or remains stationary. In the latter case, we deduce that we have reached the conditions for the formation of a zero-velocity magnetic soliton with $\Omega \approx -0.91$. The length scale x_0 is equal to $1.61 \mu\text{m}$ in this particular case.

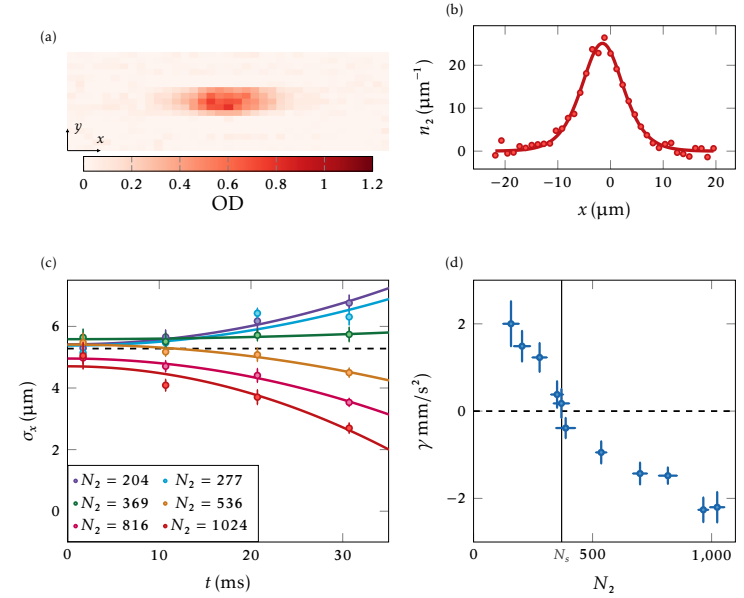


Figure IV.11. *a,b*: Visualization of the density $\rho_2(x)$ of the minority component of a magnetic soliton. The density ρ_0 of the majority component (not visible here) is 370 atoms/ μm . *c,d*: Expansion of the wave packet ψ_2 as a function of the atom number N_2 . The magnetic soliton state is reached for $N_2 = 370$. Figure taken from Franco Rabec's thesis (see also Rabec, Chauveau, et al. (2024)).

A typical result is shown in figure IV.11. For the value chosen for κ , the number of atoms ensuring stationarity is $N_2 = 370$. This yields the interaction parameter of the experiment $g_s = \hbar \times 0.06$ Hz $\cdot\mu\text{m}$; this result is in good agreement with what we expected, given the 3D scattering lengths and the geometry of the trap confining the atoms. We will return to the magnetic soliton thus produced in section 4, to study Bloch oscillations under the effect of a constant force.

3-4 The magnetic soliton in motion

We now turn to the solution of the system (IV.77) for any velocity v . As the corresponding calculations are fairly lengthy, we will simply give the main results here. The angle θ is given by

$$\boxed{\frac{\rho_2(x)}{\rho_0} = \sin^2 \frac{\theta}{2} = \frac{2\kappa^2}{2 + \Omega + \sqrt{\Omega^2 + v^2} \cosh(2\kappa x)}} \quad (\text{IV.91})$$

with

$$\boxed{\kappa = \sqrt{1 + \Omega - v^2/4}} \quad (\text{IV.92})$$

which generalizes the result (IV.82-IV.83) to the case $v \neq 0$. The phase ϕ is no longer uniform and it is given by:

$$\tan \left(\phi(x) + \frac{1}{2}xv \right) = \frac{2\Omega - v^2 + 2\sqrt{\Omega^2 + v^2}}{2\kappa v} \tanh(\kappa x) \quad (\text{IV.93})$$

The number of atoms of the minority species 2 in this structure is:

$$\cosh \tilde{N}_2 = \frac{2 + \Omega}{\sqrt{\Omega^2 + v^2}} \quad (\text{IV.94})$$

where we have set $\tilde{N}_2 \equiv N_2/\rho_0 x_0$.

To gain some intuition from these complicated equations, it is interesting to represent the state of the soliton in the plane (v, Ω) (figure IV.12). First, we note that the definition of κ in (IV.92) puts a constraint on the domain of the accessible plane. As the argument of the square root must be positive, we must choose the pair (v, Ω) such that

$$\Omega > -1 + \frac{v^2}{4}, \quad (\text{IV.95})$$

which represents a domain bounded by a parabola of axis z . The condition $\Omega > -1$ found in (IV.81) corresponds to the special case $v = 0$ of this general condition.

In the plane (v, Ω) , the curves corresponding to constant N_2 are ellipses, with their vertices located in $v = 0, \Omega < 0$ and in $v = 0, \Omega > 0$. These vertices correspond to the two solutions identified earlier for $v = 0$, and

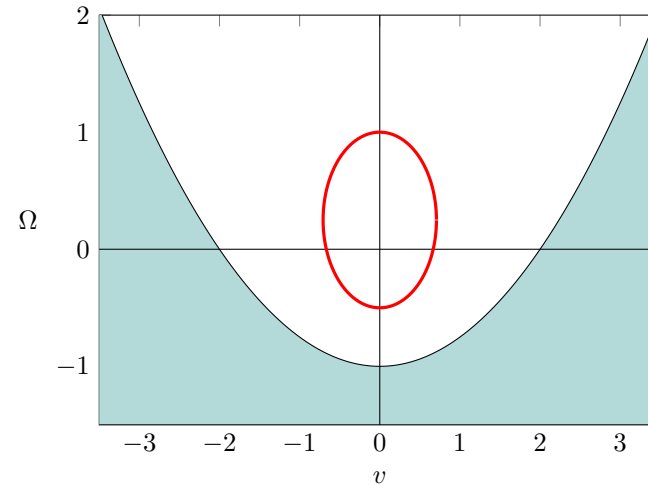


Figure IV.12. Red curve: ellipse representing the possible states of a magnetic soliton in the (v, Ω) plane for a fixed number of \tilde{N}_2 particles (here $\tilde{N}_2 \approx 1.7$). The colored area corresponds to the (v, Ω) parameters for which there is no solution. As \tilde{N}_2 increases, the ellipse contracts around the point $(0, 0)$.

we can now see that these particular solutions are linked by a continuum of solutions corresponding to non-zero velocity. The question, open at this stage, is to find a way to set the soliton in motion and make it travel along this ellipse. In the next section, we will show how this is possible.

The energy of the soliton is always given by the simple relation $E = 2\kappa$. From this result, we find that the momentum P deduced from the canonical relation

$$\left(\frac{\partial E}{\partial P} \right)_{\tilde{N}_2} = v \quad (\text{IV.96})$$

is related to the velocity by

$$\boxed{v = 2 \frac{\sin P}{\sinh \tilde{N}_2}} \quad (\text{IV.97})$$

This last relationship allows us to write the energy as

$$E(\tilde{N}_2, P) = 2 \tanh(\tilde{N}_2/2) + 4 \frac{\sin^2(P/2)}{\sinh \tilde{N}_2} \quad (\text{IV.98})$$

In this particular case of the magnetic soliton, we can verify the general relationship $P = -\hbar\rho_0 \Delta\varphi_1$ given in (IV.63), linking the momentum P and the phase variation of the bath $\Delta\varphi_1$ around the zone where component 2 is localized.

The fact that energy and velocity are periodic functions of momentum is remarkable. This will play an essential role in the next section, where we will study the motion of the magnetic soliton under the effect of a force. In mathematical terms, this periodicity is explained by the fact that the momentum is proportional to the phase variation of the bath $\Delta\varphi_1$, and that a phase is generally defined modulo 2π .

Here we have used the fact that the momentum P and the velocity v are conjugate quantities. Since the energy (IV.98) depends on the two independent variables P and \tilde{N}_2 , a natural question is to find the variable conjugate to \tilde{N}_2 . A straightforward calculation yields

$$\left(\frac{\partial E}{\partial \tilde{N}_2} \right)_P = -\Omega, \quad (\text{IV.99})$$

which shows that Ω plays (up to a minus sign) the role of a chemical potential, i.e. the energy required to modify the number of particles \tilde{N}_2 by one unit, at constant momentum.

A reminder on units. Position and time are expressed here in units of x_0 and t_0 given in (IV.56-IV.57). The unit of velocity is x_0/t_0 , the unit of energy is $\frac{\hbar}{t_0} \rho_0 x_0$ and the unit of momentum is $\hbar\rho_0$. We have set $\tilde{N}_2 = N_2/\rho_0 x_0$.

4 Bloch oscillations of a magnetic soliton

4-1 "Usual" Bloch oscillations

The phenomenon of Bloch oscillations is one of the most spectacular manifestations of quantum physics for a single particle. Provided this particle is placed in a suitable environment, the action of an external force f , uniform and constant in time, does not lead to a uniformly accelerated motion, but to an oscillating motion. We have encountered and studied this phenomenon in detail in previous courses (see in particular the lecture series 2012-13), so we will just briefly introduce it here.

The environment that gives rise to the phenomenon of Bloch oscillations is a periodic potential in space, which we will denote $V(x)$, limiting ourselves to a one-dimensional problem for the sake of simplicity. Let a be the spatial period of the potential, $V(x+a) = V(x)$. The temporal period of the Bloch oscillation is then

$$t_B = \frac{2\pi\hbar}{fa} \quad (\text{IV.100})$$

The explanation of this phenomenon lies in the structure of the dispersion relation that links the particle's energy E to its momentum, or rather quasi-momentum, noted here as p . In the periodic potential $V(x)$ and in the absence of the external force f , this dispersion relation is composed of energy bands $E_n(p)$ with periodicity $2\pi\hbar/a$:

$$E_n\left(p + \frac{2\pi\hbar}{a}\right) = E_n(p). \quad (\text{IV.101})$$

The eigenstates $|\phi_{n,p}\rangle$ of the Hamiltonian are also periodic in p , apart from phase factors of no importance here. A momentum domain of width $2\pi\hbar/a$, for example $[-\pi\hbar/a, +\pi\hbar/a]$, is called a *Brillouin zone*.

Let us assume, for example, that the particle is prepared in the lowest energy band, $n = 0$, in the form of a wave packet obtained by superimposing a continuum of quasi-momentum values:

$$|\psi(t=0)\rangle = \int c(p) |\phi_{n=0,p}\rangle dp \quad (\text{IV.102})$$

Now let us apply the additional force f : each quasi-momentum p will evolve according to $\dot{p} = f$. Let us further assume that this force f is sufficiently weak that during its motion, the particle remains in the lower band $n = 0$. After the time t_B , the quasi-momentum of each eigenstate involved in the integral (IV.102) has increased by the quantity $2\pi\hbar/a$, and this quasi-momentum has therefore described the entire Brillouin zone. We deduce that the particle's state has returned to its initial value (apart from one global phase). In particular, the average particle position is back to its initial value.

This phenomenon was first demonstrated for electrons in superlattices (Feldmann, Leo, et al. 1992), then for atoms in standing light waves (Ben Dahan, Peik, et al. 1996; Wilkinson, Bharucha, et al. 1996). The essential ingredient is the periodic variation of physical observables (energy, velocity, position, etc.) with momentum. The response of the momentum to a force ($\dot{p} = f$) then immediately implies an oscillating motion for the physical object involved.

4-2 Force on a magnetic soliton

Let us now consider a magnetic soliton initially at rest. This soliton is composed with N_2 atoms immersed in a bath of type 1 particles, with asymptotic density $\rho_1(x) = \rho_0$. Suppose we apply a force f to each particle of type 2, without affecting the particles of type 1. If the force is sufficiently weak, the soliton will (at least at short times) be accelerated as a whole: particles 2 will start moving in the direction of the force, and the hole they create in the bath of particles 1 will follow this motion. If this were not the case, we would generate an excitation of the total density of the mixture, which we have seen is costly in terms of energy because it is proportional to g .

Assuming that the fluid mixture can continue to be described as a magnetic soliton that retains its integrity under the action of the force f , the canonical momentum of the system varies as follows

$$\boxed{\frac{dP}{dt} = F \quad \text{with} \quad F = N_2 f} \quad (\text{IV.103})$$

This relationship is deduced from the conservation of total energy in the

presence of the potential $U(x)$ associated with the force f ($f = -dU/dx$):

$$E_{\text{tot}} = E(\tilde{N}_2, P) + \tilde{N}_2 U(x_s) \quad (\text{IV.104})$$

where $E(\tilde{N}_2, P)$ is given in (IV.98) and x_s represents the position of the center of the soliton. Since N_2 remains constant, we find

$$0 = \frac{dE_{\text{tot}}}{dt} = \left(\frac{\partial E}{\partial P} \right)_{\tilde{N}_2} \frac{dP}{dt} + \tilde{N}_2 \frac{dU}{dx} \frac{dx_s}{dt} \quad (\text{IV.105})$$

which leads to, using the soliton velocity $v = \frac{dx_s}{dt} = \left(\frac{\partial E}{\partial P} \right)_{\tilde{N}_2}$:

$$0 = v \frac{dP}{dt} - \tilde{N}_2 f v \quad \Rightarrow \quad \frac{dP}{dt} = \tilde{N}_2 f. \quad (\text{IV.106})$$

The uniformly accelerated motion of the soliton will last as long as the corresponding velocity v , expressed in reduced units x_0/t_0 , is smaller than 1. In this regime we have [cf (IV.97-IV.98)]:

$$v \approx \frac{P}{m_{\text{eff}}} \quad E(\tilde{N}_2, P) \approx E_0(\tilde{N}_2) + \frac{P^2}{2m_{\text{eff}}} \quad (\text{IV.107})$$

with the effective mass

$$m_{\text{eff}} = \frac{1}{2} \sinh \tilde{N}_2. \quad (\text{IV.108})$$

Once out of this regime, we must return to the complete dispersion relation $E(\tilde{N}_2, P)$ to determine the soliton's motion. As this dispersion relation is periodic in P with the period 2π in reduced units, i.e., $2\pi\hbar\rho_0$ in physical units, we deduce that the soliton will have an oscillating motion with the time period

$$\boxed{t_B = \frac{2\pi\hbar\rho_0}{F}} \quad (\text{IV.109})$$

as initially predicted by Kosevich, Gann, et al. (1998) and Kosevich (2001). We thus find typical Bloch oscillation dynamics, even though no underlying periodic structure is present in this system (Gangardt & Kamenev 2009; Schecter, Gangardt, et al. 2012). The correspondence between the traditional result (IV.100) and that found for a magnetic soliton is as follows:

$$\begin{aligned} a &\leftrightarrow \rho_0^{-1} \\ f &\leftrightarrow F = N_2 f \end{aligned} \quad (\text{IV.110})$$

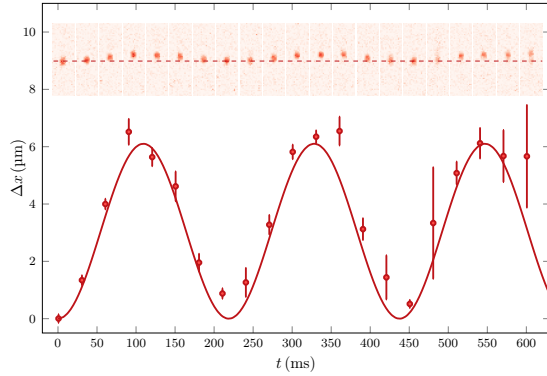


Figure IV.13. Bloch oscillations of a magnetic soliton prepared as shown in figure IV.11. The bath of particles 1 is present, but not visible in this series of images, as the light beam used to image the system is not resonant with atoms in the $|1\rangle$ state. Figure taken from Rabec, Chauveau, et al. (2024).

It is important to note that we are dealing here with a collective phenomenon: the period is a function of $N_2 f$ and not of f alone. In other words, the soliton's oscillation is not the superposition of individual motions of type 2 particles each subjected to the force f , but it corresponds to the dynamics of a "mesoscopic" object (for $N_2 \gg 1$) subjected to the force $F = N_2 f$.

For the graphical representation in the plane (v, Ω) , this oscillating motion is equivalent to travelling along the ellipse of figure IV.12 in the counterclockwise direction. The two turning points of the motion, at which the soliton's velocity cancels out, correspond to the two states of the soliton at rest found in §3-2 [see also Zhao, Wang, et al. (2020) for a description in terms of effective mass whose sign depends on time].

4-3 Observation of Bloch oscillations

The magnetic soliton whose preparation we described in §3-3 can be set in motion by a magnetic field gradient, since the two sublevels involved, $|1\rangle \equiv |F = 1, m = -1\rangle$ and $|2\rangle \equiv |F = 1, m = +1\rangle$ experience opposing

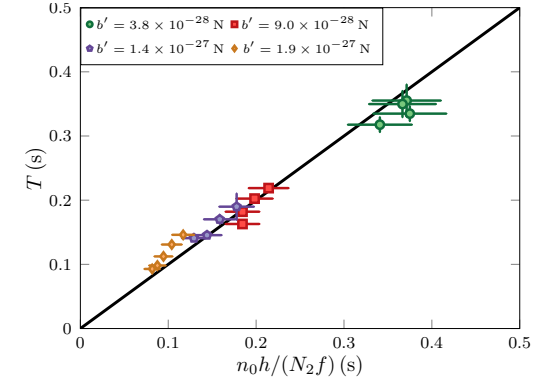


Figure IV.14. Variation of the period measured for Bloch oscillations as a function of N_2 and the force $f = \mu_B b'$.

forces in this gradient. In practice, we prepare the cloud in the state $|1\rangle$ in the presence of the gradient b' , chosen to be sufficiently small that the equilibrium density ρ_1 remains practically uniform. We use $b' = 1 \text{ G/m}$, which corresponds to an energy difference ΔU between the two ends of the segment of the order of a nanokelvin, well below the chemical potential of the gas. The force f introduced earlier is equal to the difference in forces felt by the atoms on the states $|1\rangle$ and $|2\rangle$, corresponding to $f = \mu_B b'$ where μ_B is the Bohr magneton.

The period of Bloch oscillations is a few hundred milliseconds, which is very long compared to the time it takes a sound wave to travel from one end of the sample to the other (ten milliseconds). The assumption made in (IV.52) of a zero current J is therefore legitimate: the phonons generated by the soliton's motion make several round trips between the ends of the tube and the soliton itself in a period t_B ; this ensures that the phase of the bath of particles 1 can be considered uniform on either side of the soliton.

An example of oscillations is shown in figure IV.13. The measured period is in excellent agreement with the prediction (figure IV.109).

Using atom interferometry, we can study the state of the bath at the turning points of the motion. At initial times as well as after an integer number of oscillations, the bath is expected to have a uniform phase [cf. eq.

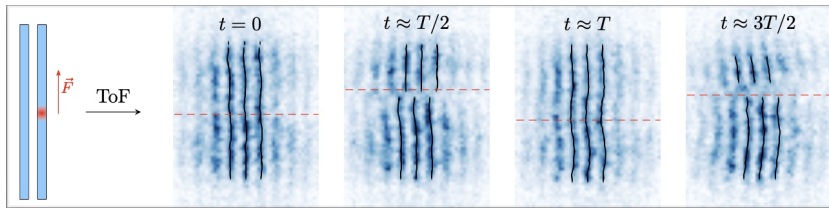


Figure IV.15. Study of the phase of the bath of particles $|1\rangle$ at the turning points of the Bloch oscillation. The segment of atoms containing the soliton is made to interfere with a test segment of uniform phase.

(IV.89)], which corresponds to the lower point of the ellipse in figure IV.12. On the other hand, after one half of the oscillation period (or $3/2, 5/2, \dots$), the bath phase is expected to have a jump of $\pm\pi$ at the soliton center, which corresponds to the upper point of the ellipse in figure IV.12 [cf. eq. (IV.88)].

These predictions concerning the bath phase can be checked by preparing a second segment, parallel to the first one, for which all atoms are in state $|1\rangle$. This second segment is then used as a phase reference. At a given time, the confinement of the two segments is released. The atoms expand ballistically and the interference between the two segments is observed. When the segment with the soliton is associated with a uniform phase for the wave function $\psi_1(x)$, the interference fringes are expected to be rectilinear. On the other hand, when $\psi_1(x)$ has a phase jump of π , the fringes are expected to exhibit a dislocation at the soliton position. This is indeed what we observe experimentally (see figure IV.15).

This experimental result presents a strong analogy with that of a Josephson junction subjected to a potential difference V constant over time (Bresolin, Roy, et al. 2023). Denoting φ the phase difference of the superconductor on either side of the junction, the behavior of this junction is governed by the following two equations:

$$I = I_c \sin \varphi \quad (\text{IV.111})$$

$$\frac{d\varphi}{dt} = \frac{qV}{\hbar} \quad (\text{IV.112})$$

where I is the current flowing through the junction and I_c is the junction's

characteristic current. These equations lead to a sinusoidal current $I(t)$.

$$I(t) = I_c \sin(\omega t) \quad \text{with} \quad \omega = qV/\hbar. \quad (\text{IV.113})$$

The correspondence with the soliton oscillation is made by the following identification:

$$I \longleftrightarrow v \quad (\text{IV.114})$$

$$\varphi \longleftrightarrow P/\hbar\rho_0 = \varphi_1(x_-) - \varphi_1(x_+) \quad (\text{IV.115})$$

$$qV \longleftrightarrow N_2 f / \rho_0 \quad (\text{IV.116})$$

Equations (IV.111) and (IV.112) are equivalent to (IV.97) and (IV.103) respectively, which we rewrite here in physical units:

$$v = v_c \sin(P/\hbar\rho_0) \quad \text{with} \quad v_c = \frac{2}{\sinh \tilde{N}_2} \frac{x_0}{t_0} \quad (\text{IV.117})$$

$$\frac{dP}{dt} = N_2 f. \quad (\text{IV.118})$$

4-4 The origin of the periodicity of $E(P)$

As mentioned above, the origin of the Bloch oscillation phenomenon lies in the periodicity of the dispersion relation $E(P)$, from which we deduce the periodicity $v(P)$ since $v = \partial E / \partial P$. If the momentum evolves linearly in time under the effect of a constant and uniform external force F , with $\dot{P} = F$, the energy, velocity and position of the system under study will be oscillating functions of time.

The periodicity of $E(P)$ (or rather $E_{\text{rel}}(P)$ in what follows) with period $2\pi\hbar\rho_0$ is in fact a general property of a 1D gas. To show this, we will follow a line of reasoning due to Bloch (1973) and Bloch (1974) [see also Haldane (1981)]. Consider a set of N particles of mass m on a ring of perimeter L , which amounts to imposing periodic boundary conditions on the wave function $\Psi(x_1, \dots, x_N)$. Let us separate the N position variables into a center-of-mass variable

$$X = \frac{1}{N}(x_1 + \dots + x_N) \quad (\text{IV.119})$$

and $N - 1$ relative variables ξ_1, \dots, ξ_{N-1} that we will not have to define explicitly. The Hamiltonian is written as

$$\hat{H} = \frac{\hat{P}^2}{2M} \otimes \hat{1}_{\text{rel}} + \hat{1}_{\text{com}} \otimes \hat{H}_{\text{rel}} \quad (\text{IV.120})$$

where $M = Nm$ denotes the total mass, $\hat{P} = \sum \hat{p}_i$ is the total momentum, and \hat{H}_{rel} contains the kinetic terms related to the relative momenta as well as the effect of interactions between particles, which depend only on the position differences $x_i - x_j$. We can then search for the eigenfunctions of \hat{H} in the form

$$\Psi_P(x_1, \dots, x_N) = e^{iPX/\hbar} \Phi_P(\xi_1, \dots, \xi_{N-1}) \quad (\text{IV.121})$$

where P is a possible eigenvalue of the total momentum operator \hat{P} and where

$$\hat{H}_{\text{rel}} \Phi_P = E_{\text{rel}}(P) \Phi_P. \quad (\text{IV.122})$$

The total energy associated with Ψ_P is therefore

$$\frac{P^2}{2M} + E_{\text{rel}}(P). \quad (\text{IV.123})$$

At this point, it may come as a surprise to see P appear in the eigenvalue equation (IV.122) for the Hamiltonian \hat{H}_{rel} : the latter depends only on the relative variables ξ_i and we might naively have expected a complete decoupling between the degree of freedom of the center of mass and the relative variables. In fact, this complete decoupling does not occur, due to the constraints of the periodic boundary conditions adopted here. To explain this point, we will make these constraints explicit by exploiting two types of transformations.

- If we perform the translation $x_i \rightarrow x_i + L$ for each particle, the relative coordinates are unchanged and $X \rightarrow X + L$. Since the wave function Ψ_P must remain unchanged, we deduce that $e^{iPL/\hbar} = 1$, i.e.

$$P = 2\pi n\hbar/L \quad \text{with} \quad n \in \mathbb{Z}. \quad (\text{IV.124})$$

This is the usual quantization relation for the momentum of a particle (here, the center of mass) in a box of size L .

- If we perform the translation $x_i \rightarrow x_i + L$ for just one of the N particles, the prefactor $e^{iPX/\hbar}$ is multiplied by $e^{iPL/N\hbar} = e^{iP/\hbar\rho_0}$ with $\rho_0 = N/L$. As for the relative variables, they are modified in a way that we will not specify explicitly, but which we can write as $\xi_j \rightarrow \xi'_j$. Since Ψ_P must remain unchanged in this translation, we deduce that the function of the relative variables is modified according to:

$$\Phi_P(\xi'_1, \dots, \xi'_{N-1}) = e^{-iP/\hbar\rho_0} \Phi_P(\xi_1, \dots, \xi_{N-1}). \quad (\text{IV.125})$$

Here we explicitly see that a value of P obeying the quantization condition (IV.124) generally leads to a change of the boundary conditions of the function Φ_P . This is precisely why the eigenfunctions Φ_P of the relative motion and the associated eigenvalues $E_{\text{rel}}(P)$ depend on the momentum of the center of mass.

However, if we choose P such that $e^{-iP/\hbar\rho_0} = 1$, i.e. P multiple of $2\pi\hbar\rho_0$, then the eigenfunctions satisfy the same boundary conditions as those for $P = 0$. Since the relative Hamiltonian \hat{H}_{rel} does not depend on P , we deduce that its spectrum for $P = 2\pi\hbar\rho_0$ is the same as that for $P = 0$.

Furthermore, in the thermodynamic limit $N \rightarrow \infty$, $L \rightarrow \infty$ with $\rho_0 = N/L$ constant, the mass $M = Nm$ tends towards infinity so that the kinetic energy of the center of mass $P^2/2M$ also tends towards 0 when $P = 2\pi\hbar\rho_0$. In particular, this provides the desired periodicity for the ground-state energy of the system, which is what interests us here for the magnetic soliton.

In the Bloch oscillation experiment we described earlier, the magnetic soliton can be seen as a mesoscopic impurity that enables us to inject momentum into the bath in a controlled manner via the force F , and thus probe the general periodicity of $E(P)$ that we have just explained. Another experiment exploiting this same periodicity is described in Meinert, Knap, et al. (2017), where the impurity is then microscopic since it is composed of a single atom, of a different nature to that of the bath (see also Grusdt, Shashi, et al. (2014), Petković & Ristivojevic (2016), and Will & Fleischhauer (2023)).

Références

- Ablowitz, Mark J, David J Kaup, Alan C Newell & Harvey Segur (1974), “The inverse scattering transform-Fourier analysis for nonlinear problems”, in *Studies in applied mathematics* **53**, pp. 249–315.
- Ablowitz, Mark J & Harvey Segur (1981), *Solitons and the inverse scattering transform*, SIAM.
- Aftalion, Amandine, Philippe Gravejat & Etienne Sandier (2024), “Bifurcating solitonic vortices in a strip”, in *arXiv preprint arXiv:2411.16482*.
- Aftalion, Amandine & Etienne Sandier (2023), “Solitons and solitonic vortices in a strip”, in *Nonlinear Analysis* **228**, p. 113184.
- Akhmediev, Nail (2021), “Waves that appear from nowhere: complex rogue wave structures and their elementary particles”, in *Frontiers in Physics* **8**, p. 612318.
- Akhmediev, Nail, JM Soto-Crespo & Natasha Devine (2016), “Breather turbulence versus soliton turbulence: Rogue waves, probability density functions, and spectral features”, in *Phys. Rev. E* **94**, p. 022212.
- Anderson, BP, PC Haljan, CA Regal, DL Feder, LA Collins, Charles W Clark & Eric A Cornell (2001), “Watching dark solitons decay into vortex rings in a Bose-Einstein condensate”, in *Phys. Rev. Lett.* **86**, p. 2926.
- Bakkali-Hassani, B, C Maury, S Stringari, S Nascimbene, J Dalibard & J Beugnon (2023), “The cross-over from Townes solitons to droplets in a 2D Bose mixture”, in *New Journal of Physics* **25**, p. 013007.
- Bakkali-Hassani, B, C Maury, Y-Q Zou, É Le Cerf, R Saint-Jalm, Patricia Christina Marques Castilho, Sylvain Nascimbene, Jean Dalibard & Jérôme Beugnon (2021), “Realization of a Townes soliton in a two-component planar Bose gas”, in *Phys. Rev. Lett.* **127**, p. 023603.
- Bastianello, Alvise, Alexey Tikan, Francois Copie, Stephane Randoux & Pierre Suret (2025), “Observation of a generalized Gibbs ensemble in photonics”, in *arXiv preprint arXiv:2503.16526*.
- Becker, C, K Sengstock, P Schmelcher, PG Kevrekidis & R Carretero-González (2013), “Inelastic collisions of solitary waves in anisotropic Bose-Einstein condensates: sling-shot events and expanding collision bubbles”, in *New Journal of Physics* **15**, p. 113028.
- Becker, Christoph, Simon Stellmer, Parvis Soltan-Panahi, Sören Dörscher, Mathis Baumert, Eva-Maria Richter, Jochen Kronjäger, Kai Bongs & Klaus Sengstock (2008), “Oscillations and interactions of dark and dark-bright solitons in Bose-Einstein condensates”, in *Nature Physics* **4**, pp. 496–501.
- Ben Dahan, M., E. Peik, J. Reichel, Y. Castin & C. Salomon (1996), “Bloch Oscillations of Atoms in an Optical Potential”, in *Phys. Rev. Lett.* **76** (24), p. 4508.
- Benjamin, T Brooke & James E Feir (1967), “The disintegration of wave trains on deep water Part 1. Theory”, in *Journal of Fluid Mechanics* **27**, pp. 417–430.
- Bersano, TM, V Gokhroo, MA Khomehchi, J D’Ambrose, DJ Frantzeskakis, P Engels & PG Kevrekidis (2018), “Three-component soliton states in spinor $F=1$ Bose-Einstein condensates”, in *Phys. Rev. Lett.* **120**, p. 063202.
- Bloch, F (1973), “Superfluidity in a Ring”, in *Phys. Rev. A* **7**, p. 2187.
- (1974), “Reply to” Free-energy minima for helium in a ring”, in *Phys. Rev. A* **10**, p. 716.
- Brand, Joachim & William P Reinhardt (2002), “Solitonic vortices and the fundamental modes of the “snake instability”: Possibility of observation in the gaseous Bose-Einstein condensate”, in *Phys. Rev. A* **65**, p. 043612.
- Brazhnyi, VA & VV Konotop (2003), “Evolution of a dark soliton in a parabolic potential: Application to Bose-Einstein condensates”, in *Phys. Rev. A* **68**, p. 043613.
- Brazhnyi, VA, VV Konotop & LP Pitaevskii (2006), “Dark solitons as quasi-particles in trapped condensates”, in *Phys. Rev. A* **73**, p. 053601.

- Bresolin, S., A. Roy, G. Ferrari, A. Recati & N. Pavloff (2023), “Oscillating Solitons and ac Josephson Effect in Ferromagnetic Bose-Bose Mixtures”, in *Phys. Rev. Lett.* **130** (22), p. 220403.
- Bromberg, Yaron & Hui Cao (2014), “Generating non-Rayleigh speckles with tailored intensity statistics”, in *Phys. Rev. Lett.* **112**, p. 213904.
- Burger, S., K. Bongs, S. Dettmer, W. Ertmer, K. Sengstock, A. Sanpera, G. V. Shlyapnikov & M. Lewenstein (1999), “Dark solitons in Bose–Einstein condensates”, in *Phys. Rev. Lett.* **83**, pp. 5198–5201.
- Busch, Th & JR Anglin (2000), “Motion of dark solitons in trapped Bose–Einstein condensates”, in *Phys. Rev. Lett.* **84**, p. 2298.
- (2001), “Dark-bright solitons in inhomogeneous Bose–Einstein condensates”, in *Phys. Rev. Lett.* **87**, p. 010401.
- Caretta, Lucas, Se-Hyeok Oh, Takian Fakhrol, Dong-Kyu Lee, Byung Hun Lee, Se Kwon Kim, Caroline A Ross, Kyung-Jin Lee & Geoffrey SD Beach (2020), “Relativistic kinematics of a magnetic soliton”, in *Science* **370**, pp. 1438–1442.
- Carr, LD & J Brand (2004), “Spontaneous soliton formation and modulational instability in Bose–Einstein condensates”, in *Phys. Rev. Lett.* **92**, p. 040401.
- Carr, Lincoln D & Yvan Castin (2002), “Dynamics of a matter-wave bright soliton in an expulsive potential”, in *Phys. Rev. A* **66**, p. 063602.
- Carr, Lincoln D, Charles W Clark & Wilhelm P Reinhardt (2000), “Stationary solutions of the one-dimensional nonlinear Schrödinger equation. I. Case of repulsive nonlinearity”, in *Phys. Rev. A* **62**, p. 063610.
- Cartwright, Julyan HE & Hisami Nakamura (2009), “What kind of a wave is Hokusai’s Great wave off Kanagawa?”, in *Notes and Records of the Royal Society* **63**, pp. 119–135.
- Castin, Yvan & Jean Dalibard (1997), “Relative phase of two Bose–Einstein condensates”, in *Phys. Rev. A* **55**, p. 4330.
- Castin, Yvan & Christopher Herzog (2001), “Bose–Einstein condensates in symmetry breaking states”, in *Comptes Rendus de l’Académie des Sciences-Series IV-Physics* **2**, pp. 419–443.
- Chai, X., D. Lao, K. Fujimoto, R. Hamazaki, M. Ueda & C. Raman (2020), “Magnetic Solitons in a Spin-1 Bose–Einstein Condensate”, in *Phys. Rev. Lett.* **125** (3), p. 030402.
- Chai, X., L. You & C. Raman (2022), “Magnetic solitons in an immiscible two-component Bose–Einstein condensate”, in *Phys. Rev. A* **105** (1), p. 013313.
- Cheiney, P, CR Cabrera, J Sanz, B Naylor, L Tanzi & L Tarruell (2018), “Bright soliton to quantum droplet transition in a mixture of Bose–Einstein condensates”, in *Phys. Rev. Lett.* **120**, p. 135301.
- Congy, T, GA El, G Roberti, A Tovbis, S Randoux & P Suret (2024), “Statistics of extreme events in integrable turbulence”, in *Phys. Rev. Lett.* **132**, p. 207201.
- Congy, Thibault, Anatoly Kamchatnov & Nicolas Pavloff (2016), “Dispersive hydrodynamics of nonlinear polarization waves in two-component Bose–Einstein condensates”, in *SciPost Physics* **1**, p. 006.
- Copie, François, Pierre Suret & Stéphane Randoux (2023), “Space–time observation of the dynamics of soliton collisions in a recirculating optical fiber loop”, in *Optics Communications* **545**, p. 129647.
- Danaila, I, MA Khamehchi, V Gokhroo, P Engels & PG Kevrekidis (2016), “Vector dark-antidark solitary waves in multicomponent Bose–Einstein condensates”, in *Phys. Rev. A* **94**, p. 053617.
- Darrigol, Olivier (2003), “The spirited horse, the engineer, and the mathematician: water waves in nineteenth-century hydrodynamics”, in *Archive for history of exact sciences* **58**, pp. 21–95.
- Dauxois, Thierry (2008), “Fermi, Pasta, Ulam, and a mysterious lady”, in *Physics today* **61**, pp. 55–57.
- Dauxois, Thierry & Michel Peyrard (2006), *Physics of solitons*, Cambridge University Press.
- De Jager, EM (2006), “On the origin of the Korteweg–de Vries equation”, in *arXiv preprint math/0602661*.
- Del Vecchio Del Vecchio, Giuseppe, Alvisè Bastianello, Andrea De Luca & Giuseppe Mussardo (2020), “Exact out-of-equilibrium steady states in the semiclassical limit of the interacting Bose gas”, in *SciPost Physics* **9**, p. 002.
- Delande, Dominique & Krzysztof Sacha (2014), “Many-body matter-wave dark soliton”, in *Phys. Rev. Lett.* **112**, p. 040402.
- Denschlag, J, J.E. Simsarian, D.L. Feder, C.W. Clark, L.A Collins, et al. (2000), “Generating solitons by phase engineering of a Bose–Einstein condensate”, in *Science* **287**, p. 97.
- Des Cloizeaux, Jacques & Michel Gaudin (1966), “Anisotropic linear magnetic chain”, in *Journal of Mathematical Physics* **7**, pp. 1384–1400.
- Di Carli, Andrea, Craig D Colquhoun, Grant Henderson, Stuart Flannigan, Gian-Luca Oppo, Andrew J Daley, Stefan Kuhr & Elmar Haller (2019),

- “Excitation modes of bright matter-wave solitons”, in *Phys. Rev. Lett.* **123**, p. 123602.
- Donadello, Simone, Simone Serafini, Marek Tylutki, Lev P Pitaevskii, Franco Dalfovo, Giacomo Lamporesi & Gabriele Ferrari (2014), “Observation of solitonic vortices in Bose-Einstein condensates”, in *Phys. Rev. Lett.* **113**, p. 065302.
- Drazin, Philip G & Robin Stanley Johnson (1989), *Solitons: an introduction*, Cambridge University Press.
- Dreischuh, Alexander, Dragomir N Neshev, Dan E Petersen, Ole Bang & Wieslaw Krolikowski (2006), “Observation of attraction between dark solitons”, in *Phys. Rev. Lett.* **96**, p. 043901.
- Dudley, John M, Goëry Genty, Arnaud Mussot, Amin Chabchoub & Frédéric Dias (2019), “Rogue waves and analogies in optics and oceanography”, in *Nature Reviews Physics* **1**, pp. 675–689.
- Dudley, John M, Véronique Sarano & Frédéric Dias (2013), “On Hokusai’s Great wave off Kanagawa: localization, linearity and a rogue wave in sub-Antarctic waters”, in *Notes and Records of the Royal Society* **67**, pp. 159–164.
- Dudley, John Michael, Christophe Finot, Goëry Genty & J Taylor (2023), “Fifty years of fiber solitons”, in *Optics and photonics news* **34**, pp. 26–33.
- Dunjko, Vanja & Maxim Olshanii (2015), “Resilience of constituent solitons in multisoliton scattering off barriers”, in *arXiv preprint arXiv:1501.00075*.
- Dutton, Zachary, Michael Budde, Christopher Slowe & Lene Vestergaard Hau (2001), “Observation of quantum shock waves created with ultra-compressed slow light pulses in a Bose-Einstein condensate”, in *Science* **293**, pp. 663–668.
- Dziarmaga, Jacek (2004), “Quantum dark soliton: Nonperturbative diffusion of phase and position”, in *Phys. Rev. A—Atomic, Molecular, and Optical Physics* **70**, p. 063616.
- Everitt, PJ, MA Sooriyabandara, Massimiliano Guasoni, PB Wigley, CH Wei, GD McDonald, KS Hardman, P Manju, JD Close, CCN Kuhn, et al. (2017), “Observation of a modulational instability in Bose-Einstein condensates”, in *Phys. Rev. A* **96**, p. 041601.
- Farolfi, A., D. Trypogeorgos, C. Mordini, G. Lamporesi & G. Ferrari (2020), “Observation of Magnetic Solitons in Two-Component Bose-Einstein Condensates”, in *Phys. Rev. Lett.* **125** (3), p. 030401.
- Feldmann, J., K. Leo, J. Shah, D.A.B. Miller, J.E. Cunningham, T. Meier, G. von Plessen, A. Schulze, P. Thomas & S. Schmitt-Rink (1992), “Optical investigation of Bloch oscillations in a semiconductor superlattice”, in *Phys. Rev. B* **46** (11), p. 7252.
- Fermi, Enrico, P Pasta & Stanislaw Ulam (1955), *Studies of the nonlinear problems*, tech. rep., Los Alamos National Laboratory (LANL), Los Alamos, NM (United States).
- Frantzeskakis, DJ (2010), “Dark solitons in atomic Bose–Einstein condensates: from theory to experiments”, in *Journal of Physics A: Mathematical and Theoretical* **43**, p. 213001.
- Gammal, A, T Frederico & Lauro Tomio (2001), “Critical number of atoms for attractive Bose-Einstein condensates with cylindrically symmetrical traps”, in *Phys. Rev. A* **64**, p. 055602.
- Gangardt, D.M. & A. Kamenev (2009), “Bloch Oscillations in a One-Dimensional Spinor Gas”, in *Phys. Rev. Lett.* **102** (7), p. 070402.
- Gardner, Clifford S, John M Greene, Martin D Kruskal & Robert M Miura (1967), “Method for solving the Korteweg-deVries equation”, in *Phys. Rev. Lett.* **19**, p. 1095.
- Gelash, Andrey, Dmitry Agafontsev, Vladimir Zakharov, Gennady El, Stéphane Randoux & Pierre Suret (2019), “Bound state soliton gas dynamics underlying the spontaneous modulational instability”, in *Phys. Rev. Lett.* **123**, p. 234102.
- Ginsberg, Naomi S, Joachim Brand & Lene Vestergaard Hau (2005), “Observation of hybrid soliton vortex-ring structures in Bose-Einstein condensates”, in *Phys. Rev. Lett.* **94**, p. 040403.
- Gordon, JP (1983), “Interaction forces among solitons in optical fibers”, in *Optics letters* **8**, pp. 596–598.
- Greenberger, Daniel M (1979), “Some remarks on the extended Galilean transformation”, in *American Journal of Physics* **47**, pp. 35–38.
- Grusdt, F., A. Shashi, D. Abanin & E. Demler (2014), “Bloch oscillations of bosonic lattice polarons”, in *Phys. Rev. A* **90** (6), p. 063610.
- Haldane, FDM (1981), “Effective harmonic-fluid approach to low-energy properties of one-dimensional quantum fluids”, in *Phys. Rev. Lett.* **47**, p. 1840.
- Hamner, C., J.J. Chang, P. Engels & M.A. Hoefer (2011), “Generation of Dark-Bright Soliton Trains in Superfluid-Superfluid Counterflow”, in *Phys. Rev. Lett.* **106** (6), p. 065302.
- Hasegawa, Akira (2022), “Optical soliton: Review of its discovery and applications in ultra-high-speed communications”, in *Frontiers in Physics* **10**, p. 1044845.

- Hasegawa, Akira & Frederick Tappert (1973), “Transmission of stationary nonlinear optical pulses in dispersive dielectric fibers. I. Anomalous dispersion”, in *Applied Physics Letters* **23**, pp. 142–144.
- Haus, Hermann A & William S Wong (1996), “Solitons in optical communications”, in *Rev. Mod. Phys.* **68**, p. 423.
- Ivanov, Sergey K, Anatoly M Kamchatnov, Thibault Congy & Nicolas Pavloff (2017), “Solution of the Riemann problem for polarization waves in a two-component Bose-Einstein condensate”, in *Phys. Rev. E* **96**, p. 062202.
- Jackson, B, NP Proukakis & CF Barenghi (2007), “Dark-soliton dynamics in Bose-Einstein condensates at finite temperature”, in *Phys. Rev. A—Atomic, Molecular, and Optical Physics* **75**, p. 051601.
- Javanainen, Juha & Sung Mi Yoo (1996), “Quantum phase of a Bose-Einstein condensate with an arbitrary number of atoms”, in *Phys. Rev. Lett.* **76**, p. 161.
- Kamchatnov, AM, YV Kartashov, P-É Larré & N Pavloff (2014), “Nonlinear polarization waves in a two-component Bose-Einstein condensate”, in *Phys. Rev. A* **89**, p. 033618.
- Karjanto, Natanael (2021), “Peregrine soliton as a limiting behavior of the Kuznetsov-Ma and Akhmediev breathers”, in *Frontiers in Physics* **9**, p. 599767.
- Katsimiga, GC, Simeon I Mistakidis, TM Bersano, MKH Ome, SM Mossman, K Mukherjee, P Schmelcher, P Engels & PG Kevrekidis (2020), “Observation and analysis of multiple dark-antidark solitons in two-component Bose-Einstein condensates”, in *Phys. Rev. A* **102**, p. 023301.
- Kaup, DJ (1990), “Perturbation theory for solitons in optical fibers”, in *Phys. Rev. A* **42**, p. 5689.
- Khaykovich, L., F. Schreck, G. Ferrari, T. Bourdel, J. Cubizolles, L. D. Carr, Y. Castin & C. Salomon (2002), “Formation of a matter-wave bright soliton”, in *Science* **296**, p. 1290.
- Kibler, Bertrand, Julien Fatome, Christophe Finot, Guy Millot, Frédéric Dias, Goëry Genty, Nail Akhmediev & John M Dudley (2010), “The Peregrine soliton in nonlinear fibre optics”, in *Nature Physics* **6**, p. 790.
- Kibler, Bertrand, Julien Fatome, Christophe Finot, Guy Millot, Goëry Genty, Benjamin Wetzol, Nail Akhmediev, Frédéric Dias & John M Dudley (2012), “Observation of Kuznetsov-Ma soliton dynamics in optical fibre”, in *Scientific reports* **2**, p. 463.
- Kivshar, Yuri S & Wiesław Królikowski (1995), “Lagrangian approach for dark solitons”, in *Optics communications* **114**, pp. 353–362.
- Kivshar, Yuri S, Dmitry E Pelinovsky, Thierry Cretegy & Michel Peyrard (1998), “Internal modes of solitary waves”, in *Phys. Rev. Lett.* **80**, p. 5032.
- Komineas, S & N Papanicolaou (2003), “Solitons, solitonic vortices, and vortex rings in a confined Bose-Einstein condensate”, in *Phys. Rev. A* **68**, p. 043617.
- Konotop, Vladimir V & Lev Pitaevskii (2004), “Landau dynamics of a grey soliton in a trapped condensate”, in *Phys. Rev. Lett.* **93**, p. 240403.
- Korepin, Vladimir E, Vladimir E Korepin, NM Bogoliubov & AG Izergin (1997), *Quantum inverse scattering method and correlation functions*, vol. 3, Cambridge university press.
- Kosevich, AM (2001), “Bloch oscillations of magnetic solitons as an example of dynamical localization of quasiparticles in a uniform external field”, in *Low Temperature Physics* **27**, pp. 513–541.
- Kosevich, AM, VV Gann, AI Zhukov & VP Voronov (1998), “Magnetic soliton motion in a nonuniform magnetic field”, in *Journal of Experimental and Theoretical Physics* **87**, pp. 401–407.
- Kosevich, Arnold Markovich, BA Ivanov & AS Kovalev (1990), “Magnetic solitons”, in *Physics Reports* **194**, pp. 117–238.
- Kraych, Adrien E, Dmitry Agafontsev, Stéphane Randoux & Pierre Suret (2019), “Statistical properties of the nonlinear stage of modulation instability in fiber optics”, in *Phys. Rev. Lett.* **123**, p. 093902.
- Ku, Mark JH, Wenjie Ji, Biswaroop Mukherjee, Elmer Guardado-Sanchez, Lawrence W Cheuk, Tarik Yefsah & Martin W Zwierlein (2014), “Motion of a Solitonic Vortex in the BEC-BCS Crossover”, in *Phys. Rev. Lett.* **113**, p. 065301.
- Ku, Mark JH, Biswaroop Mukherjee, Tarik Yefsah & Martin W Zwierlein (2016), “Cascade of solitonic excitations in a superfluid fermi gas: From planar solitons to vortex rings and lines”, in *Phys. Rev. Lett.* **116**, p. 045304.
- Kundu, A & O Pshaev (1983), “Comments on the gauge equivalence between Heisenberg spin chains with single-site anisotropy and nonlinear Schrodinger equations”, in *Journal of Physics C: Solid State Physics* **16**, p. L585.
- Kuznetsov, Evgenii Aleksandrovich (1977), “Solitons in a parametrically unstable plasma”, in *Akademiia Nauk SSSR Doklady*, vol. 236, , pp. 575–577.

- Lakshmanan, M, Th W Ruijgrok & CJ Thompson (1976), “On the dynamics of a continuum spin system”, in *Physica A: Statistical Mechanics and its Applications* **84**, pp. 577–590.
- Lakshmanan, Muthusamy (1988), *Solitons: Introduction and Applications*, Springer Science & Business Media.
- Landau, Lev & Evgeny Lifshitz (1935), “On the theory of the dispersion of magnetic permeability in ferromagnetic bodies”, in *Phys. Z. Sowjetunion* **8**, pp. 101–114.
- Lannig, Stefan, Christian-Marcel Schmied, Maximilian Prüfer, Philipp Kunkel, Robin Strohmaier, Helmut Strobel, Thomas Gasenzer, Panayotis G Kevrekidis & Markus K Oberthaler (2020), “Collisions of three-component vector solitons in Bose-Einstein condensates”, in *Phys. Rev. Lett.* **125**, p. 170401.
- Lax, Peter (1968), “Integrals of nonlinear equations of evolution and solitary waves”, in *Commun. Pure Appl. Math.* **21**, p. 46.
- Lepoutre, S, L Fouché, A Boissé, Gwenaël Berthet, G Salomon, Alain Aspect & Thomas Bourdel (2016), “Production of strongly bound K 39 bright solitons”, in *Phys. Rev. A* **94**, p. 053626.
- Lieb, Elliott H. & Werner Liniger (1963), “Exact Analysis of an Interacting Bose Gas. I. The General Solution and the Ground State”, in *Phys. Rev.* **130** (4), pp. 1605–1616.
- Long, KA & AR Bishop (1979), “Nonlinear excitations in classical ferromagnetic chains”, in *Journal of Physics A: Mathematical and General* **12**, p. 1325.
- Luo, De, Yi Jin, Jason HV Nguyen, Boris A Malomed, Oleksandr V Marchukov, Vladimir A Yurovsky, Vanja Dunjko, Maxim Olshanii & RG Hulet (2020), “Creation and characterization of matter-wave breathers”, in *Phys. Rev. Lett.* **125**, p. 183902.
- Ma, Yan-Chow (1979), “The perturbed plane-wave solutions of the cubic Schrödinger equation”, in *Studies in Applied Mathematics* **60**, pp. 43–58.
- Malomed, Boris A (2022), “Soliton models: Traditional and novel, one- and multidimensional”, in *Low Temperature Physics* **48**, pp. 856–895.
- (2024), “Multidimensional soliton systems”, in *Advances in Physics: X* **9**, p. 2301592.
- Marchukov, Oleksandr V, Boris A Malomed, Vladimir A Yurovsky, Maxim Olshanii, Vanja Dunjko & Randall G Hulet (2019), “Splitting of nonlinear-Schrödinger-equation breathers by linear and nonlinear localized potentials”, in *Phys. Rev. A* **99**, p. 063623.
- Marin, François (2012), “Solitons: Historical and physical introduction”, in *Solitons*, Springer, , pp. 1561–1575.
- McGuire, James B (1964), “Study of exactly soluble one-dimensional N-body problems”, in *Journal of Mathematical Physics* **5**, pp. 622–636.
- Meinert, Florian, Michael Knap, Emil Kirilov, Katharina Jag-Lauber, Mikhail B Zvonarev, Eugene Demler & Hanns-Christoph Nägerl (2017), “Bloch oscillations in the absence of a lattice”, in *Science* **356**, pp. 945–948.
- Meng, Ling-Zheng, Xi-Wang Luo & Li-Chen Zhao (2025), “Self-Adapted Josephson Oscillation of Dark-Bright Solitons under Constant Forces”, in *arXiv preprint arXiv:2501.15841*.
- Menotti, Chiara & Sandro Stringari (2002), “Collective oscillations of a one-dimensional trapped Bose-Einstein gas”, in *Phys. Rev. A* **66**, p. 043610.
- Mežnaršič, Tadej, Tina Arh, Jure Brenc, Jaka Pišljar, Katja Gosar, Žiga Gosar, Rok Žitko, Erik Zupanič & Peter Jeglič (2019), “Cesium bright matter-wave solitons and soliton trains”, in *Phys. Rev. A* **99**, p. 033625.
- Mikeska, H-J & M Steiner (1991), “Solitary excitations in one-dimensional magnets”, in *Advances in Physics* **40**, pp. 191–356.
- Mitschke, Fedor M & Linn F Mollenauer (1987), “Experimental observation of interaction forces between solitons in optical fibers”, in *Optics letters* **12**, pp. 355–357.
- Mollenauer, Linn F, Roger H Stolen & James P Gordon (1980), “Experimental observation of picosecond pulse narrowing and solitons in optical fibers”, in *Phys. Rev. Lett.* **45**, p. 1095.
- Mossman, Sean M, Garyfallia C Katsimiga, Simeon I Mistakidis, Alejandro Romero-Ros, Thomas M Bersano, Peter Schmelcher, Panayotis G Kevrekidis & Peter Engels (2024), “Observation of dense collisional soliton complexes in a two-component Bose-Einstein condensate”, in *Communications Physics* **7**, p. 163.
- Muñoz Mateo, A & J Brand (2014), “Chladni solitons and the onset of the snaking instability for dark solitons in confined superfluids”, in *Phys. Rev. Lett.* **113**, p. 255302.
- Muryshev, A, GV Shlyapnikov, Wolfgang Ertmer, K Sengstock & M Lewenstein (2002), “Dynamics of dark solitons in elongated Bose-Einstein condensates”, in *Phys. Rev. Lett.* **89**, p. 110401.
- Muryshev, AE, HB van Linden van den Heuvell & GV Shlyapnikov (1999), “Stability of standing matter waves in a trap”, in *Phys. Rev. A* **60**, R2665.
- Nakamura, K & T Sasada (1982), “Gauge equivalence between one-dimensional Heisenberg ferromagnets with single-site anisotropy and

- nonlinear Schrodinger equations”, in *Journal of Physics C: Solid State Physics* **15**, p. L915.
- Nguyen, Jason HV, De Luo & Randall G Hulet (2017), “Formation of matter-wave soliton trains by modulational instability”, in *Science* **356**, pp. 422–426.
- Nguyen, J.H.V., P. Dyke, D. Luo, B.A. Malomed & R.G. Hulet (2014), “Collisions of matter-wave solitons”, in *Nat. Phys.* **10**, p. 918.
- Novikov, S, Sergei V Manakov, Lev Petrovich Pitaevskii & Vladimir Evgenovič Zakharov (1984), *Theory of solitons: the inverse scattering method*, Springer Science & Business Media.
- Olshanii, Maxim (1998), “Atomic scattering in the presence of an external confinement and a gas of impenetrable bosons”, in *Phys. Rev. Lett.* **81**, p. 938.
- Parker, NG, SL Cornish, CS Adams & AM Martin (2007), “Bright solitary waves and trapped solutions in Bose–Einstein condensates with attractive interactions”, in *Journal of Physics B: Atomic, Molecular and Optical Physics* **40**, p. 3127.
- Pelinovsky, Dmitry E, Yuri S Kivshar & Vsevolod V Afanasjev (1998), “Internal modes of envelope solitons”, in *Physica D: Nonlinear Phenomena* **116**, pp. 121–142.
- Peregrine, D Howell (1983), “Water waves, nonlinear Schrödinger equations and their solutions”, in *The ANZIAM Journal* **25**, pp. 16–43.
- Perez-Garcia, Victor M, Humberto Michinel & Henar Herrero (1998), “Bose-Einstein solitons in highly asymmetric traps”, in *Phys. Rev. A* **57**, p. 3837.
- Petković, Aleksandra & Zoran Ristivojevic (2016), “Dynamics of a mobile impurity in a one-dimensional Bose liquid”, in *Phys. Rev. Lett.* **117**, p. 105301.
- Pitaevskii, Lev P (2019), “Magnetic solitons in binary mixtures of Bose–Einstein condensates”, in *Rendiconti Lincei. Scienze Fisiche e Naturali* **30**, pp. 269–276.
- Pitaevskii, Lev Petrovich (2016), “Dynamics of solitary waves in ultracold gases in terms of observable quantities”, in *Physics-Uspekhi* **59**, p. 1028.
- Qu, C., M. Tylutki, S. Stringari & L.P. Pitaevskii (2017), “Magnetic solitons in Rabi-coupled Bose-Einstein condensates”, in *Phys. Rev. A* **95** (3), p. 033614.
- Qu, Chunlei, Lev P Pitaevskii & Sandro Stringari (2016), “Magnetic solitons in a binary Bose-Einstein condensate”, in *Phys. Rev. Lett.* **116**, p. 160402.
- Rabec, F, G Chauveau, G Brochier, S Nascimbene, J Dalibard & J Beugnon (2024), “Bloch Oscillations of a Soliton in a 1D Quantum Fluid”, in *arXiv preprint arXiv:2412.04355*.
- Reinhardt, W. P. & C. W. Clark (1997), “Soliton dynamics in the collisions of Bose-Einstein condensates: an analogue of the Josephson effect”, in *Phys. Rev. B* **30**, p. L785.
- Roberti, Giacomo, Gennady El, Alexander Tovbis, François Copie, Pierre Suret & Stéphane Randoux (2021), “Numerical spectral synthesis of breather gas for the focusing nonlinear Schrödinger equation”, in *Physical Review E* **103**, p. 042205.
- Romero-Ros, A, Garyfallia C Katsimiga, Simeon I Mistakidis, S Mossman, G Biondini, P Schmelcher, P Engels & PG Kevrekidis (2024), “Experimental realization of the Peregrine soliton in repulsive two-component Bose-Einstein condensates”, in *Phys. Rev. Lett.* **132**, p. 033402.
- Russell, J Scott (1844), “Report on waves”, in *Report of the fourteenth meeting of the British Association for the Advancement of Science*, vol. 25.
- Safari, Akbar, Robert Fickler, Miles J Padgett & Robert W Boyd (2017), “Generation of caustics and rogue waves from nonlinear instability”, in *Phys. Rev. Lett.* **119**, p. 203901.
- Saha, Abhik Kumar & Romain Dubessy (2025), “Characterizing far from equilibrium states of the one-dimensional nonlinear Schrödinger equation”, in *SciPost Physics Core* **8**, p. 028.
- Salasnich, Luca, Alberto Parola & L Reatto (2003), “Modulational instability and complex dynamics of confined matter-wave solitons”, in *Phys. Rev. Lett.* **91**, p. 080405.
- Satsuma, Junkichi & Nobuo Yajima (1974), “B. Initial value problems of one-dimensional self-modulation of nonlinear waves in dispersive media”, in *Progress of Theoretical Physics Supplement* **55**, pp. 284–306.
- Schechter, Michael, DM Gangardt & Alex Kamenev (2012), “Dynamics and Bloch oscillations of mobile impurities in one-dimensional quantum liquids”, in *Annals of Physics* **327**, pp. 639–670.
- Schweigler, Thomas, Valentin Kasper, Sebastian Erne, Igor Mazets, Bernhard Rauer, Federica Cataldini, Tim Langen, Thomas Gasenzer, Jürgen Berges & Jörg Schmiedmayer (2017), “Experimental characterization of a quantum many-body system via higher-order correlations”, in *Nature* **545**, pp. 323–326.

- Scott, Robin George, Franco Dalfovo, LP Pitaevskii & Sandro Stringari (2011), "Dynamics of dark solitons in a trapped superfluid Fermi gas", in *Phys. Rev. Lett.* **106**, p. 185301.
- Shamailov, Sophie S & Joachim Brand (2019), "Quantum dark solitons in the one-dimensional Bose gas", in *Phys. Rev. A* **99**, p. 043632.
- Shrira, Victor I & Vladimir V Geogjaev (2010), "What makes the Peregrine soliton so special as a prototype of freak waves?", in *Journal of Engineering Mathematics* **67**, pp. 11–22.
- Siovitz, Ido, Stefan Lannig, Yannick Deller, Helmut Strobel, Markus K Oberthaler & Thomas Gasenzer (2023), "Universal dynamics of rogue waves in a quenched spinor Bose condensate", in *Phys. Rev. Lett.* **131**, p. 183402.
- Solli, Daniel R, Claus Ropers, Prakash Koonath & Bahram Jalali (2007), "Optical rogue waves", in *nature* **450**, pp. 1054–1057.
- Soto-Crespo, Jose M, Natasha Devine & Nail Akhmediev (2016), "Integrable turbulence and rogue waves: breathers or solitons?", in *Phys. Rev. Lett.* **116**, p. 103901.
- Sroyngoen, Waranon & James R Anglin (2025), "Soliton resuscitations: asymmetric revivals of the breathing mode of an atomic bright soliton in a harmonic trap", in *arXiv preprint arXiv:2502.09016*.
- Suret, Pierre, Rebecca El Koussaifi, Alexey Tikan, Clément Evain, Stéphane Randoux, Christophe Schwaj & Serge Bielawski (2016), "Single-shot observation of optical rogue waves in integrable turbulence using time microscopy", in *Nature communications* **7**, p. 13136.
- Suret, Pierre, Stephane Randoux, Andrey Gelash, Dmitry Agafontsev, Benjamin Doyon & Gennady El (2024), "Soliton gas: Theory, numerics, and experiments", in *Phys. Rev. E* **109**, p. 061001.
- Syrwid, Andrzej (2021), "Quantum dark solitons in ultracold one-dimensional Bose and Fermi gases", in *Journal of Physics B: Atomic, Molecular and Optical Physics* **54**, p. 103001.
- Theocharis, G, P Schmelcher, MK Oberthaler, PG Kevrekidis & DJ Frantzeskakis (2005), "Lagrangian approach to the dynamics of dark matter-wave solitons", in *Phys. Rev. A—Atomic, Molecular, and Optical Physics* **72**, p. 023609.
- Togawa, Y, T Koyama, K Takayanagi, S Mori, Y Kousaka, J Akimitsu, S Nishihara, K Inoue, AS Ovchinnikov & J-i Kishine (2012), "Chiral magnetic soliton lattice on a chiral helimagnet", in *Phys. Rev. Lett.* **108**, p. 107202.
- Tsuzuki, Toshio (1971), "Nonlinear waves in the Pitaevskii-Gross equation", in *Journal of Low Temperature Physics* **4**, pp. 441–457.
- Wadkin-Snaith, Dominic C & Dimitri M Gangardt (2012), "Quantum gray solitons in confining potentials", in *Phys. Rev. Lett.* **108**, p. 085301.
- Walczak, Pierre, Stéphane Randoux & Pierre Suret (2015), "Optical rogue waves in integrable turbulence", in *Phys. Rev. Lett.* **114**, p. 143903.
- Weller, A, JP Ronzheimer, C Gross, J Esteve, MK Oberthaler, DJ Frantzeskakis, G Theocharis & PG Kevrekidis (2008), "Experimental observation of oscillating and interacting matter wave dark solitons", in *Phys. Rev. Lett.* **101**, p. 130401.
- Wilkinson, S.R., C.F. Bharucha, K.W. Madison, Q. Niu & M.G. Raizen (1996), "Observation of Atomic Wannier-Stark Ladders in an Accelerating Optical Potential", in *Phys. Rev. Lett.* **76** (24), p. 4512.
- Will, M. & M. Fleischhauer (2023), "Dynamics of polaron formation in 1D Bose gases in the strong-coupling regime", in *New J. Phys.* **25**, p. 083043.
- Wybo, Elisabeth, Alvise Bastianello, Monika Aidelsburger, Immanuel Bloch & Michael Knap (2023), "Preparing and analyzing solitons in the sine-Gordon model with quantum gas microscopes", in *PRX Quantum* **4**, p. 030308.
- Yefsah, T., A.T. Sommer, M.J.H. Ku, L.W. Cheuk, W. Ji, W.S. Bakr & M.W. Zwierlein (2013), "Heavy solitons in a fermionic superfluid", in *Nature* **499**, p. 426.
- Yu, X. & P.B. Blakie (2022), "Propagating Ferrodark Solitons in a Superfluid: Exact Solutions and Anomalous Dynamics", in *Phys. Rev. Lett.* **128** (12), p. 125301.
- Zabusky, Norman J & Martin D Kruskal (1965), "Interaction of "solitons" in a collisionless plasma and the recurrence of initial states", in *Phys. Rev. Lett.* **15**, p. 240.
- Zakharov, Vladimir & Aleksei Shabat (1972), "Exact theory of two-dimensional self-focusing and one-dimensional self-modulation of waves in nonlinear media", in *Sov. Phys. JETP* **34**, p. 62.
- Zakharov, Vladimir Evgenevich, ed. (1991), *What is integrability?*, Springer-Verlag.
- Zhao, Li-Chen, Wenlong Wang, Qinglin Tang, Zhan-Ying Yang, Wen-Li Yang & Jie Liu (2020), "Spin soliton with a negative-positive mass transition", in *Phys. Rev. A* **101**, p. 043621.